Exploration of Histone Deacetylase Ligand Binding Modes by Photoaffinity Probes

By

He Bai

M.S., University of Illinois at Chicago, 2007
B.S., Zhejiang University, 2003

THESIS

Submitted as a partial fulfillment of the requirements For the degree of Doctor of Philosophy in Medicinal Chemistry
In the Graduate College of the University of Illinois at Chicago, 2012

Chicago, Illinois

Defense Committee:

Pavel A. Petukhov, Chair and Advisor
Richard B. van Breemen
Joanna E. Burdette
Brian T. Murphy
Jonna Frasor, Physiology and Biophysics

This thesis is dedicated to my father, Nanping Bai, my mother, Shirong He, and my wife, Wenli Wang, without whom it would never have been accomplished.

ACKNOWLDEGMENTS

I would like to thank my advisor and mentor, Professor Pavel A. Petukhov, for his support and invaluable guidance over the last five years. It has truly been a privilege and honor of mine to be one of his students. He is one of the most intelligent, passionate, knowledgeable and considerate scientists I have ever encountered. I have learned far more important values than knowledge from him, which is by no means short. I am also deeply thankful to my committee member, Dr. Richard B. van Breemen for his help throughout the course of my graduate studies. The knowledge he has taught me in graduate courses, as well as many insightful suggestions on my research have been of incalculable value in this process. In addition, I'd like to express my gratitude to Dr. Joanna Burdette, Dr. Jonna Frasor and Dr. Brian Murphy for serving on my committee.

I have had the wonderful opportunity to work with a number of amazing collaborators on very interesting projects. I've had the pleasure of working closely with Dr. Raghupathi Neelarapu, Dr. Bhargava Karumudi, Dr. Subash Velaparthi, Dr. Michael Brunsteiner in Dr. Petukhov's lab on a variety of challenging drug discovery projects. Outside our lab, I appreciate the collaboration with Dr. Yongsoo Choi and Dr. Christopher Pennington, the post-doctoral researchers in Dr. van Breemen's lab, who are both very knowledgeable and intelligent. The dedication and talents of all my collaborators have contributed tremendously to the success of my Ph.D. project.

Over the years in Dr. Petukhov's lab, I was fortunate to be surrounded by brilliant colleagues who have been always willing to lend a hand when needed. In particular, I would like to give my special thanks to Dr. Boobalan Pachaiyappan who provided initial orientation when I joined the group and is a very good friend throughout and after my graduate career. I am also very grateful to Dr. Sylvie Y Blond, who spent a lot of time training me in cell biology and molecular

biology experimental skills. Additionally, my thanks would go to my past officemates at MBRB, where I spent almost all my time in the past five years. I have greatly enjoyed working with every single member in Dr. Petukhov's group and I feel proud to be one of this remarkable team.

Finally, my whole-hearted thanks go to my loving family. My wife, Wenli Wang, has made my Ph.D. journey not only possible, but also enjoyable by always giving her unconditional love, continuous encouragement and inexhaustible support. Without her by my side, I would not have come so far. I would like to sincerely thank my parents, Shirong He and Nanping Bai, for always believing in me, being proud of me and encouraging me whenever, wherever I needed.

HB

TABLE OF CONTENTS

CHAPTERS **PAGE**

TABLE OF CONTENTS (continued)

CHAPTERS **PAGE**

TABLE OF CONTENTS (continued)

CHAPTERS **PAGE**

LIST OF TABLES

TABLE **PAGE**

LIST OF FIGURES

FIGURE **PAGE**

LIST OF FIGURES (continued)

FIGURE **PAGE**

LIST OF FIGURES (continued)

FIGURE **PAGE**

LIST OF ABBREVIATIONS

ABPP	Activity-based protein profiling
ABPs	Activity-based probes
APL	Acute promyelocytic leukemia
BEProFL	Binding ensemble profiling with (f)photoaffinity labeling
BT	Biotin tag
CaMK	Ca^{2+}/calmodulin-dependent kinase
CAPRI	Critical Assessment of PRedicted Interactions
CoREST	Co-repressor for element-1-silencing transcription factor
DAD	Deacetylase activating domain
DMSO	Dimethyl sulfoxide
ECD	Electron capture dissaociation
ECL	Enhanced chemiluminescence
ETD	Electron transfer dissociation
Fluor-de-Lys	Fluorescent deacetylation of lysine
HATs	Histone acetyltransferases
HDACs	Histone deacetylases
HDLP	Histone deacetylase-like protein
HID	Histone interaction domain
HM	Homemade
HRP	Horseradish peroxidase
IT	Ion-Trap
LBT	Long biotin analog
LC-MS/MS	Liquid chromatography coupled with tandem mass spectrometry
MALDI	Matrix-assisted laser desporption ionization
MW	Molecular weight
NAD^+	Nicotinamine adenine dinucleotide
NCoR	Nuclear co-repressor
OPD	o-phenylenediamine
PBS-T	Phosphate buffer saline, supplemented with 0.05% Tween-20

LIST OF ABBREVIATIONS (continued)

pI	Isoelectric point
PML	Promyelocytic leukemia gene
PMSF	Phenylmethylsulfonyl fluoride
PTMs	Post-translational modifications
PVDF	Polyvinylidiene difluoride
RAR	Retinoic acid receptor gene
SAHA	Suberoylanilide hydroxamic acid
SAR	Structure-activity relationship
SBG	Surface binding group
Strep-HRP	Streptavidin-Horseradish Peroxidase
TBTA	tris((1-benzyl-1H-1,2,3-triazol-4-yl)methyl)amine
TCEP	Tris(2-carboxyethyl)phosphine
TFs	Transcription factors
ToF	Time-of-Flight
TSA	Trichostatin A
ZBG	Zinc binding group

SUMMARY

Histone deacetylases (HDACs) regulate chromatin structure and function. Since much of the literature has reported aberrant expression and recruitment of HDAC in malignant tissues, the role of HDACs in regulating the genes that are involved in cell cycle progression and arrest makes them attractive therapeutic targets for the treatment of cancer. Even though the pan-HDAC inhibitor showed promising antiproliferative activity, their application may be limited due to their toxicity and negative side-effects. To address this gap, design of isoform-selective HDAC inhibitors might be of significant importance for the treatment of cancer, making the knowledge of how inhibitors interact with HDACs and their binding mode crucial for isoform-specific inhibitor discovery. This study focused on investigating the interaction between HDAC probes and HDACs at the molecular level by using a combination of in vitro bioassays, immunoblotting, fluorescence spectroscopy, and protein mass spectrometry.

In Chapter 1, a brief introduction to HDACs and HDAC inhibitors was presented. First, the roles of HDACs play in gene transcription regulation were introduced, followed by the discussion of the classification and cellular distribution of HDACs in biological systems. It was noted that, due to the aberrant recruitment and expression of HDACs in tumor tissues, HDAC is recognized as an attractive therapeutic target for cancer treatment. Extensive research conducted in this field during the past few decades revealed promising antiproliferative activity of HDAC inhibitors, even though numerous side-effects such as fatigue, nausea, vomiting, diarrhea, and neutropenia have been associated with the use of pan-HDAC inhibitors. Thus, it is believed that the development of isoform-selective HDAC inhibitors would be a significant step in reducing the off-target effects of HDAC-based therapeutics. One of the key challenges in designing isoform-selective HDAC inhibitors is a poor understanding of the binding modes of

the HDAC inhibitors targeting the protein surface. As a part of the study presented here, the use of diazide-based photoaffinity labeling probes, liquid chromatography-tandem mass spectrometry, and molecular dynamic simulations was introduced for the first time to map the ensemble of the poses of HDAC inhibitors upon binding. We also discussed the strategy of using photolabeling as a tool to explore probe binding. The "click-chemistry" conditions with catalysis by Cu(I) generated *in situ* were used to attach a biotin tag (BT) to the adduct between HDAC and photoaffinity probes. By applying this method, photolabeling efficiency can be visualized with BT by Streptavidin-Horseradish Peroxidase (Strep-HRP) on western blot. The application of mass spectrometry to study the protein-probe and protein-protein interactions was described in the last section. In this way, the significance, methodology and scope of our study were discussed.

In Chapter 2, the process of HDAC8 protein purification and characterization was described, with respect to its activity and stability. Additionally, the assay conditions were optimized in order to accurately assess the potency of photolabeling probes. The results revealed that, when formulated in an appropriate buffer, the specific activity of "homemade" (HM) HDAC8 was higher than that measured for the commercially available HDAC8. The fluorometric assay was then developed and optimized. The established assay conditions were thus chosen for evaluating the inhibition potency of photoaffinity probes that were designed and synthesized as described in Chapter 3.

In Chapter 3, a Binding Ensemble Profiling with (F)photoaffinity Labeling (BEProFL) approach that utilizes photolabeling of HDAC8 with a probe containing a UV-activated

aromatic azide, mapping of the covalent modifications by liquid chromatography-tandem mass spectrometry, was described. The IC_{50} of the hydroxamic acid-based HDAC photoaffinity probes developed in Dr. Petukhov's laboratory was measured under the optimized assay conditions. The probes were confirmed to be potent inhibitors for HDAC3 and HDAC8 and other class I and class II HDAC isoforms, which was prerequisite to our photolabeling study. Non-ionic detergent was applied in the HDAC assay buffer to explore its impact on the possible aggregation of HDAC inhibitors, as this allows for separation of micelles. The tagging of the diazide photoaffinity probe attached to HDAC with BT resulted in a concentration-dependent increase in biotinylation of the protein as the concentration of the probe increased. The selectivity of the diazide probe for the active site of HDAC8 was demonstrated by blocking it with SAHA. MALDI-ToF mass spectrometry was utilized to examine the total mass of native HDAC protein and HDAC modified by different probes. The modified HDAC protein was further digested by trypsin and analyzed by FT-ICR mass spectrometry in order to identify the sites where modifications occurred. Upon computational modeling analysis, two distinct binding poses of the HDAC8 probe were identified. The data also suggest that an "upside-down" pose with the surface binding group of the probe bound in an alternative pocket near the catalytic site may contribute to the binding. The photolabeling methodology is therefore proved a suitable method for investigating the probe-binding pose to HDAC8.

In Chapter 4, the interactions between HDAC3 and its co-repressor NCoR2 were explored by applying photolabeling technique. The binding of probe to HDAC3 active site at the time of photoactivation was demonstrated through competitive binding of diazide probe and SAHA. On the other hand, binding to the NCoR2-DAD can occur only if the NCoR2-DAD is positioned in

proximity of the UV-activated nitrene moiety of the diazide probe bound to HDAC3. In order to test this hypothesis, potent HDAC diazide probe was incubated with NCoR2-DAD only and inactive diazide probe that lacks a hydroxamate portion to form the metal-probe complex with HDAC active site was incubated with HDAC3/NCoR2-DAD. The results showed that, in absence of HDAC3, the potent diazide probe does not react in a dose-dependent manner with NCoR2, and that inactive diazide probe reacts, albeit weakly, with NCoR2-DAD but not with HDAC3 at the higher molar ratio investigated. Thus, it is concluded that the diazide probe was able to photocrosslink to both HDAC3 and NCoR2-DAD, indicating the presence of NCoR2 in proximity of HDAC3 active site. Selective modification of both HDAC3 and NCoR2-DAD by the photoaffinity probe was further confirmed using MALDI-ToF mass spectrometry. Modification of HDAC3/NCoR2-DAD by the photoaffinity probe was observed using MALDI mass spectrometry as a dose-dependent increase in protein mass. After confirming that significant covalent modification of the HDAC3/NCoR2-DAD complex occurs in the experimental conditions chosen for this study, in order to locate modification sites of HDAC3 and NCoR2-DAD by the photoaffinity probe, a tryptic digestion and peptide mapping was performed using microcapillary HPLC coupled with an FTICR mass spectrometer. MassMatrix proteomics data analysis software was used to identify modified peptides and, as a result, one HDAC3 tryptic peptide (amino acids 283 to 300) and two NCoR2-DAD tryptic peptides (amino acids 407 to 424 and 444 to 461) were found to be modified by the photoaffinity diazide probe at an equimolar protein/probe ratio. With the help of computational modeling performed by Dr. Michael Brunsteiner, structural information on the type of interaction between HDAC3 and NCoR2-DAD was obtained. Therefore, the concept of small photoreactive “nanorulers” was

proposed, whereby these entities target both HDAC3 catalytic site and the surface regions in NCoR2-DAD, most likely involved in the protein-protein interaction and a structural model that delineates some of the contact residues was developed.

The photolabeling research described in Chapters 3 and 4 revealed that the HDAC inhibitory potency of the photoaffinity probe did not correlate with its photolabeling efficiency. In other words, some photoaffinity probes, despite being potent HDAC inhibitors exhibited poor photolabeling outcome. Although the potency of inhibitor is usually the main criterion to evaluate photoaffinity probes, several research groups reported that the photolabeling signal could not be solely ascribed to potency in protein binding. Finally, the last chapter describes a series of experiments conducted in order to explore the factors affecting the photoaffinity labeling outcomes. Three diazide probes with different scaffolds, namely regular aromatic ring, isoxazole-, and pyrozole-, were compared for their inhibitory potency against HDAC3 and HDAC8. All probes showed promising HDAC inhibiting activity at the micro- and nanomolar level. In particular, probe **3** inhibited HDAC8 and HDAC3 with the lowest potency, and HD-55 exhibited the highest potency inhibiting HDAC8, whereas HD-74 was the most active inhibitor for HDAC3. A comparison of V_{max} and K_m obtained in the presence or absence of all the diazide probes showed only a marginal difference in the values of the parameters indicating competitive inhibition for HDACs. The reactivity/specificity of the photoreactive group on different probes was evaluated by IT-TOF mass spectrometry. In the chromatogram, multiple peaks with same MW of photoactivation product were identified at different retention times, suggesting that several reactive intermediates were generated during photo-irradiation.

The effects of non-ionic detergent on the aggregation of probes/tags were also evaluated. After the introduction of non-ionic detergent, the background noise levels decreased and the photolabeling signal intensity increased in a dose-dependent manner as probe concentration was raised. Accessibility of the reactive groups for click chemistry ligation was confirmed by varying the length of the linker group of photoaffinity probes. Similar to the accessibility study for click chemistry ligation, the availability of the biotin tag to Strep-HRP was explored through the application of a longer biotin tag. As a result, in comparison with a regular biotin tag, weaker photolabeling signal intensity was observed when visualized by a longer biotin tag, which may be ascribed to unfavorable orientation of tags, higher activation energy and the effect of steric hindrance during the click chemistry ligation.

CHAPTER 1 BACKGROUND AND INTRODUCTION

1.1 Histone Deacetylase

Histone deacetylases (HDACs) and histone acetyl-transferases (HATs) are enzymes that regulate chromatin structure and function through removal or addition of acetyl group from lysine residue on N terminal of histone of nucleosome core.[1] Histones are nuclear proteins wrapped with DNA to form nucleosomes. The structure of histones is critical for both packaging of DNA and regulation of transcription in chromosomes. Among post-translational modifications (PTMs), histone acetylation and deacetylation play an important role in transcription regulation of eukaryotic cells. Since the identification and characterization of the first histone deacetylases by Taunton,[2] 18 HDACs have been identified and classified based on homology to yeast HDACs. The increase of histone deacetylation is usually associated with transcriptional repression. Elevated expression levels of HDACs in malignant tissues suggest its association with cancer.

1.1.1. Histone, nucleosome, chromatin and chromosome

Histones are proteins found in eukaryotic cell nuclei. Among the five major families of histones- H1/H5, H2A, H2B, H3 and H4,[3] H2A, H2B, H3 and H4 are known as the core histones to form one histone octamer, whereas histones H1 and H5 function as the linker histones. The basic unit of eukaryotic chromatin, the nucleosome, consisting of 146 pairs of DNA helix wrapped around an histone octamer.[4] Due to the presence of primary amines as a part of lysines on histone proteins, the isoelectric point (pI) of core

histones is very high and ranges from 9.8 to 10.25.[5] Under physiological condition, the amino groups on lysines of histones are positively charged, resulting in tight binding of histones to negatively charged DNA.

Nucleosome forms the fundamental repeating units of eukaryotic chromatin, which is used to package DNA into smaller volume in the cell, to control gene expression and DNA replication. Core histones wrapped with DNA construct chromosomes through a series of folding process into higher order of structure.

1.1.2. Histone deacetylase, histone acetyltransferase and transcription regulation

One of the best characterized post-translational modifications - histone acetylation and deacetylation - is thought to modulate the accessibility of transcription factors to their respective nucleosomal DNA. These processes are a part of epigenetic regulation of gene expression machinery.[6] The ε-amino groups of lysine residues in the N-terminal tails of core histones (H2A, H2B, H3 and H4) that protrude from the nucleosome are shown to be substrates for HATs and HDACs. Acetylation of the amino groups on lysine residues neutralizes the positive charge on histone proteins and leads to the weaker electrostatic interactions between the histone protein and the negatively-charged DNA. The overall acetylation status of histones is determined by the dynamic equilibrium of HAT and HDAC catalyzed acetylation and deacetylation, respectively.[7, 8] In general, histone hyperacetylation is associated with an open chromatin structure and better accessibility for transcription factors, whereas histone deacetylation promotes chromatin condensation and transcriptional repression (Figure 1).[9] In addition, many non-histone proteins such as hormone receptors, transcription factors, chaperone proteins, and

cytoskeleton proteins regulating cell proliferation and cell cycle arrest are shown to be substrates for HATs and HDACs.[10]

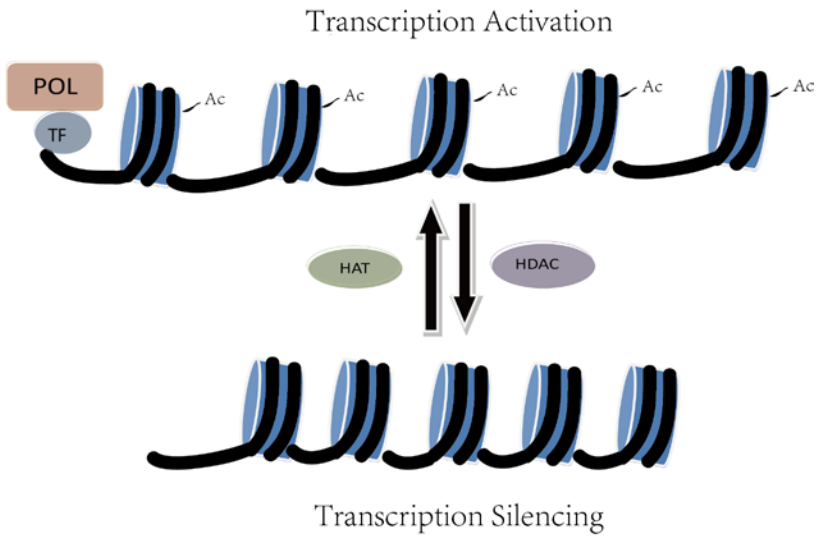

Figure 1: Regulation of chromatin condensation and gene transcription by histone acetylation and deacetylation.

Histone acetylation by HAT results in an open chromatin structure that allows binding of transcription factors and RNA polymerase and promotes gene transcription as a consequence. Upon histone deacetylation, the accessibility of nucleosomal DNA for transcription factors decreased, leading to transcriptional silencing.

1.1.3. HDAC Isoforms Distribution

The 18 human HDAC isoforms are subdivided into four classes based on their homology to yeast analogs.[11] The class I (HDAC1, 2, 3, 8), class II (HDAC4, 5, 6, 7, 9, 10) and class IV (HDAC11) are Zn^{2+} dependent metalloproteins, whereas class III (Sirt1

2, 3, 4, 5, 6, 7) (which will not be discussed further in this dissertation) requires nicotinamine adenine dinucleotide (NAD^+) as cofactor to regulate gene expression.[12] The class I, II, III HDAC proteins are homologous to yeast HDAC Rpd3, Hda1, and Sir2, respectively.

Class I HDACs are ubiquitously expressed and generally reside in nucleus, class II and III HDACs are expressed only in certain types of tissues and may shuttle between cytoplasm and nucleus with the help of Ca^{2+}/calmodulin-dependent kinase (CaMK).[13] The general distribution of HDAC isoforms can be found in TABLE I.

TABLE I: CLASSIFICATION AND DISTRIBUTION OF HDAC ISOFORMS

Class	**Members**	**Catalytic Domain**	**subcellular localization**	**Tissue distribution**
I	HDAC1	1	Nucleus	Ubiquitous
	HDAC2	1	Nucleus	Ubiquitous
	HDAC3	1	Nucleus	Ubiquitous
	HDAC8	1	Nucleus	Ubiquitous
IIA	HDAC4	1	Nucleus/cytoplasm	Tissue restricted
	HDAC5	1	Nucleus/cytoplasm	Tissue restricted
	HDAC7	1	Nucleus/cytoplasm	Tissue restricted
	HDAC9	1	Nucleus/cytoplasm	Tissue restricted
IIB	HDAC6	2	Mostly cytoplasm	Tissue restricted
	HDAC10	2*	Mostly cytoplasm	Tissue restricted
III	SIRT1-7	-	Nucleus/Cytoplasm/Mitochondrial	-
IV	HDAC11	2	Nucleus/cytoplasm	Tissue restricted

*: One active catalytic domain, one inactive domain.

1.1.4. Research Significance

1.1.4.1. Histone Deacetylase, Cancer and HDAC inhibitors

The deacetylation on lysine residues of histones recovers the positive charge, strengthens the electrostatic interaction, leads to a compact chromatin structure and precludes the access of transcription factors to their DNA binding site and represses cellular differentiation, apoptosis and cell cycle arrest. The current data indicated that there is more than one mechanism of how HDAC function in the progression of cancer. HDACs can be recruited to their target promoters through the interaction with fusion proteins and repress the transcription of the tumor suppressors, cell cycle inhibitors, differentiation factors and apoptosis inducers.[14] An example of this model is acute promyelocytic leukemia (APL). The fusion of promyelocytic leukemia gene (PML) and retinoic acid receptor gene (RAR) creates a hybrid protein which recruits HDAC with high affinity. This product can hinder the binding of retinoic acid, and repress the expression of genes which regulate the normal differentiation and proliferation of myeloid cells.[15] On the other hand, elevated expression level of certain HDAC had also been reported in different tumor types (Table II). For example, overexpression of HDAC1 was observed in gastric[16], prostate[17], colon,[18] and breast cancers.[19] High level expression of HDAC2 was reported in cervical[20] and gastric cancers.[21],[22] The transcriptional repression of tumor-suppressor genes by overexpression and abnormal recruitment of HDACs to their promoter region could be the common cause for tumor initiation and progression. The cyclin-dependent kinase inhibitor $p21^{WAF1}$ which inhibits cell-cycle progression serves as ideal example. The $p21^{WAF1}$ was found epigenetically inactivated by hypoacetylation of the promoter and

thus failed to express in some tumors. The treatment with HDAC inhibitors has been shown to be efficacious not only stopping the growth of tumor-cell, but also boosting both the acetylation of the promoter and gene expression.[23]

TABLE II: RELEVANCE OF HDACS TO CANCER

Group	Relevance to cancer	Expression in tumor
Class I		
HDAC1	Possible prognostic indicator for lung and breast cancers. Overexpressed in prostate cancers (hormone-refractory), gastric, colorectal	++
HDAC2	Overexpressed in colorectal and gastric cancers. Loss of antigen presenting cells in colorectal cancers gave HDAC2 over expression	++
HDAC3	Overexpressed in lung cancer and several solid tumors.	++
HDAC8	Knock down inhibits cell growth in several human tumor cells	++
Class IV		
HDAC11	Unknown	
Class II		
HDAC4	Unknown	++
HDAC5	Down regulated in colon cancer and acute myeloid leukemia	−−
HDAC6	Ambiguous prognostic in breast cancer	
HDAC7	Unknown	
HDAC9	Unknown	
HDAC10	Unknown	

++ indicates an overexpression in tumor, −− indicates a reduced expression.

It was demonstrated that HDAC inhibitors are able to induce growth arrest, activation of apoptotic pathways, cell death and senescence.[7] According to Dokmanovic et al., the HDAC inhibitors can be roughly categorized into four groups based on their similarity in structure: aliphatic acid, hydroxamates, benzamides and cyclic peptides.[24] The structures are given in Table III.

TABLE III: CLASSIFICATION OF HDAC INHIBITORS BASED ON THEIR STRUCTURES [11, 24]

Compound	Representative Examples	HDAC target	Potency (cells)
Aliphatic acids 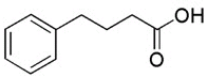	Sodium butyrate	Class I, IIa	mM
	Valproate (VP-101)	Class I, IIa	mM
	Phenylbutyrate	Class I, IIa	mM
	Baceca	Class I	NA
Benzamides 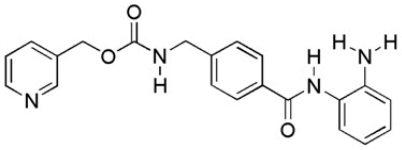	MS-275	HDAC1,2,3	μM
	CI-991	HDAC1,3	μM
	MGCD0103	Class I	NA
Hydroxamates 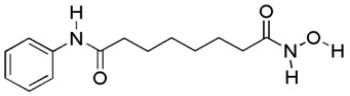	SAHA	Class I, II	μM
	LBH589	Class I, II	nM
	PXD101	Class I, II	μM
	ITF2357	Class I, II	nM
	PCI-24781	Class I, II	NA
Cyclic peptides 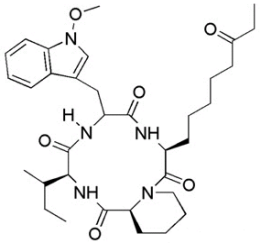	FK228	HDAC1,2	nM
	Trapoxin	Class I, IIa	nM
	Apicidin	Class I	nM
	CHAP1	Class I, IIa	nM

Apart from SAHA (Vorinostat) and Romidepsin which are already approved by FDA, a number of HDAC inhibitors are currently undergoing clinical trials as anticancer drugs[25-27]. Most of the nonselective HDAC inhibitors being investigated in clinical trials show promising efficacy against leukemia and solid tumors.[25, 27, 28] However, numerous side effects are also observed, including bone marrow depression, diarrhea, weight loss, taste disturbances, electrolyte changes, disordered clotting, fatigue and

cardiac arrhythmias.[29, 30] Since HDACs are diversely implied in various cancer progression and other diseases, the expression and localization differ significantly between isoforms. It is hypothesized that depending on isoform selectivity HDAC probes can be either cytotoxic or neuroprotective.[31] Therefore, identifying specific biomarkers to maximize patient therapies and reduce side-effect is an emerging area. The development of isoform-selective HDAC inhibitors would be a significant step in reducing off-target effects of HDAC-based therapeutics.

Class I HDACs are generally considered as the most relevant targets for cancer therapy because class I HDAC inhibitors usually show strong anti-proliferative and apoptosis-inducing activity.[30, 32] High level of HDAC 1, 2 and 3 is usually associated with poor prognosis in most gastric, prostate and colorectal cancer samples.[33-36] The over-expression of HDAC8 is correlated with advanced disease stage, clinical and genetic risk factors and poor long term survival in childhood neuroblastoma.[37] Unlike HDAC1, 2 and 3 which form a multi-protein complex to function, HDAC8 has not been found to be a component of any co-repressor complex so far. In this thesis, I will focus on HDAC8 and HDAC3 as representatives of class I HDAC in isoform-selective drug discovery.

1.1.4.2. Histone Deacetylases and their co-repressors

Most HDACs act via the formation of large multiprotein deacetylase complexes. The HDACs may require other DNA binding proteins to achieve optimal enzymatic activity. It has been reported that the HDACs interact with co-repressors such as silencing mediator for retinoid and thyroid (SMRT) receptor, nuclear co-repressor (NCoR)[38, 39] , corepressor for element-1-silencing transcription factor (CoREST), nucleosome

remodeling and histone deacetylation (NuRD) and SIN3a. This complex is recruited to a variety of transcription factors (TFs).[40] For example, HDAC3 requires an interaction with SMRT/NCoR for its deacetylation activity.[41] Feed-forward model of how the match between HDAC3 substrate specificity and NCoR/SMRT histone-binding preference serves to stabilize the repression complex. Nuclear receptor (NR) recruitment of HDAC3 by means of NCoR/SMRT favors deacetylation of H4 K5, leading to increased chromatin association of NCoR/SMRT, and thereby enhancing deacetylation and maintaining the repressed state. Therefore, we can interrupt the interaction between HDACs and their protein partners such as SMRT, NCoR, CoREST to inhibit the HDAC enzyme activity, which makes these co-repressors potential targets for isoform-selective HDAC inhibition.

1.1.4.3. HDAC substrates and mechanism of histone deacetylation

Over the past decade, studies have revealed that histones are not the only targets of deacetylation as many non-histone proteins involved in transcription, nuclear transport, cytoskeleton and signal transduction are known to be HDAC substrates (Table IV).[11, 25, 28, 42-45] The findings from recent structural studies of histone deacetylases are critical to study substrate recognition. Understanding the catalytic reaction and enzyme-substrate interactions can facilitate the design of HDAC inhibitors in return.[46-48]

TABLE IV: ACETYLATED PROTEIN SUBSTRATES OF HDACS

Function	**Proteins**
Histones	H2a, H2b, H3, H4
DNA binding transcriptional factors	p53, c-Myc, AML1, BLC-6, E2F1, E2F2, E2F3, Ying Yang 1 (YY1), MEF2, CREB, IRF-2, SRY, EKLF
Steroid receptors	Androgen receptor, estrogen receptor α, glucocorticoid receptor
Transcription coregulators	Rb, DEK, MSL-3, CtBP2, PGC-1α
Nuclear import	Rch1, importin-α7
Chaperone protein	HSP90
Cytoskeleton protein	α-Tubulin
Viral proteins	E1A, L-HDAg, S-HDAg, T antigen, HIV Tat

As a pioneer in HDAC research, Finn et al. developed an X-ray structure of *Aquifex aeolicus* HDAC homologue- HDLP (35.2% identity with HDAC1), as a complex with two inhibitors, (R)-TSA and SAHA.[49] For the first time, the authors also provided a detailed mechanism of deacetylation reactions based on the crystal structures (Figure 2).[49]

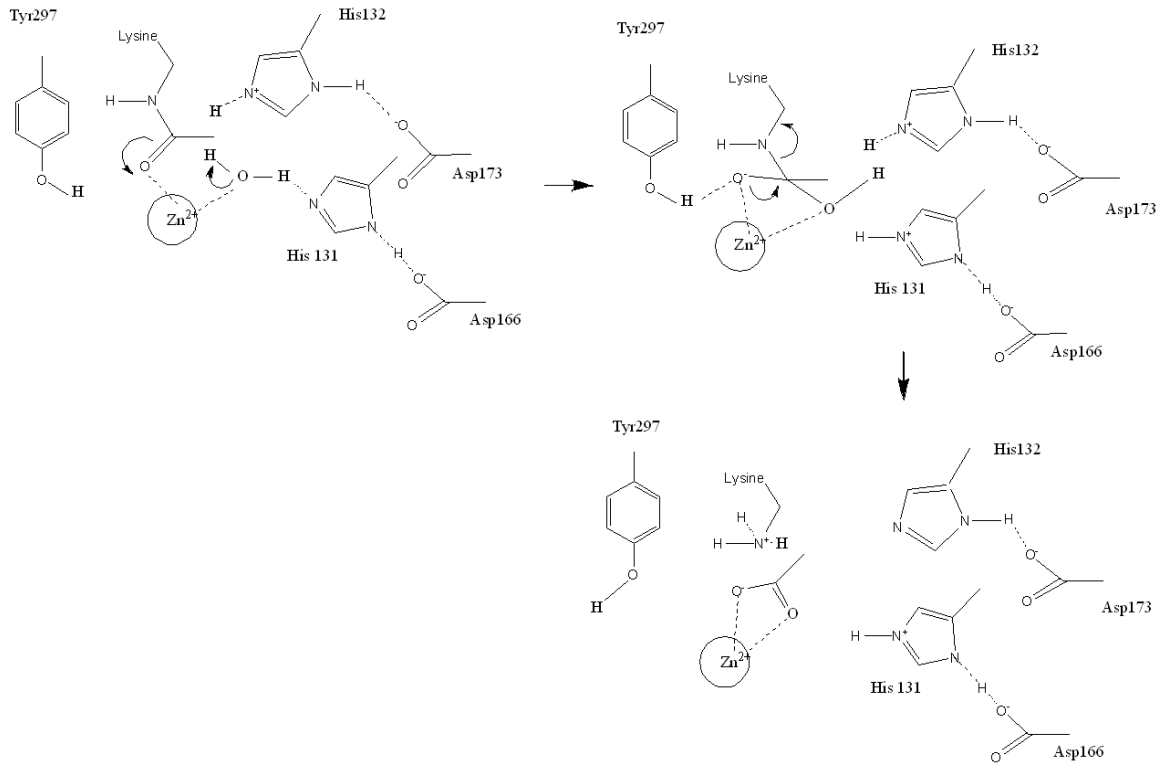

Figure 2: Proposed mechanism for histone deacetylation

The carbonyl oxygen of the N-acetylamide is thought to coordinate to and be activated by the zinc cation in HDAC active site. The activated carbon of carbonyl group undergoes nucleophilic attack by a water molecule nearby. The nucleophilicity of the water molecule, in turn, could be enhanced by an interaction with the negative charge of the buried Asp166-His131 charge-relay system. The attack of the water molecule on the carbonyl carbon would produce an oxy-anion intermediate, stabilized by the zinc ion and hydrogen bond to Tyr297. The collapse of this intermediate would result in cleavage of the carbon-nitrogen bond, with the nitrogen accepting a proton from the His132 residue, and would thereby produce the observed acetate and lysine products.[50]

1.2 Activity Based Protein Profiling and Photolabeling

In the study of proteins function and their interactions with other macromolecules or small probes, the activity-based protein profiling (ABPP)[51, 52] became an attractive strategy in recent years. ABPP makes use of relatively small molecules to label a specific enzyme in its active state. Therefore, the application of ABPP is based on the enzyme's activity rather than its expression level. Considering the high abundance of inactive proenzymes expressed in biological system, ABPP strategy is especially well suited for mechanism-based biomarker identification and characterization.[53] Here in this section we will discuss ABPP studies, with specific focus on the implementation of photoreactive probes.

1.2.1. General aspects of activity based protein profiling

The ABPP utilizes small organic molecules to label the active sites of a specific enzyme. The molecules used are called activity-based probes (ABPs) which usually are consist of three major parts.[54] The recognition moiety is designed to mimic the structural and functional motif of natural substrate of the target enzyme. It directs the ABP to the target enzyme and establishes a covalent bond between the ABP and enzyme. A reporter group (tag) which allows visualization or purification of the bound enzyme is connected to the recognition moiety through linker group. The most widely used tags are radioactive labels, epitope tags, fluorophores and biotin, of which the latter can serve for purposes of both visualization and purification (Figure 3, top). In some circumstances, the bulky size of reporter group may interfere with the interaction between ABP and enzyme or significantly lower the ability to cross cell membrane, which is of special

interest for labeling living cells. An alternative 2-step labeling approach is therefore developed. In this approach, the reporter group of ABP is replaced by a ligation handle, where the reporter group will be attached after the enzyme has been captured (Figure 3, bottom).[52]

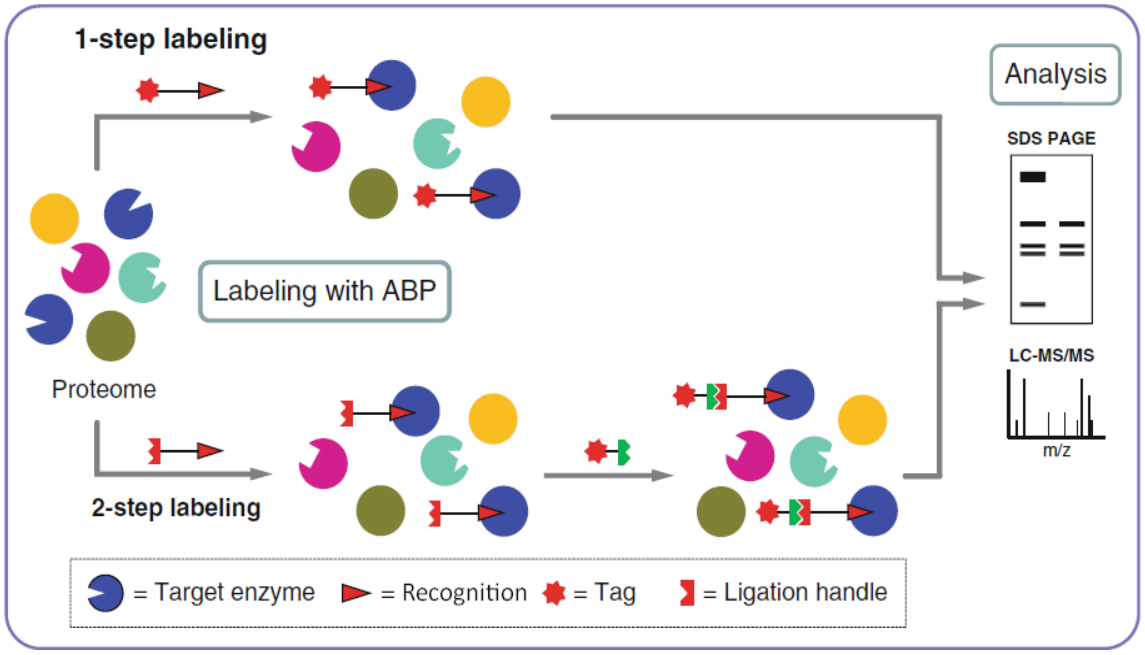

Figure 3: The mechanism of ABPP[54]

In the ABPP approach shown in Figure 3, the ABP recognition group is designed to react with the nucleophilic residues in the active site of target enzyme to form a covalent bond.[55-58] However, for enzymes that do not rely on nucleophilic residue in their active site such as metalloproteases, histone deacetylases (HDACs) and kinases, the application of ABP approach is limited. The photoaffinity labeling (PAL) utilizing affinity based probe (AfBP) is developed as an alternative for ABP.[59] In this approach, AfBP noncovalently binds the target enzyme through electrostatic or hydrophobic

interactions, and forms an irreversible covalent bond to the enzyme via a photoreactive group upon activation by light (Figure 4).

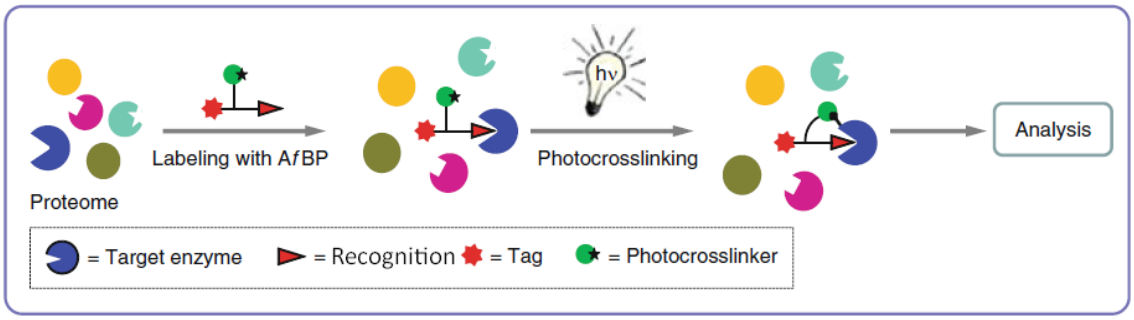

Figure 4: Basic principle of photoaffinity labeling (PAL)[54]

1.2.2. Photoaffinity labeling and photoaffinity probes

The prevalent application of photoaffinity labeling can be attributed to two key advantages they possessed over conventional approaches. The first resides in the appropriate chemical stability of photoreactive moiety in the absence of light, which permits them to be targeted to the specified compartment or component prior to activation. The second one results from the exceptional reactivity of intermediates upon photo-irradiation, and their ability to attack a broad range of functional groups of biomolecules nearby.[60] Since the first use of PAL in enzyme modifications was first described in 1962,[61] numerous research on the development of new PAL reagents has been reported.[62-64] Among AfBPs developed for PAL, aryl azides, diazirines and benzophenones are widely used nowadays.

Aryl azides are perhaps the most widely used because of its universality, reactivity, and relative simplicity in implementation.[65] Upon activation of an aryl azide (**1**, Figure 5) by UV irradiation, molecular nitrogen is released and a singlet nitrene (**2**) is formed. The singlet nitrene is highly energetic and is quickly converted into triplet nitrene (**3**) via intersystem crossing,[66] or it can undergo rearrangement into the corresponding benzazirine (**10, 11**). The singlet acts as electrophiles and inserts into C-H bond directly to give (**6**), whereas triplet nitrene undergo a two-step reaction which first abstracts a hydrogen radical from a nearby C-H followed by coupling to the formed carbon radical. Noteworthy, the product of this two different reaction mechanism is the same (**6**). The triplet phenyl nitrene tends to form dimer – azobenzene (**8**). The benzazirine (**10, 11**) and its rearrangement product dehydroazepine (a.k.a kentenimine) (**13, 14**) are long-lived electrophiles which can react with nucleophile to yield compound **15** and **16**, respectively.[66, 67] Therefore, the reaction of kentenimine and the side chains of nucleophilic amino acids is the dominating reaction when aryl azide is used for PAL with protein. For side reactions, the aryl azides can be reduced to amine (**5**) in the presence of dithiols such as dithiothreitol,[68] triplet nitrene can be oxidized to corresponding nitro species (**4**) by oxygen gas. The relative small size of aryl azide, the flexibility to incorporate them into natural biological surroundings and its relative ease of preparation render it great popularity in PAL studies.

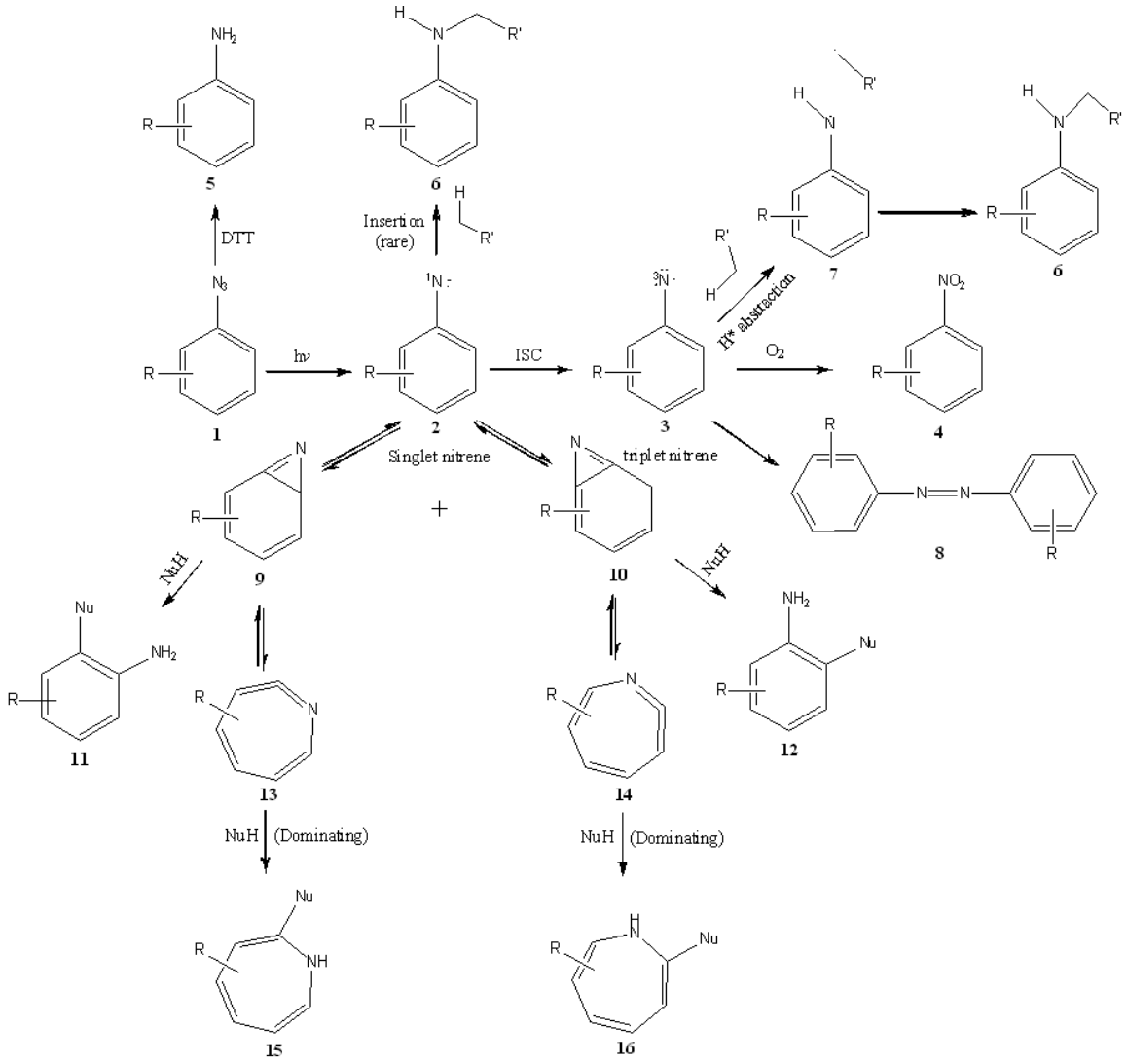

Figure 5: Possible reaction mechanism of aryl azides after photolysis

One of the major advantages of the photoreactive diazirine group over aryl azides is that the wavelength used to activate it ranges from 350-380 nm. This is much higher than 300 nm limit and therefore, it causes no damage to biological systems. The singlet carbene generated upon activation of diazirine also undergo intersystem crossing to form triplet carbene. The singlet and triplet carbenes display a similar behavior compared to their nitrene counterparts. A singlet carbene can react as an electrophile, nucleophile or ambiphile while triplet carbenes behave like diradicals. The formation of non-reactive

diazo species after photolysis and complicate synthesis of diazirine restrict the application of diazirine in PAL.

Similar to diazirines, benzophenone can be excited at wavelength of 350-360 nm. The absorption of a photon of the proper wavelength by a benzophenone results in the formation of a triplet state benzhydril diradial. The diradical can be inserted into a nearby X-H bond through H abstraction and recombination. A big advantage of benzophenone group is that its photoactivated product is more reactive towards C-H bonds compared to nitrenes, and is less prone to intramolecular rearrangements than carbenes. At the mean time, the water adduct of benzophenone diradical dehydrates quickly and forms ketone again, which can be recycled to form diradical through irradiation. Therefore, the overall crosslink efficiency of benzophenones is higher than the other two moieties described above. On the other hand, the relative bulky size of benzophenone may have negative impact on the interaction between enzyme and substrate. The resulting steric hindrance can give rise to discrimination between reaction sites and lead to biased labeling.

Due to the different activation mechanisms, it is not surprising that the outcome of a photolabeling experiment heavily depend on the type of photoaffinity probe applied. In the study Weber and Beck-Sinckinger conducted to compare the photochemical behavior of different photophores,[69] they found the conversion and product formation of both the diazirine and aryl azide were much faster than benzophenone. Diazirine gave a relatively pure solvent adduct product whereas aryl azide yielded numerous unidentified products that may arising from intramolecular rearrangements and insertion reactions.

Balancing between cost, flexibility, simplicity and implementation of photolabeling experiment, aryl azide was adopted in this study.

1.3 Click-Chemistry

Ligation reaction is needed in two-step ABPP to connect the reporter group to the ligation handle of AfBP after the enzyme was captured. The Staudinger-Bertozzi ligation,[70] the Cu(I)-catalyzed[71, 72] and copper-free click reaction,[73, 74] and photoclick reaction[75] are commonly used (Figure 6). One of the recent advances in the photoaffinity labeling probe development is application of "click-chemistry" and bioorthogonal probes for activity-based proteomics profiling by Cravatt et al[72, 76-81] Click chemistry is a modular approach utilizing a few highly reliable and refined chemical transformations for organic synthesis.[82] A typical click reaction should be easy to perform with high yields. Additionally, the reaction should be oxygen and water tolerant, using only readily available reagents, and requiring minimum product isolation. The energy-favored nature of transformation drives a spontaneous and irreversible linkage reaction between building blocks. The click-chemistry is applied widely in the drug discovery, including lead identification, combinatorial chemistry, and proteomics/DNA research through bioconjugation reactions.[82] Among different click reactions (Figure 6), Huisgen's 1,3-dipolar cycloaddition of alkynes and azides yielding triazoles is the most commonly used (Figure 7).[83]

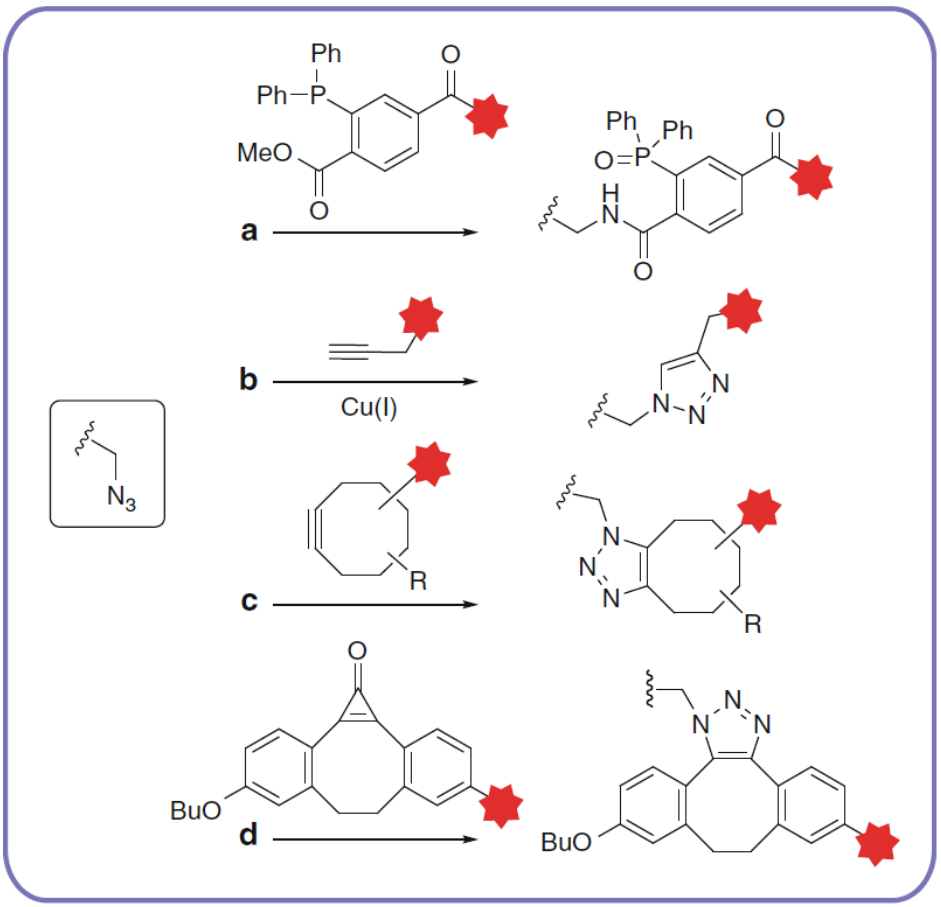

Figure 6: Ligation reaction used in two-step ABPP[54]
(a) Staudinger-Bertozzi ligation, (b) Cu(I)-catalyzed click reaction, (c) copper-free click reaction, (d) photoclick reaction

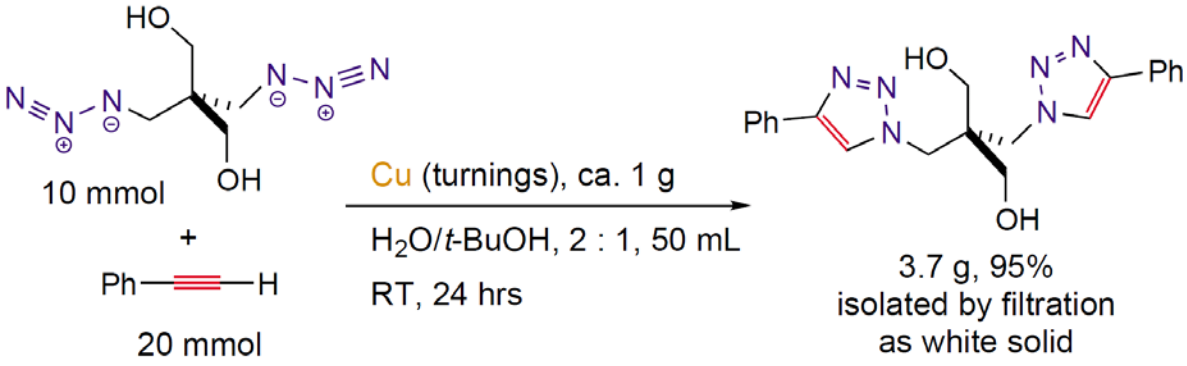

Figure 7: The coupling of azides and terminal acetylenes catalyzed by Cu(I) creates 1,4-di-substituted 1,2,3-triazole linkages, which are not susceptible to cleavage.[71]

1.4 Protein Mass Spectrometry and Proteomics

Proteomics has emerged as an experimental approach to study global gene expression profiles at the protein level. In general, proteomics involves protein identification, protein characterization and quantitative proteomics in biological systems.[84] It addresses the following questions: what proteins are there or not there? What are the post-translational modifications that are different in state 1 versus state 2? How much of a change in protein amount is there between state 1 and state 2? Mass spectrometry is a powerful tool to help us answer above questions.

Mass spectrometry based proteomics can be categorized into two methods: top-down proteomics and bottom-up proteomics. In top-down proteomics, the protein identification (protein ID) and characterization are carried out in the form of intact-protein analysis. On the other hand, enzymatically or chemically generated peptides were targets of interest for bottom-up proteomics. The two strategies are complementary, each with its pros and cons (Figure 8).[85, 86] The bottom-up approach (shotgun proteomics) involves direct digestion of a biological sample using a proteolytic enzyme that cleaves at well-defined sites to create a complex peptide mixture. The digested samples are then separated and analyzed on liquid chromatography coupled to tandem mass spectrometry for protein ID and characterization.[86] The main advantage of bottom-up strategy is the ability to achieve high-resolution separations and comprehensive coverage of proteins with limited samples. Therefore, it has been proven successful for the profiling and identification of proteins. However, due to the great complexity of generated peptides mixture, all methods using the bottom-up approach require the use of instrumentation with high

sensitivity and resolution. Information may lost for small peptides lack proper proteolytic cleavage sites, peptides with unexpected modifications and the ones present at low abundance.

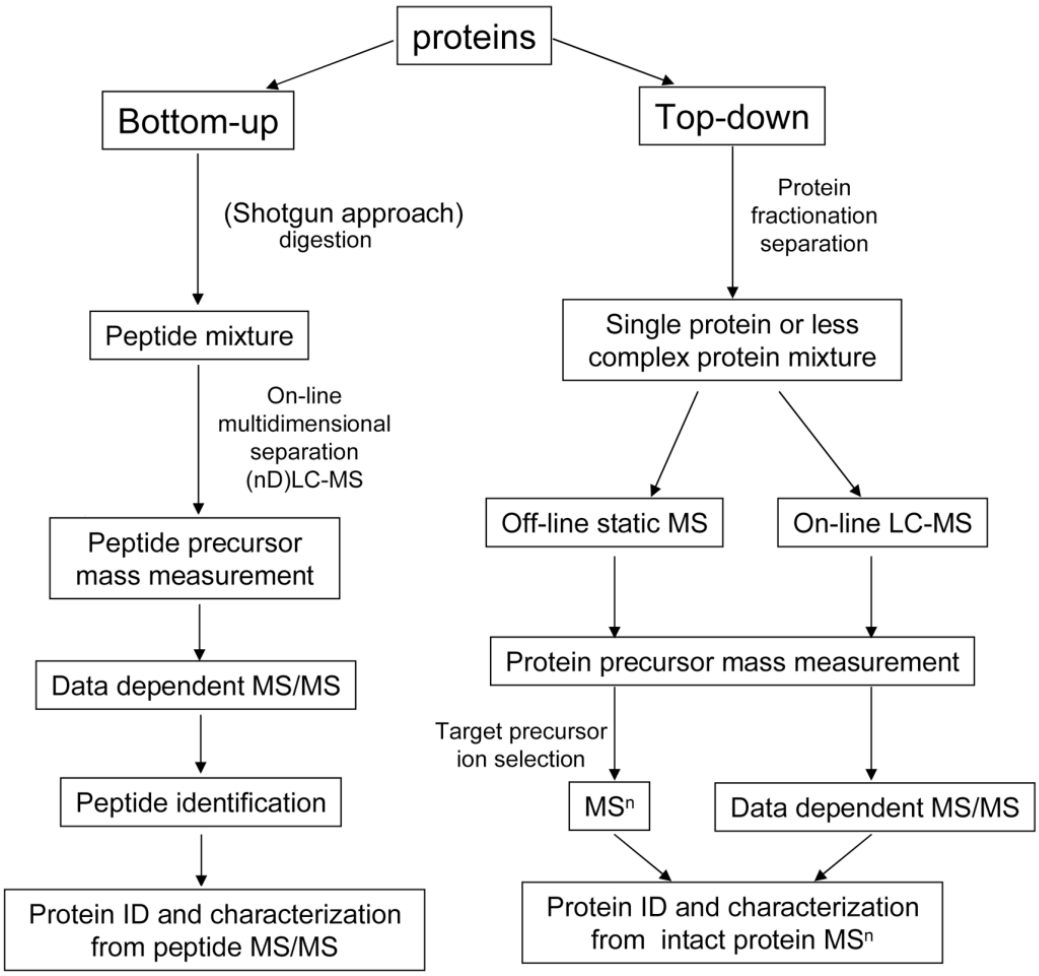

Figure 8: Strategies for MS based protein identification and characterization.

In the top-down approach, proteins in mixture are fractionated and separated into pure protein or less complex protein mixtures, followed by off-line static infusion into the mass spectrometer for intact protein mass measurement and fragmentation. In rare cases,

on-line LC-MS strategy can also be used for large scale protein analysis. The strength of top-down approaches lies in direct detection of the native molecular mass of biological protein species. Top-down proteomic strategies have demonstrated 100% protein sequence coverage and allowed for the identification of protein isoforms, proteolytic processing events and post translational modifications (PTMs).[85] Nevertheless, top-down proteomic approaches suffer from limited sensitivity and throughput.[87, 88] Although the fragmentation of small to midsize intact proteins is greatly enhanced by the development of electron capture dissociation (ECD) and electron transfer dissociation (ETD) [89-95], large proteins could not be easily analyzed due to the increasing complexity of the gas-phase protein ion's tertiary structure with many non-covalent interactions.[86] Also, since top-down proteomic is performed with direct infusion of single protein separated off-line, the analytical throughput and efficiency for large-scale proteome analysis is limited.

1.5 Scope of the current study

In recent years, it has been widely accepted that HDACs are promising targets for epigenetically treatment of aberrant regulation of gene transcription, [96, 97] which serves as hallmark of cancer. The therapeutic application of HDAC inhibitors is believed to depend on their HDAC class and isoform selectivity profile,[98, 99] making development of isoform selective inhibitors an important issue in the design and development of novel HDAC-based therapeutics. One of the key challenges in HDAC inhibitor design is the limited amount of information regarding the binding modes

available to the highly solvent exposed surface binding groups (SBG) of HDAC inhibitors.

In the present study, in order to address this problem, we utilized a diazide photoaffinity probe to map experimentally the multiple binding poses of the SBGs of HDAC. The method requires availability of the active HDAC probe containing a photoreactive group, which can covalently crosslink to the protein of interest upon UV-irradiation, and an aliphatic azide group, which can be attached by a biotin tag through click-chemistry cycloaddition for future purification and visualization. Protein mass spectrometry was applied synergistically with molecular dynamics simulations to identify and map the ensemble of the poses of HDAC inhibitors upon binding. Therefore, the enzymatic active HDAC protein and photoaffinity probe as potent HDAC inhibitor were prerequisite to the study.

CHAPTER 2 PROTEIN PURIFICATION AND ENZYME KINETICS STUDY ON HDAC3/8

2.1 Introduction

2.1.1 HDAC expression and purification in different systems

E.coli is the most commonly used system for the expression and purification of recombinant protein. Because bacteria grow much faster than insect cells, mammalian cells, or yeasts, high amounts of recombinant proteins can be produced faster than in those eukaryotic production systems. The major drawback of the bacteria-expressing system is its lack of ability to produce proteins that require PTMs for function, stability, or folding. The eukaryotic-expressing systems, such as yeast, baculovirus/insect cells or mammalian cells are therefore applied instead. Although several potential post-translational modification sites were identified on HDAC8,[100, 101] bacteria-expressed HDAC8 was still enzymatically active.[102] In contrast, all other Class I and II HDACs produced in E.coli displayed very little enzymatic activity due to the lack of PTMs. When no PTMs are required, the expression of recombinant protein in E.coli is a preferred choice, when the final application requires large quantities of pure proteins such as in-vitro assays and western blot analysis. Therefore, in the study described here, E.coli was applied for the expression and purification of HDAC8, and we will use HDAC3 (BPS Bioscience) expressed in a baculovirus-expressing system.

2.1.2 HDAC fluorometric assay

The HDAC fluorometric activity assay was applied to examine the enzymatic activity of HDAC and the inhibition potency of HDAC inhibitors. The *Fluor-de-Lys* (Fluorescent deacetylation of lysine) assay system was developed for a simple, nonradioactive measurement of deacetylase activity (Figure 9).[103, 104] The assay relied on the specificity of the proteolytic enzyme trypsin for peptides with deacetylated lysine, with R-(N^{ε}-acetyl-Lys)-AMC (7-Amino-4-Methyl-coumarin) used as *Fluor-de-Lys* substrate. Trypsin, as the main component of *Fluor-de-Lys* developer, cleaves the carboxyl side of lysine and releases AMC. By itself, the substrate showed no reaction with trypsin. The active HDAC enzyme catalyzes the removal of the acetyl group to yield R-Lys-AMC and sensitizes the substrate so that, in a second step, it can react with the *Fluor-de-Lys* developer to liberate AMC. The excitation and emission wavelength for AMC is 360 nm and 460 nm, respectively. The increase in fluorescence at 460 nm from the generation of AMC was used to measure HDAC activity.

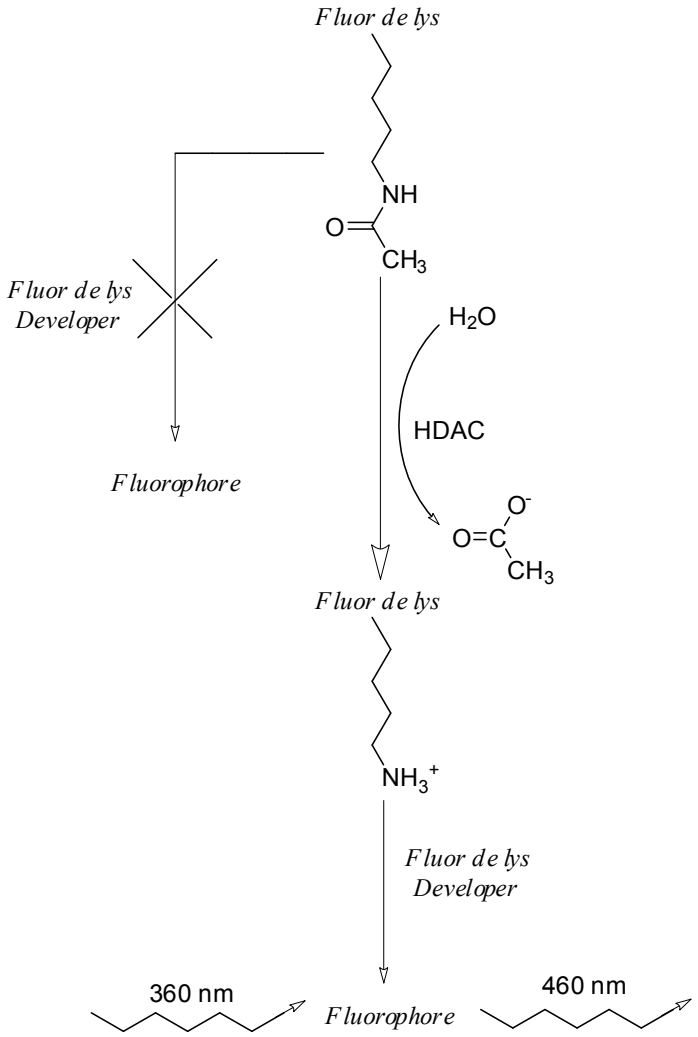

Figure 9: Mechanism of HDAC fluorometric assay

2.2 Methods and Materials

The HDAC8 fluorescent assay kit and the human recombinant HDAC8 protein were purchased from Enzo Life (formerly Biomol international; Plymouth Meeting, PA). Purified HDAC8 from E.coli was used for photoaffinity labeling. The primary anti-HDAC8 antibody was from Santa Cruz Biotech. (Santa Cruz, CA) and pHD2-Xa-His HDAC8 expressing plasmid was a generous gift from Dr. Carol A. Fierke (University of Michigan). The anti-rabbit secondary antibody conjugated to horseradish peroxidase

(HRP) was from GE (Piscataway, NJ). Finally, streptavidin and the colorimetric HRP substrate o-phenylenediamine (OPD) were sourced from Pierce (Rockford, IL) and the 96-well plates were from Nunc (Rochester, NY).

2.2.1 Expression, purification, and activity testing of HDAC8 in E.coli

BL21(DE3) pHD2-Xa-His cells were grown in LB-CB media (Lysogeny Broth-Carbenicillin) (1000:1) at 37 °C and induced by the addition of isopropyl-β-D-thiogalactoside (0.4 mM) and $ZnSO_4$ (0.2 mM) when A_{600}= 0.7-0.8. The temperature was subsequently decreased to 25 °C at induction, and protease inhibitor PMSF (10 µg/mL of phenylmethylsulfonyl fluoride) was added 3 hours after induction. The cells were incubated at 25 °C for an additional 14 hours and harvested by centrifugation (6000 g, for 15 minutes, at 4 °C). The cell pellet was resuspended and washed in an equilibration buffer of anti-His column (40 mM Na_3PO_4, pH 7.8 and 1M NaCl).

After the cells were thawed, they were homogenized in lysis buffer (0.1% Triton X-100 in 40 mM Na_3PO_4, pH 7.8, 1M NaCl, 10 µL PMSF (2.5mM, 1000X) and 20 µL leupeptin) on ice for 30 minutes. A sonic dismembrator (Fisher Scientific) was used to lyse the cell, and lysate was centrifuged at 15000 rpm for 25 minutes at 4 °C. The cleared lysate was loaded onto a GE HiTrap $NiSO_4$-charged immobilized metal affinity column (Ni-IMAC, GE Healthcare), after which they were washed with two steps of wash buffer (10 and 50 mM imidazole in 40 mM Na_3PO_4, pH 7.8 and 1M NaCl). The bound His_6-tagged HDAC8 protein was eluted with elution buffer (250 mM imidazole in 40 mM Na_3PO_4, pH 7.8, 1M NaCl), concentrated to <2 mL before being loaded onto a monoQ anion

exchange column preequilibrated in equilibration buffer (50 mM Tris-HCl, pH 8.0, 5% glycerol). The protein was eluted with a stepwise gradient from 0 to 500 mM KCl.

2.2.2 HDAC3/HDAC8 activity assay and enzyme kinetics

The assay proceeded through a simple two-step procedure that can be carried out in 96-well half-volume microtitration plates. Homemade or commercial HDAC8 was diluted with HDAC8 assay buffer KI-311 (Enzo Life; Farmingdale, NY) (25 mM Tris [pH 8.0], 137 mM NaCl, 2.7 mM KCl, 1 mM $MgCl_2$, supplemented with 0.5 mg/mL BSA) and pre-incubated with 25 μL of 10 μM HDAC substrate KI-178 (Enzo Life; Farmingdale, NY) at RT. After 45 minutes, the reaction was quenched with 50 µL of 50 μg/mL trypsin supplemented with 5 μM trichostatin-A in KI-143 (Enzo Life; Farmingdale, NY). The plate was read on a POLARStar Optima microtitration plate reader (BMG Labtech; Durham, NC) with λ_{excit} = 360 nm and λ_{emis} = 460 nm. The IC_{50} values were determined using the GraphPad Prism5 software (GraphPad Software Inc.; La Jolla, CA).

Next, 10 ng of HDAC3/NCoR2-DAD (BPS Bioscience; San Diego, CA) was diluted with KI-311 and pre-incubated with 10 μL, 125 μM. After HDAC fluorescent substrate Boc-L-Lys (AC)-AMC (Chem-Impex; Wood Dale, IL) was added the mixture was incubated for 30 minutes at RT. The reaction was quenched with 50 μL of 1 mg/mL trypsin and 5 μM trichostatin-A in KI-143 for 30 minutes. The plate was read on an OptimaPolar Starmicroplate reader (BMG Labtech; Germany) at excitation and emission wavelength of 360 nm and 460 nm, respectively.

2.2.3 Gel electrophoresis and western blot analysis of purified HDAC

Western blot was performed using 10 μg of total protein from cell lysate or elution from each step with a 5× loading buffer containing 10% SDS, 0.05% bromophenol blue, 50% glycerol, and β-mercaptoethanol. Protein samples were boiled for 5 minutes and allowed to cool before loading on a denaturing 4–20% polyacrylamide gel electrophoresis (SDS-PAGE). Following the electrophoresis, protein was either directly visualized for purity by staining in commassie blue stain buffer (10% (v/v) acetic acid, 0.006% (w/v) Coomassie Blue dye, 90% ddH_2O) or transferred to a polyvinylidiene difluoride (PVDF) membrane (Imobilon-Millipore; Bedford, MA). The membrane was incubated for 1 hour with 1% albumin fraction V (USB; OH) and washed three times with 1× phosphate buffer saline, supplemented with 0.05% Tween-20 (PBS-T). The membrane was subsequently incubated with an anti-HDAC antibody (1:3000) for 2 hours at room temperature with slight agitation. After three washes in PBS-T, the membranes were incubated with a secondary antibody anti-rabbit-HRP for 1 hour at room temperature. Finally, the signals were detected using the enhanced chemiluminescence (ECL) kit from Pierce (Pierce Biotechnology; Rockford, IL) and densitometry scanning of the films was performed using the ImageJ software provided by NIH.[105-107]

2.3 Results and Discussions

2.3.1 Expression and purification of HDAC8

His-tagged HDAC8 was expressed in *E. coli* and purified using (1) a GE Hitrap Ni-IMAC column and (2) a MonoQ anion exchange column. The purity of the protein after the first step was estimated to be around 80% as determined by SDS-PAGE, followed by

coomassie staining and densitometry quantification. The second step resulted in further improvement of the purity to approximately 95% (Figure 10, left panel). The cell pellet harvested from 1 L cultured media yielded about 90 mg of lysate, whereby 10 mg of protein was recovered after first column purification and 2 mg of pure protein was collected after the second column (Table V).

The purified protein was identified to be HDAC8 by performing the western blot using anti-HDAC8 primary antibody and anti-rabbit secondary antibody (Figure 10, right panel). Strong bands were observed at around 44 kDa. Since the anti-HDAC8 antibody was highly specific to its antigen-HDAC8, these bands were identified as the monomer of human recombinant HDAC8. The enzymatic activity of HM HDAC8 was assessed and compared to the commercial HDAC8 in the later sections.

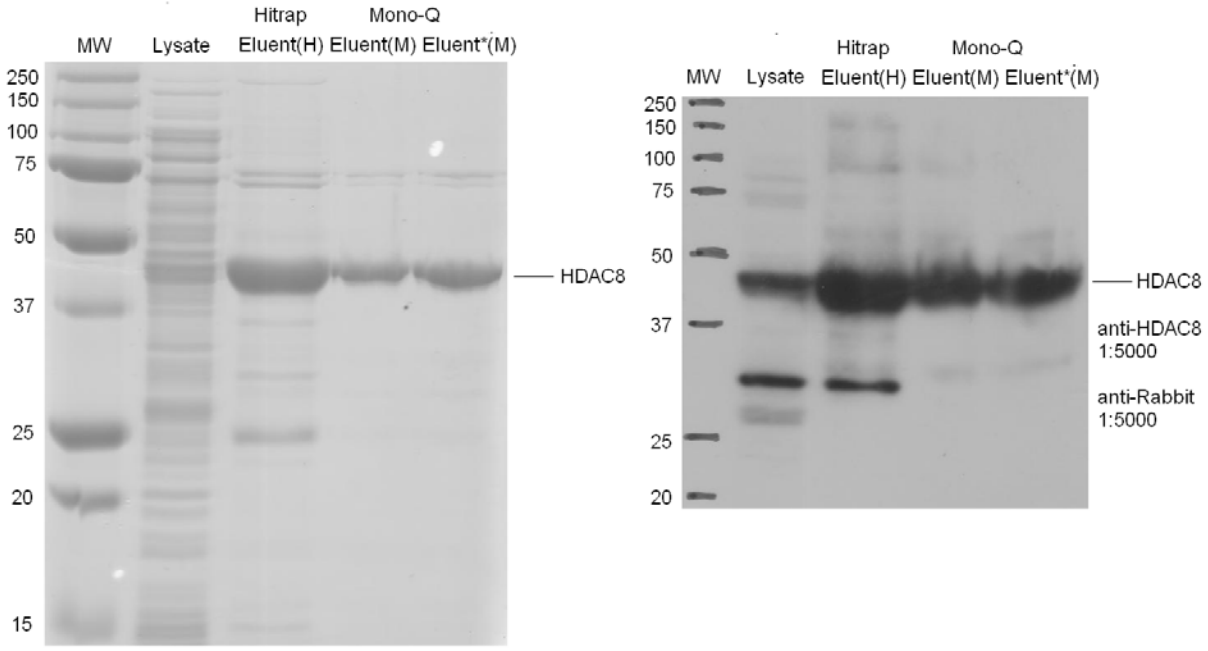

Figure 10: Purity and specificity of the purified HDAC protein

TABLE V: PROTEIN ACTIVITY AND RECOVERY OF HDAC8 PURIFICATION.

	c (µg/µL)	V (µL)	Total protein (µg)	Signal (AFU)	Protein/well (µg)	Specific activity (AFU/µg)
Lysate	6.5	14000	90832	20113	97.4	206.6
Eluent (HiTrap)	4.6	2050	9504	25553	69.6	367.1
Eluent (HiTrap)*	5.4	2050		22759	81.2	280.3
Eluent (MonoQ)	0.6	3200	1888	24919	8.9	2815.6
Eluent (MonoQ)$	0.6			20698	8.9	2338.7
Eluent (MonoQ)@	0.5			10607	8.1	1309.4
Eluent (MonoQ)#	0.6			2538	9.1	278.9
Biomol HDAC8				6472	0.6	10354.4

Eluent (HiTrap)*: Eluent from HiTrap column dialyzed in 50 mM Tris PH 8.0, 5% Glycerol.
Eluent (MonoQ)$: Eluent from MonoQ column stored at 4 °C for 8 h.
Eluent (MonoQ)@: Eluent from MonoQ column dialyzed in Biomol HDAC8 storage buffer: (10 mM Tris PH 7.5, 100 mM NaCl, 3 mM $MgCl_2$, 10% Glycerol)
Eluent (MonoQ)#: Eluent from MonoQ column dialyzed in BPS HDAC8 storage buffer: (50 mM Tris PH 8.0, 138 mM NaCl, 10% Glycerol)

2.3.2 Enzyme activity and K_m determination

Since buffer characteristics, such as the ionic strength (salt concentration), major cation (sodium or potassium), pH and working temperature may have significant effect on enzyme activity, the storage conditions of the purified enzyme were optimized with the aim to enhance HDAC8 stability and activity (Table V).

The purified HDAC8 that was eluted from MonoQ column was dialyzed in the Biomol and BPS HDAC8 storage buffer for 4 hours at 4 °C. The enzyme activity test of HDAC8 was carried out using the *Fluor-de-Lys* HDAC8 activity assay described in Section 2.1.2 (Table V). The specific activity of HDAC8 in MonoQ elution buffer (50 mM Tris, pH

8.0, 5% glycerol, 300 mM KCl) was about 2- and 10- fold higher than its counterparts dialyzed in Biomol HDAC8 and BPS storage buffer, respectively. Following the comparison of the three storage buffers tested, MonoQ column elution buffer proved to be the best buffer for HDAC8 enzyme activity. The short-term stability of the purified HDAC8 in the MonoQ elution buffer was confirmed, and similar specific activity of HDAC8 was observed after 8 hours of incubation at 4 °C before the activity test. As a result, the elution buffer of MonoQ column (50 mM Tris, pH 8.0, 5% glycerol, 300 mM KCl) was chosen for the storage of HM HDAC8 protein, unless otherwise specified.

Before the optimization of the assay conditions was carried out by *Fluor-de-Lys* HDAC8 activity assay (Enzo Life; Farmingdale, NY), the optimal amount of the enzyme to be used in the assay needed to be determined. However, as 5 μM of substrate (KI-178) was used in the Enzo Life HDAC8 activity assay protocol, it was an appropriate choice for the assay condition optimization until K_m was determined. The steady-state kinetic parameter should be obtained under conditions of subsaturating substrate and enzyme. Therefore, as shown in Figure 11, when 5 μM of substrate (KI-178) reacted with an increasing amount of HM HDAC8, the linear region of resulting reaction rate curve was chosen and re-plotted (Figure 11, lower panel). Commercial HDAC8 (Enzo Life; Farmingdale, NY) was used as the positive control (Figure 11, depicted in red).

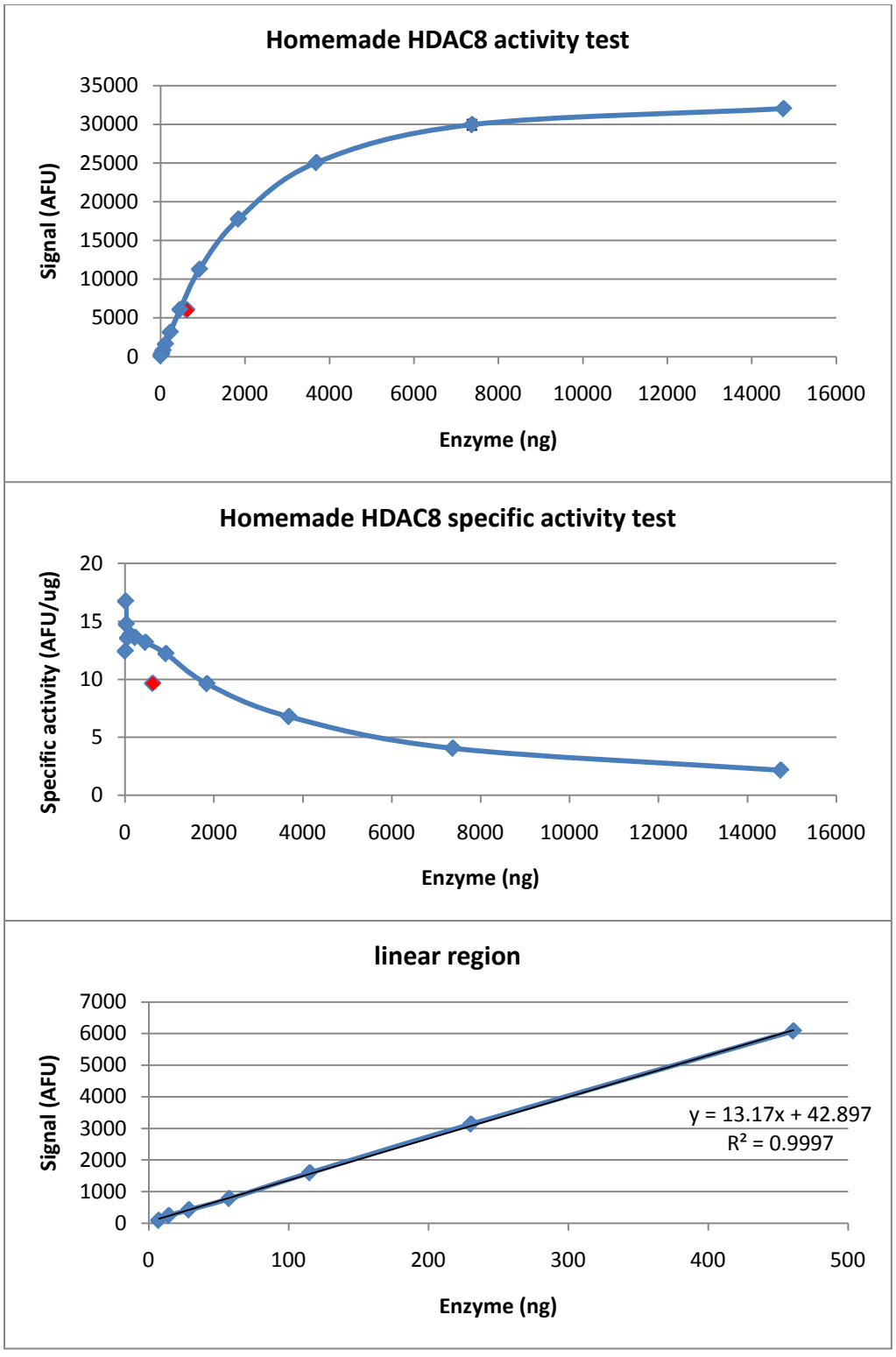

Figure 11: HM HDAC steady state test. The commercial HDAC8 is depicted in red.

As expected, the reaction rate ceases to increase, as the substrate is consumed by increasing amount of enzyme (Figure 11, upper panel). The fluorescence signal produced by the commercial HDAC8 was somewhat weaker than the one produced by the HM protein. (Figure 11, middle panel), it implies that the specific activity of HM HDAC8 is slightly better than that of the commercial HDAC8. Given that, after incubating with substrate for 30 minutes, 0 to 450 ng of HDAC8 was in the linear region of the signal increase (see Figure 11, lower panel). Thus, it was decided that 400 ng of HDAC8 should be used in the future assay, due to its optimal signal-to-noise ratio.

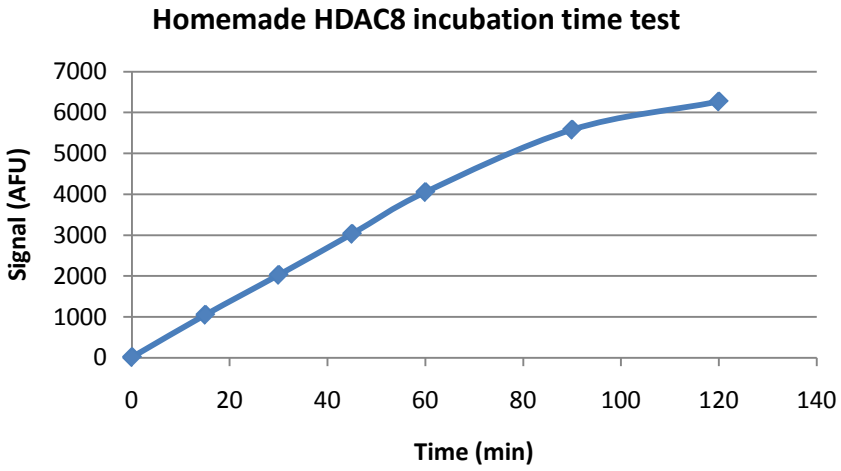

Figure 12: Temporal representation of HM HDAC8 with KI-178

A representative temporal evolution of the reaction of HM HDAC8 with substrate KI-178 is shown in Figure 12. The incubation time of substrate to enzyme was varied in order to maximize signal-to-noise ratio, while at the same time assuring a linear upward trend in signal intensity (see Figure 12). The fluorescent signal was read at 0, 15, 30, 45, 60, 90,

and 120 minutes of incubation of HDAC8 with the substrate. The graph was plotted and a good linear relationship was observed at the incubation time interval from 0 and 60 minutes. As the maximum signal-to-noise ratio exceeding 50 (data not shown), in the linear region corresponding to the incubation of 45 minutes was measured. We chose 45 minutes as the incubation time for the enzyme with its substrate.

The K_m value of substrate KI-178 for HM HDAC8 was determined by increasing the substrate concentrations while the concentration of the enzyme remained constant. Data from three independent experiments were analyzed using GraphPad Prism 5.0 software. V_{max} and K_m were deduced from the nonlinear regression models using variable slope equations (Figure 13).

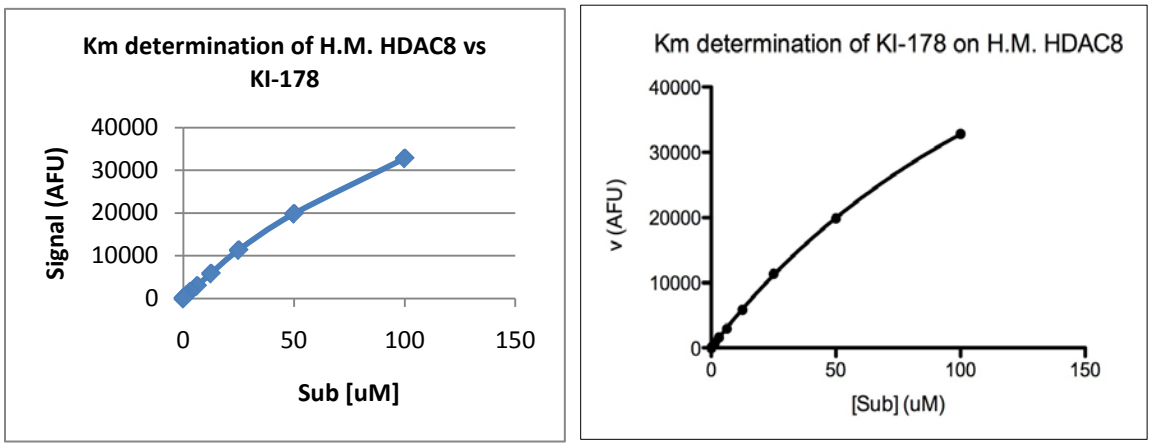

Figure 13: K_m determination of KI-178 for HM HDAC8.

Given that K_m of substrate KI-178 for HM HDAC8 measured at 182.4 μM, any substrate concentration below the K_m can be considered for the screening assay of competitive

inhibitors. In this work, due to the need to balance between signal-to-noise ratio and cost, the assay conditions were set at: 5 μM of substrate KI-178 that incubated with 400 ng of HM HDAC8 for 45 minutes, followed by 30 minutes of trypsin digestion and fluorescence signal measurement on Optima plate reader, using 360 nm and 460 nm wavelengths for excitation and emission, respectively.

2.4 Conclusions

The availability of active HDAC enzyme and an appropriate assay for the screening of HDAC probes is a prerequisite for photolabeling study of HDAC probe binding modes. In this chapter, the methodology for successfully obtaining pure and active HM HDAC8, as well as optimizing the fluorescent assay using this HM HDAC8 protein was described. As a result of the HM HDAC8 purification process, 95% pure HDAC8 was yielded through a two-step column separation. Next, the enzymatic activity of the HM HDAC8 was assessed by using a *Fluor-de-Lys* HDAC activity assay. Thus, 50 mM Tris, pH 8.0, 5% glycerol and 300 mM KCl was identified as the most optimal storage condition that would yield expected HDAC8 activity and stability and, by conducting a combination of enzyme kinetic experiments, the HM HDAC8 assay conditions were established and optimized. Consequently, in the work described in the subsequent chapters, 400 ng of HM HDAC8 will be incubated with 5 μM of KI-178 HDAC substrate for 45 minutes, followed by a tryptic digest and the fluorophore generated will be quantified on an Optima plate reader. This assay will be applied to evaluate the inhibitory potency of all synthesized photoaffinity probes.

This study was a prerequisite for the mapping of the probe binding pose by photolabeling, which will be discussed in Chapters 3–5, where the pure and active HM HDAC8 will be used to assess the inhibition potency of different photoaffinity probes, perform photolabeling experiments and protein mass spectrometry analysis.

CHAPTER 3 MAPPING THE BINDING POSES OF HDAC8 BY PHOTO-AFFINITY PROBES

3.1 Introduction

One of the key challenges in designing isoform-selective HDAC inhibitors is a poor understanding of the binding modes (poses) available to the highly solvent exposed surface binding group (SBG) of HDAC inhibitors targeting the grooves and ridges on the protein surface directly adjacent to the catalytic well of HDACs. It has been hypothesized by us in our preliminary experiments and a recent publication by Wiest and colleagues[108] that the SBG groups may have more than one preferred position on the surface and each of them contributes to the overall binding affinity. Although the available HDAC X-ray data provide information on structure of proteins and binding of probes, its use is limited due to high solvent exposure of the SBG of the probes and additional copies of the same protein in the crystallographic cell that interfere with the binding of the co-crystallized probes.

Photoaffinity labeling is a strategy offering methods for the identification of drug target proteins of biologically active compounds and mapping their binding sites.[65, 109, 110] Among several photosensitive groups, aryl azide is perhaps one of the most widely used due to its universality, reactivity, and relative simplicity in implementation.[65] One of the recent advances in the photoaffinity labeling probe development is application of "click-chemistry" and bioorthogonal probes for activity-based proteomics profiling by Cravatt et al[72, 76-81] and its recent modification by Suzuki et al.[111-113] This latter study is based on a concept in which a bifunctional probe is connected to a target protein

by activation of a photoreactive group, such as an aromatic azido or 3-trifluoromethyl-3H-diazirin-3-yl group, and identification of the probe product is achieved by anchoring a detectable tag to an alkyl azido moiety, which survives photolysis, using the Staudinger-Bertozzi ligation.[70, 114-118] A similar approach was recently utilized to discover a new binding site in HIV-1 integrase.[119] In this case a different photoactivated moiety - benzophenone – facilitated by mass spectrometry and docking analysis was used to determine the exact probe binding position. The recent study by Cravatt et al.[81] presents a novel proteomics probe for histone deacetylases and is intended to discover new proteins interacting with the histone deacetylases. It does not address, however, the problem of multiple binding poses of HDAC inhibitors.

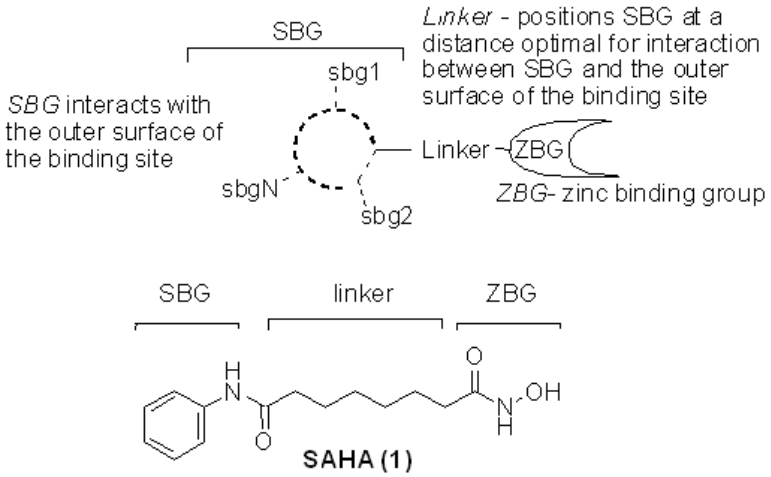

Figure 14: General structure of HDAC inhibitors

Similarly to SAHA, the general structure of HDAC inhibitor can be categorized into zinc-binding group, linker group and surface binding group (Figure 14). The inhibitor anchors to HDAC through formation of a metal-probe complex between the hydroxamate group

of the probe and Zn^{2+} in the active site. The binding was further strengthened by binding of surface-binding group to outer surface of the active site. Here we introduced for the first time the use of diazide-based photoaffinity labeling probes, liquid chromatography-tandem mass-spectrometry, and molecular dynamics simulations to map the ensemble of the poses of HDAC8 inhibitors upon binding (Figure 15).

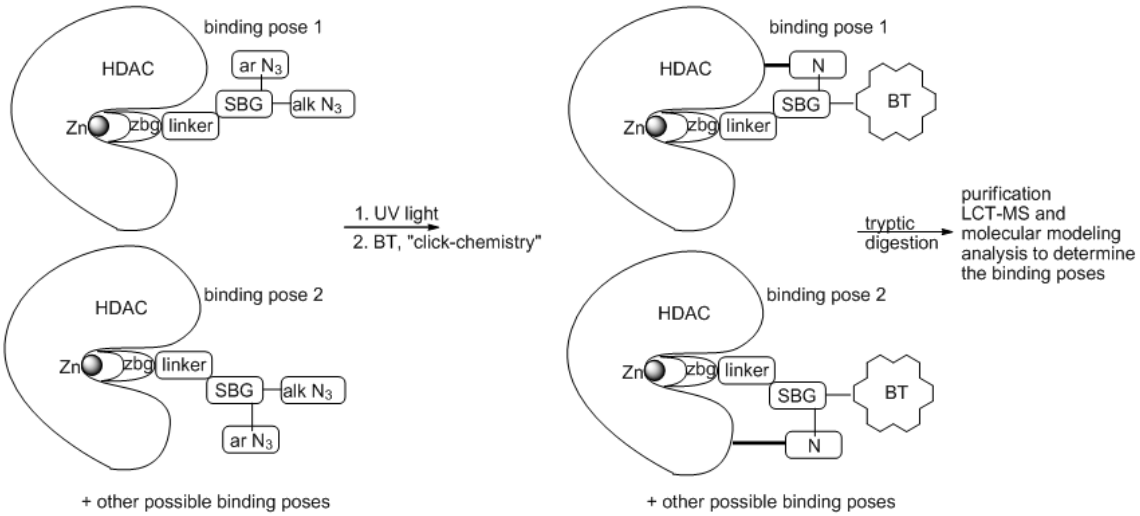

Figure 15: Application of photoaffinity probes for detection of binding poses of an HDAC probe.

The probe was first covalently crosslinked to enzyme via activation of aryl azido moiety, the biotin tag was then introduced and attached to probe-enzyme mixture through click chemistry cyclo-addition between alkyl azido moiety and alkyne group of the tag. In the final step, the binding of protein by probe/tag was examined by western blotting with strep-HRP which recognizing biotin tag or proteomic post-translational modification profiling.

3.2 Methods and Materials

Streptavidin and the colorimetric HRP substrate o-phenylenediamine (OPD) were from Pierce (Rockford, IL) and the 96-well plates from Nunc (Rochester, NY). Tris(2-carboxyethyl)phosphine (TCEP) was from (Alfa Aesar chemicals, Ward Hill, MA). CuSO4, dimethyl sulfoxide (DMSO), tris((1-benzyl-1H-1,2,3-triazol-4-yl)methyl)amine (TBTA), and all other chemicals were purchased from Sigma (St. Louis, MO) if not stated otherwise. The probes and tags were synthesized in house (Figure 16). The primary anti-HDAC8 antibody was from Santa Cruz (Santa Cruz, CA) respectively. The anti-rabbit secondary antibody conjugated to horseradish peroxidase (HRP) was from GE (Piscataway, NJ).

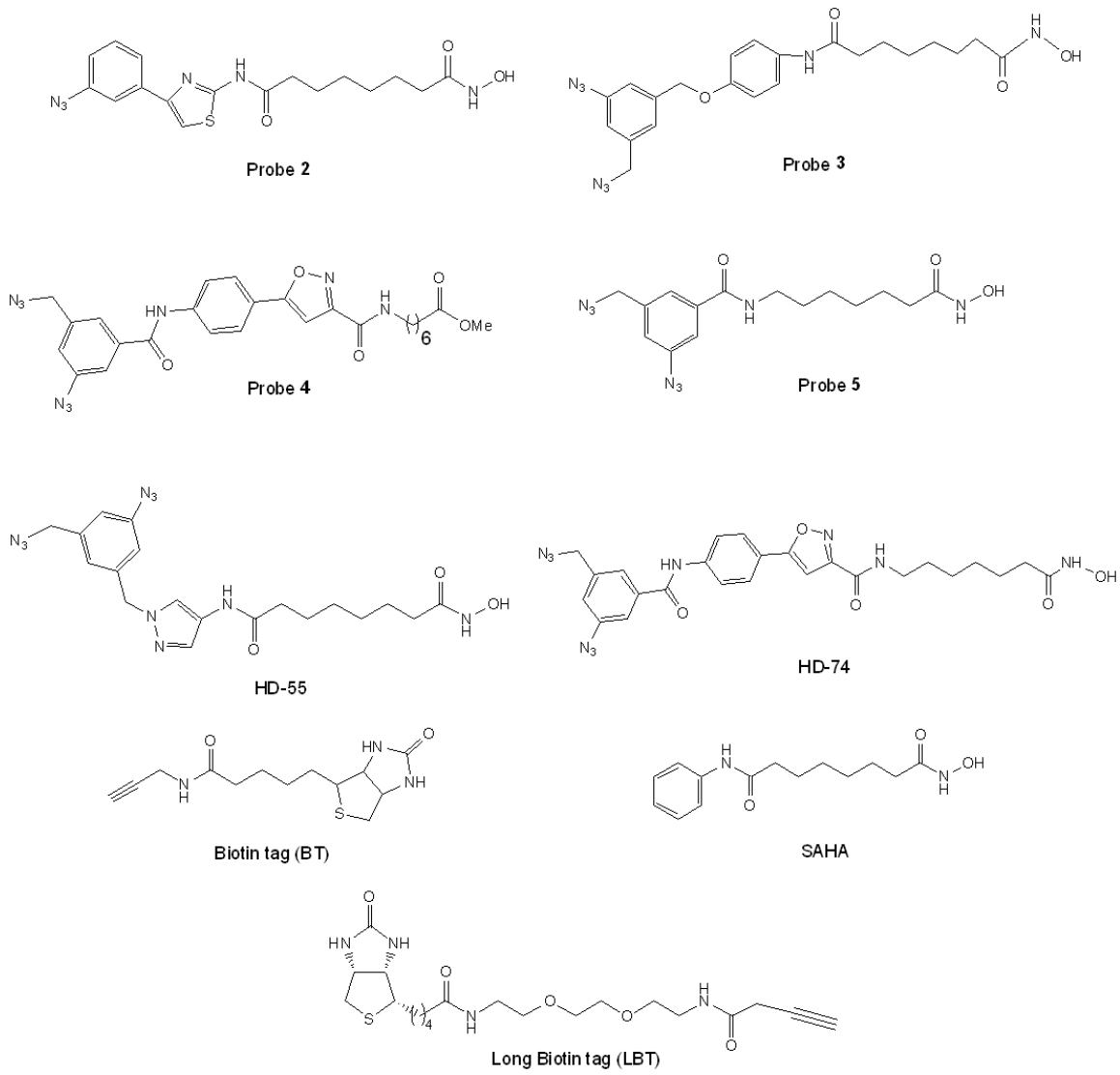

Figure 16: Structures of HDAC photoaffinity probes and tags used during this investigation.

Among photoaffinity probes, **2** is a mono-azide probe which lacks ability to be attached by visualization tags; all other probes are equipped with diazide moieties. Probe **4** is a diazide probe which lacks the HDAC binding group. Two biotin tags with different linker group length are prepared.

3.2.1 HDAC8 Activity assay

HDAC inhibition assay was performed in 96-well half-area microplate (Corning). 0.4 μg HM HDAC8 was diluted with HDAC8 assay buffer KI-311 (Enzo life) and preincubated with 10 μL of inhibitor for 5 min. The assay mixture was treated with 25 μL of 10 μM HDAC substrate KI-178 (Enzo life) for 45 min at rt. The reaction was quenched with 50 μL of 50 μg/mL trypsin and 4 μM trichostatin A in KI-143 (Enzo life) for 30 min. The plate was read on a POLARstar OPTIMA (BMG labtech) microplate reader at excitation wavelength 360 nm and emission wavelength 460 nm.

The IC_{50} values were determined using the GraphPad Prism 5 software (GraphPad Software Inc., La Jolla, CA).

3.2.2 Direct measurement of modification by MALDI-ToF mass spectrometry

HDAC8 protein was treated with different photoaffinity probes at the ratio of 1:1 to 1:20 and UV-irradiated to induce covalent cross-linking. The protein-probe complex was diluted with 50% methanol in water to make 2 μM as final concentration, mixed with saturated sinapic acid. 1 μL of the mixture was spotted onto a MALDI plate and air-dried before analysis. Positive ion MALDI TOF mass spectra were acquired using an Applied Biosystems (Foster City, CA) Voyager-DE pro MALDI-TOF mass spectrometer in linear mode. A total of 500 or more laser shots were acquired and signal averaged per mass spectrum.

3.2.3 Photolabeling experiments

Purified recombinant HDAC8 (0.5 μg in 5 μL of assay buffer or assay buffer with 0.1% triton X-100) was incubated with various concentrations of probe **2**, probe **3** with or without competent SAHA for three hours in the dark, after which the formation of a covalent bond between the azide group present in the probe and reactive side chains of the HDAC was initiated by UV irradiation (λ= 254 nm) for 3 min with 1 min rest. Then "click chemistry" was used to attach Biotin tag (BT) to the diazide probes attached covalently to the protein. The biotin tag was added to all the tubes at a final concentration of 50 μM, and the chemical reaction was initiated by addition of TCEP (0.5 mM final concentration), TBTA (0.1 mM) and $CuSO_4$ (1 mM). After 60 min incubation at room temperature, protein samples were analyzed by SDS-PAGE and western blot using an anti-biotin primary antibody, streptavidin conjugated to horseradish peroxidase (Pierce, Rockford IL) and ECL (Pierce, Rockford IL).

3.2.4 Tryptic digest and proteomic profiling of modification sites

HDAC8 protein was incubated with the photoaffinity probe **3**, exposed to UV light to form HDAC8-**3** covalent adduct, and attached with BT. Next, the modified protein was purified using avidin-agarose chromatography. Unmodified HDAC8 was used as a negative control. To facilitate the analysis of the modified protein, tryptic digestion was carried out followed by mass spectrometric liquid chromatography-tandem mass spectrometry (LC-MS/MS) and proteomics database analyses using SEQUEST proteomics software. Two proteomics data sets were generated; one used an accurate mass peptide mass tolerance of 5 ppm between the theoretical and measured peptide

masses, and second data set used a mass tolerance of 10 ppm. It should be noted that both 5 and 10 ppm are considered accurate mass measurements.

3.3 Results and Discussion

3.3.1 HDACs Activity Profiling

We followed the established assay protocol to evaluate the inhibition potency of inhibitors and probes synthesized in-house. 400 ng of homemade HDAC8 was pre-incubated with various concentrations of inhibitors for 5 min before introduction of the substrate. As illustrated above (Section 3.2.1), the reaction mixtures were quenched by the developer and residual HDAC activity was assessed by the fluorescence plate reader. The non-linear regression analysis of data on Graphpad Prism 5.0 (Graphpad software Inc. CA) was performed to calculate the IC_{50} values. An example of HDAC inhibition profile was given in Figure 17. The residual HDAC activity would fall when the concentrations of inhibitor increased. The half maximal inhibitory concentration (IC_{50}) was deduced from nonlinear regression curve fitting by GraphPad Prism (Figure 17).

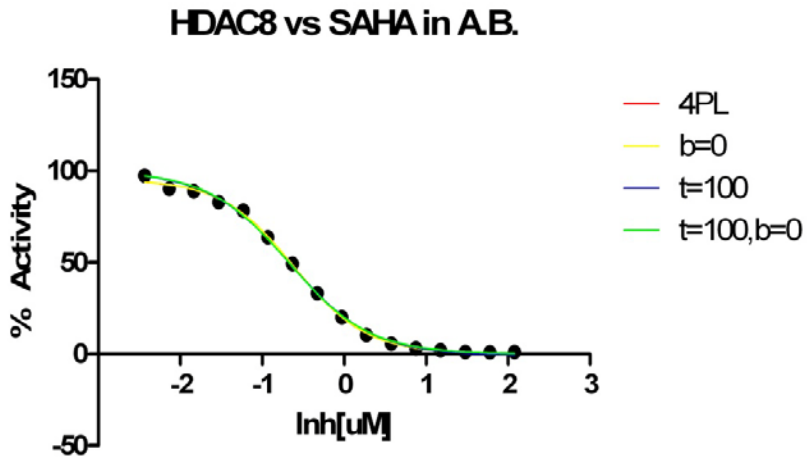

Figure 17: Inhibition profile of homemade HDAC8 by inhibitor
A.B.: Assay buffer

As shown in Table VI, the IC_{50} values of SAHA and photoaffinity probes probe **2** and probe **3** for HDAC8 range from mid nM to lower μM, indicating all probes are potent HDAC inhibitors. The strong interaction between HDAC and photoaffinity probes makes the application of activity-based protein profiling by photolabeling possible.

TABLE VI: SCREENING FOR INHIBITORY ACTIVITY (IC_{50}, *M*M) OF COMMERCIAL AVAILABLE SAHA, PROBE **2** AND PROBE **3** AGAINST HDAC8

HDAC8/A.B.	**IC_{50} (μM)**	**sd (IC_{50}) (μM)**	**Ki (μM)**
SAHA	0.236	0.021	0.235
Probe **2**	2.705	0.023	2.431
Probe **3**	2.873	0.064	2.86

3.3.2 MALDI-ToF mass shift of HDAC8 modified by different diazide probes

After confirming that the photoaffinity probes are potent HDAC inhibitors, MALDI-ToF mass spectrometry was utilized to directly examine the modification of HDAC8 by diazide probes. HDAC8 was incubated with up to 20 equiv. of probe **2** and probe **3** irradiated with UV light to activate the probe, diluted with ammonium bicarbonate (50 mM, pH 7.8) and concentrated using Centricon 10 000 molecular weight cutoff filters (Millipore). The recovered protein sample was tested on MALDI-ToF. As expected, the mass shift of modified HDAC8 compared with untreated HDAC8 changes with amount of probe added in a dose-dependent manner (Table VII).

TABLE VII: MALDI MS OF INTACT HDAC8 AND TREATED WITH PROBE **2** AND **3**

Mass shift	**1:1**		**1:5**		**1:20**	
	avg.	sd.	avg.	sd.	avg.	sd.
Probe **2**	4.0	41.3	113.5	37.1	256.8	37.1
Probe **3**	3.0	15.4	13.2	7.5	60.1	77.6

The results of the MALDI-MS analysis of the intact and modified protein supported the conclusion that the protein can be modified by the UV activated nitrene group generated from the diazide probes. We moved to the next stage – photolabeling followed by attachment of BT tag to the alkyl azide moiety of probe **3**.

3.3.3 Photolabeling and competition experiment in assay buffer

To evaluate the selectivity of photolabeling *in vitro*, purified recombinant HDAC8 was incubated with various concentrations of probes **2** and **3**. The conditions for UV crosslinking were optimized to increase signal-to-noise ratio. We found that in case of HDAC8 3×1 min exposure to UV light with 1 min rest gives the best signal to noise ratio. The "click-chemistry" conditions with catalysis by Cu(I) generated *in situ* were successfully used to attach BT to the adduct between HDAC8 and probe **3**. In our preliminary studies we also tried the Staudinger-Bertozzi ligation[19-24] as an attachment procedure of the biotin tag and determined that the "click-chemistry" approach is much faster and gives better yield as determined by Western blotting. This is consistent with the observation made by Cravatt et al.[9]

Different amount of probe **3** and **2** were used to photolabeling with HDAC8. Since **3** has additional alkyl azide group that can survive photo irradiation and attach to the biotin tag while **2** does not, the photolabeling result was compared.

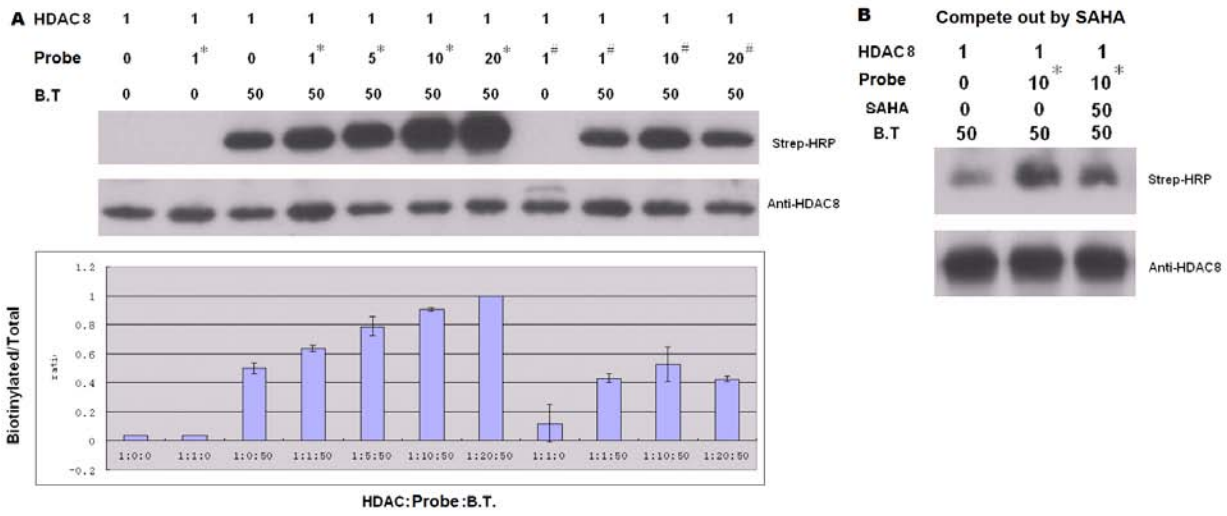

Figure 18: Characterization of biotinylated HDAC proteins and total HDAC proteins. (A) Western blot analysis of probe **2** (labeled as #) and probe **3** (labeled as *) binding to HDAC8 probed by strep-HRP and anti-HDAC8 antibodies. All the numbers stand for the concentration in μM. (B) Competition of probe **3** by SAHA.

As expected, the amount of biotinylated HDAC increases in a concentration-dependent manner in the presence of probe **3** but not with probe **2** (Figure 18 A) that lacks the alkyl azide group designed to bind the biotin tag; only non-specific, background level signals are observed. A comparison of the background levels observed in lanes 3, 9-11 shows that the background levels of biotinylation are due to non-specific modification of the HDAC8 protein with BT and do not depend on the presence of probes **2** and **3**. It appears that the non-specific biotinylation with BT may be specific to the HDAC8 protein as in a similar experiment HDAC3 protein showed negligible levels of non-specific biotinylation with BT (data not shown). In the competition experiment shown in Figure 18 B, the level of the covalent modifications with probe **3** drops by 50% when SAHA is present during the photolabeling, indicating that the cross-linking of the probe **3** to HDAC8 is likely to happen when **3** is bound at the catalytic site. The probe **3** competes with SAHA binding to the same active site. The photoaffinity probe **3** is thus proved to be able to crosslink

HDAC8 as a specific inhibitor. In the section followed, we will describe how the modification sites of HDAC8 by **3** were identified by FT-ICR mass spectrometry.

3.3.4 Modification sites identification by FT-MS and interpretation of data

The HDAC8-probe **3**-BT adduct underwent avidin-agarose enrichment was tryptic digested and tested on LTQ-FT mass spectrometry. With the help of Dr. Chris Pennington, a total of 11 modified HDAC8 peptides were identified on peptide mapping using high resolution accurate mass measurement (within 10 ppm) and peptide sequencing using MS/MS (Table VIII).[107] No modified peptides were detected in the negative control using unmodified HDAC8 (data not shown). The amino acids underlined in Table VIII correspond to the residues modified by probe **3** based on MS/MS analysis. Due to occasional missed trypsin cleavage sites, which are common in trypsinization reactions, there are some amino acid sequence overlaps among several peptides. For example, entries 1 and 2 correspond to overlapping amino acid sequences 35-55 and 37-60, respectively. Also, due to the high reactivity of the photoaffinity probe, several amino acid residues became modified in entries # 3,4,6,10, and 11 (Table VIII).

TABLE VIII: SUMMARY OF IDENTIFIED HDAC8 PEPTIDES MODIFIED WITH PROBE **3**:BT ADDUCT.

Entry No.	Peptide	Sequence (AA#s)	$[M+H]^+$	m/z	Charge state (z)	# of Mods	Mass tolerance ppm
1	IPKRASM*VHSLIEAYALHKQM*R[a,b]	034-055	3330.72571	1109.57524	3	1	5
2	RASMVHSLIEAYALHKQM*RIVKPK	037-060	3541.88969	886.22242	4	1	10
3	ASM*VHSLIEAYALHKQMRIVKPK	038-060	4105.10938	1367.70313	3	2	5
4	ASM*VHSLIEAYALHKQMRIVKPK	038-060	4105.10938	1367.70313	3	2	5
5	QM*RIVKPK.	053-060	1734.93338	867.96669	2	1	10
6	VAINWSGGWHHAKK	133-145	2901.37544	1450.18772	2	2	5
7	DEASGFCYLNDAVLGILRLRRKFER	147-171	3660.86731	609.31122	6	1	5
8	GRYYSVNVPIQDGIQDEK	222-239	2800.35061	934.11687	3	1	10
9	YYQICESVLKEVYQAFNPK	240-258	3041.46828	1521.23414	2	1	10
10	AVVLQLGADTIAGDPMCSFNMTPVGIGK	259-286	4244.03997	1060.25999	4	2	5
11	AVVLQLGADTIAGDPMCSFNMTPVGIGK	259-286	4244.03997	849.60799	5	2	10

a) * indicates an oxidized methionine

b) The underlined residues correspond to the region of the HDAC8 protein where modification by probe **3** occurred.

Our modeling group discovered that among the sites modified by probe **3** (Table VIII, Figure 19), the two nearest to the binding site amine acids located on the surface of the protein were Asp^{233} and Asp^{272}. Asp^{272} maps to the R2/G1 region of HDAC8, and Asp^{233} neighbors with the R2/G2 (Figure 22). The two other areas near the binding site corresponding to His^{142}-His^{143} (entry #6, Table VIII) and Ile^{135}-Asn^{136}-Trp^{137}-Ser^{138} (entry #6, Table VIII) are not on the surface of the protein. Photolabeling of these residues may be explained if the binding site of HDAC8 adopts a conformation similar to that found in 1T64 X-ray structure where the second molecule of TSA is bound upside down.[120] The access to these residues in other crystal structures is blocked by the loop L1 (Figure 19B) that was shown to shift its position to accommodate the second molecule of TSA. If the loop L1 swings far enough it may expose the residues in entries #1-#6 for modification by the SBG of probe **3**. The other labeled peptides correspond to sites on the

outer periphery of HDAC8 and were likely modified by excess unbound **3** upon activation by UV light. An analysis of these areas shows that they are either hydrophobic or in close proximity to hydrophobic areas and, thus, may participate in aggregation with probe **3**.

(A) 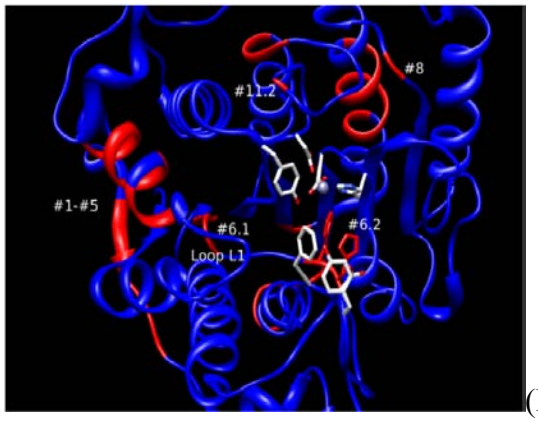

(B) 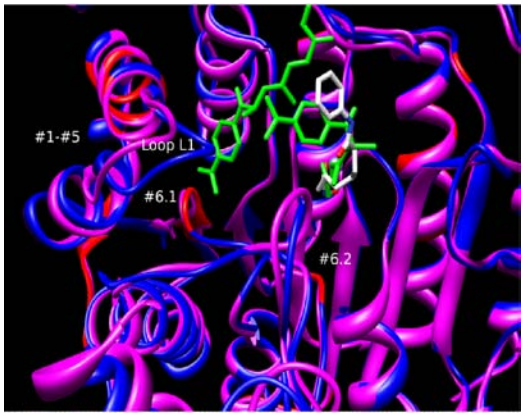

Figure 19: Location of the peptides (red) modified with probe **3** mapped on HDAC8 PDB:1T69 (blue model).
The number # corresponds to the entries in TABLE VIII. The residues rendered as "sticks" correspond to the residues in the immediate proximity to SAHA in 1T69. (B) Same as panel A. Overlay of HDAC8 1T69 (blue) and 1T64 (magenta). SAHA and TSA are rendered as "stick" models colored either by atom types (SAHA) or green color (TSA).

Modified Asp^{233} was contained in peptide GRYYSVNVPIQDGIQDEK (222-239), and the MS/MS spectrum of this modified peptide is shown in Figure 20. Based on Sequest proteomics analysis, the standard peptide fragment ions such as y_6^{+1} and a_{15}^{+2} were identified, and manual inspection of the data was used to identify additional fragment ions formed by side chain fragmentation of probe **3**. By accounting for these side chain fragments, it was possible to identify and assign the other peaks present in the MS/MS spectra.

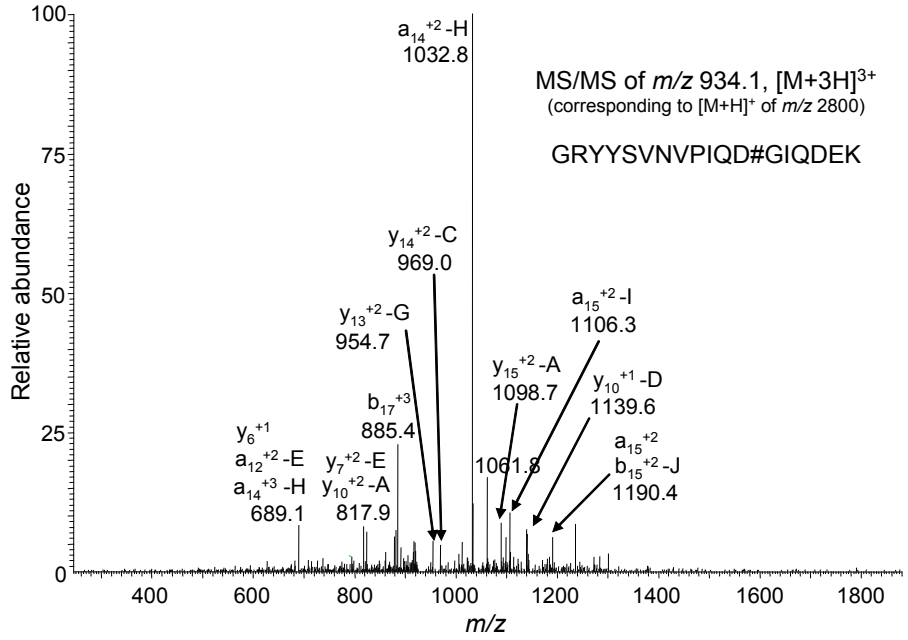

Figure 20: MS/MS spectrum of HDAC8 tryptic peptide 222-239, GRYYSVNVPIQDGIQDEK (see Table VIII, entry 8) showing alkylation at Asp^{233}. The peaks are annotated using the conventional proteomics MS/MS nomenclature (e.g., y_6^{+1}). Upper case letters denote the additional side chain cleavages of probe **3** modified by biotin tag 4 (the structures of possible fragmentation of the resulting construct are shown in Figure 21)

During MS/MS analysis of peptides from HDAC8 that had been modified by **3**, fragmentation of probe **3** was observed at the sites indicated in Figure 21.

These types of cleavages (e.g., y_{15}^{+2} -A) are indicated in the tandem mass spectra of modified HDAC8 peptides. There were a total of three fragment ions *m/z* 689.1 (y_6^{+1}), 885.4 (b_{17}^{+3}), and 1190.4 (a_{15}^{+2}), that could be directly assigned to peptide backbone bond cleavages. Of those three, only the y_6^{+1} fragment corresponds to a region of the peptide not containing probe **3**. The remaining fragment ions were assigned to peptide backbone cleavages plus fragmentation of probe **3**. For three of the fragment ions, more than one type of fragment ion could be assigned. The overall HDAC8 sequence analyses ranged

between 61 – 68 % for the control HDAC8 samples and 52 – 58 % for modified HDAC8 protein samples.

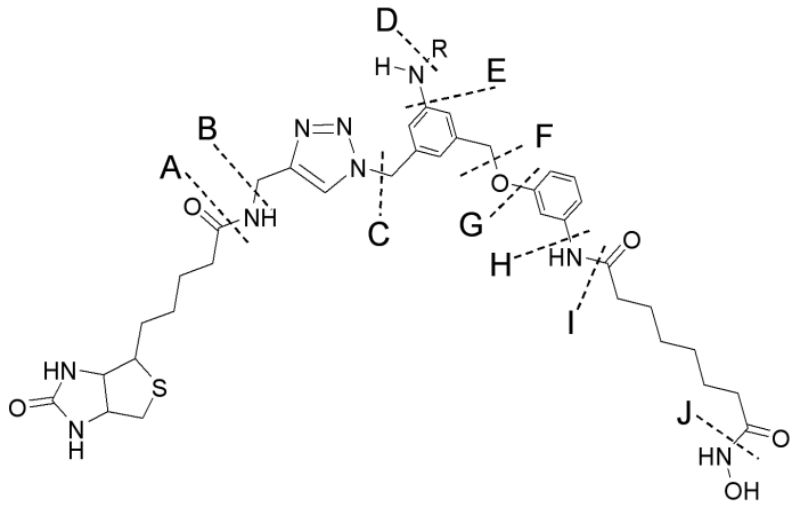

Figure 21: Structure and ten possible bond cleavages of probe **3** modified with biotin tag. Bond cleavages are labeled A through J, and R denotes the amino acid side chain.

To explore if there are more than one binding mode for HDAC probes, Michael and Gilles performed extensive MD simulations of SAHA and probe **3** bound to the HDAC8 and compared them with the outcomes of the photolabeling experiments described above for probe **3**. The binding modes of the probes are characterized by the conformation of the probe inside the binding site and the resulting interactions between the SBG of the probes and the various structural elements of the HDAC8 surface, i.e. R1-R3 and G1-G3 (Figure 22). To determine the binding modes available to the probes, identical conformations sampled during the course of an MD simulation were identified using the matrix RMSD and confirmed with an analysis of the distances between the SBGs of SAHA and probe **3** and representative amino acids in G1-G3 (data not shown).

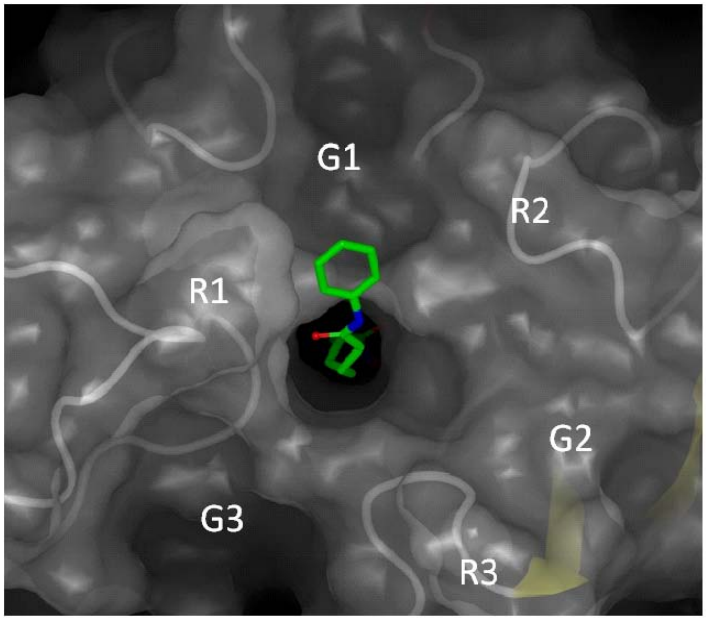

Figure 22: Description of the grooves (G1-G3) and ridges (R1-R3) formed by the protein surface of HDAC8 (PDB:1T69).

In brief, three binding modes of SAHA to HDAC8 were revealed (Figure 23). Characteristic interactions of each binding mode are determined by visual inspection of the conformation of the probe inside the binding site of HDAC8. In the first binding mode, the phenyl ring interacts with the area G2/R3 of the protein, whereas in the second binding mode the phenyl ring interacts with G2/R2 (Figure 23A). The third binding mode is similar to the binding mode of SAHA observed in X-ray as they are both characterized by strong electrostatic interaction between the amide group of SAHA and Asp101 and weak interaction between the phenyl ring of SAHA and the protein surface.

Figure 23B shows the spatial distribution of the aromatic azide group throughout the simulations. The cyan dots represent all the locations occupied by the last nitrogen atom of the azide group of probe **3**. The coordinates of this atom were taken from every frame of the simulation trajectory. The main density areas are located in the grooves and ridges

G1/R2, R2 and G2/R2. The spatial distribution of the aromatic azide group during the simulation is consistent with the modification of the residues Asp233 and Asp272 observed by LC-MS/MS analysis, as it is mostly located in the vicinity of these residues. Importantly, the modification of these residues cannot be accomplished if the probe exists only in a single binding pose as the residues modified are located too far away from each other to be reacting with any single binding pose.

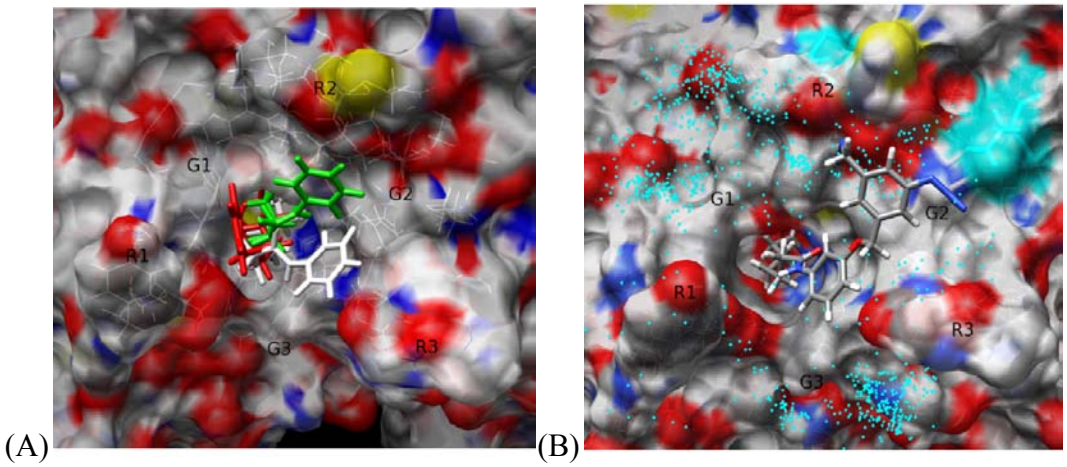

Figure 23: Docking of photoaffinity probes to HDAC8 active sites
(A) Binding mode 1, 2 and 3 of SAHA indicated in white, green and red, respectively. The surface is colored according to atom types using standard atom color convention. (B) The residues Asp233 and Asp272 modified by photoactivation of the probe **3** are indicated by a cyan surface. The locations of the aromatic azide throughout the simulations are projected on the surface and are indicated by cyan dots. Probe **3** is represented in a binding mode similar to the binding mode 2 observed for SAHA. G1-G3 and R1-R3 are - grooves and ridges on the protein surface, respectively.

The absence of modification corresponding to the azido group oriented toward G3 in the pose 1 of probe **3** is consistent with its predominant solvent exposure and the fact that G3 is relatively deeper compared to G1 and G2. The sharper curvature of the surface near G3 prevents the remotely located aromatic azide moiety of probe **3** to contact with the

surface. These observations suggest that to improve the surface contact with G3 the introduction of a more flexible moiety between the linker and the SBG portions of the HDAC probes may be necessary.

3.4 Conclusion

This is the first study where the binding poses available to the probes in HDAC8 were determined experimentally by BEProFL approach. The tagging of the probe **3** attached to HDAC8 with BT **4** resulted in a concentration dependent increase in biotinylation of the protein with the increase of the concentration of probe **3** but not with probe **2** that lacks the second azido group. The selectivity of probe **3** for the active site of HDAC8 was demonstrated by blocking it with SAHA. Using the photoaffinity experiments we show that probe **3** modifies the HDAC8 binding site at or near Asp^{233} and Asp^{272}– the interface areas between G1 and R2 and R2 and G2 that can only be reached if probe **3** adopts at least two different binding poses. The results of MD simulations are consistent with these observations. Sharper curvature of the HDAC8 protein surface in G3 explains the lack of covalent modifications in it. The modifications observed at His^{142}-His^{143} and Ile^{135}-Asn^{136}-Trp^{137}-Ser^{138} are likely attributed to the "upside-down" binding pose of probe **3** analogous to that of TSA. The other few modifications of the HDAC8 protein on the side opposite to the binding site appear to be a result of aggregation with probe **3**. Although the three major poses available to SAHA and probe **3** are similar, they are not equally populated as determined by MD analysis. Overall, the findings demonstrated that multiple binding poses of the HDAC probes are

likely to contribute to the binding. Future studies are needed to learn how this observation can be used in HDAC drug design to improve the activity and selectivity of the probes.

The study also highlights further directions in refinement of the BEProFL approach. Minimization of the fragmentation of the probe is highly desirable to facilitate the analysis of MS/MS data. The source of non-specific tagging of the HDAC8 protein upon incubation with biotin tag remains unclear, warranting further investigation.

The methodology supplies a unique power in analysis of the binding of probes to their macromolecular targets by expanding the data typically obtained in the protein X-ray crystallography or providing an alternative tool when co-crystallization of the protein with the probe of interest has failed. Most importantly, the binding poses determined by BEProFL are determined in solution and, thus, the captured "snapshots" reflect the dynamic nature of the probe and its macromolecular target conformations. Extension of the BEProFL approach to study the binding poses of the probes in cells is in progress in our laboratory. The approach has the potential not only to guide probe optimization but also to become a new tool in disciplines such as molecular modeling, development, validation and application of computer-aided drug design methods, especially those for rapid prediction of the protein-probe interactions such as docking and scoring.[107]

CHAPTER 4 EXPLORATION OF INTERACTION BETWEEN HDAC3 AND ITS CO-REPRESSOR NCOR2

4.1 Introduction

Histone deacetylase 3 (HDAC3), an enzyme involved in gene transcription, requires the direct interaction with the Deacetylase Activating Domain of Nuclear Receptor Co-repressor 2 (NCoR2-DAD) to be activated, but the geometry and the structure of the protein-protein interface involved in this complex are unknown to date. In mammalian cells, HDAC3 is found as part of a large protein complex with Nuclear Receptor Co-repressors (NCoR2, or the homologous SMRT), GPS2, TBL1, and TBLR1.[121] Direct interactions with the deacetylase activating domain (DAD), a segment of approximately 80 amino acids in NCoR2 (or SMRT), is both required and sufficient for HDAC3 activation.[122, 123] Deacetylation activation domain (DAD) of NCoR functions in activating the HDAC3, while the histone interaction domain (HID) assists in anchoring the complex to the histone tail. In a synergistic fashion, components with distinct functions in the multiprotein complex work together to repress transcription.

Insights into structural details of this complex would be of interest, as this information may also provide an alternative avenue for the design of new therapeutics. The prospect is particularly attractive as selective inhibition of particular HDAC isoforms through substrate analogues that bind to just the active sites is difficult to achieve due to the high degree of sequence homology among different HDAC isoforms. Since most of the HDAC isoforms are found as a part of various types of complexes, the structures of these complexes might hold the key for successful rational design of selective HDAC

inhibitors. In this chapter, results were presented based on the concept of small photoreactive “nanorulers” that target both HDAC3 catalytic site and surface regions in NCoR2-DAD most likely involved in the protein-protein interaction and proposed a structural model that delineate some of the contact residues.

4.2 Methods and Materials

4.2.1 HDAC activity assay

10 ng HDAC3/NCoR-DAD (BPS Bioscience) was diluted with KI-311 (Enzo life) and preincubated with 30 μL of inhibitor for 5 min then 10 μL, 125 μM HDAC fluorescent substrate Boc-$_L$-Lys (Ac)-AMC (Chem-Impex) was added, and the mixture incubated for 30 min at room temperature. The reaction was quenched with 50 μL of 1 mg/mL trypsin and 4 μM trichostatin A in KI-143 (Enzo life) for 30 min. The plate was read on an POLARstar OPTIMA (BMG labtech) microplate reader at excitation wavelength 360 nm and emission wavelength 460 nm.

4.2.2 Photolabeling and competition experiment of HDAC3/NCoR2-DAD

Commercial recombinant HDAC3 (BPS Bioscience, CA) (0.5 μg in 5 μL of assay buffer or assay buffer with 0.1% triton X-100) was incubated with various concentrations of probe **2**, probe **3**, HD-55 and HD-74 with or without competent SAHA for three hours in the dark, after which the formation of a covalent bond between the azide group present in the probe and reactive side chains of the HDAC was initiated by UV irradiation (λ= 254 nm) for 3×1 min with 1 min rest. Then “click chemistry” was used to attach Biotin tag (BT) to the diazide probes attached covalently to the protein. The biotin tag was

added to all the tubes at a final concentration of 50 μM, and the chemical reaction was initiated by addition of TCEP (0.5 mM final concentration), TBTA (0.1 mM) and $CuSO_4$ (1 mM). After 60 min incubation at room temperature, protein samples were analyzed by SDS-PAGE and western blot using an anti-biotin primary antibody, streptavidin conjugated to horseradish peroxidase (Pierce, Rockford IL) and ECL (Pierce, Rockford IL).

4.2.3 MALDI-ToF and FT-ICR of HDAC3/NCoR2-DAD modified by diazide probes

HDAC3 protein was treated with HD-74 at the ratio of 1:1 to 1:10 and UV-irradiated to induce covalent cross-linking. The protein-probe complex was diluted with 50% methanol in water to make 2 μM as final concentration, mixed with saturated sinapic acid. 1 μL of the mixture was spotted onto a MALDI plate and air-dried before analysis. Positive ion MALDI TOF mass spectra were acquired using an Applied Biosystems (Foster City, CA) Voyager-DE pro MALDI-TOF mass spectrometer in linear mode. A total of 500 or more laser shots were acquired and signal averaged per mass spectrum.

Followed by photolabeling of HDAC3/NCoR2-DAD by photoaffinity probes, a tryptic digestion and peptide sequencing using microcapillary HPLC coupled with high resolution tandem mass spectrometry on an FTICR mass spectrometer was performed to find sites of photoaffinity modification of HDAC3 and NCoR2-DAD by the inhibitor. MassMatrix proteomics data analysis software was used to identify modified peptides with less than 10 ppm mass tolerance.

4.2.4 Homology model, docking calculations and surface analysis

All computational modeling was performed by Dr. Michael Brunsteiner. In brief, the program modeller[124] was used for building HDAC3 homology models. As templates a number of HDAC8 crystal structures were used (PDB IDs: 1T64, 1T67, 1T69, 1VKG, 1W22, 2V5W, 2V5X).[120, 125-127] Altogether these crystal structures contained coordinates of 12 HDAC8 monomers, and, based on these, 12 HDAC3 homology models, including residues 4-368, were built using the settings and parameters recommended in the modeler documentation.

ZDOCK and ZRANK,[128] two programs that have repeatedly been beneath the best performers in a Critical Assessment of PRedicted Interactions (CAPRI),[129] were used for docking of the NCoR2 DAD to HDAC3. The structure of the NCoR2-DAD was taken from an NMR structure containing 28 conformers of the domain, including NCoR2 residues 420-480 (PDBID: 1XC5).[130] Separate docking runs were performed with all combinations of the 12 HDAC3 and the 28 NCoR2-DAD structures, using a sampling interval of 6 degrees, resulting in about 18 million (12x28x54000) complexes. For each HDAC3/NCoR2-DAD combination the best ranking 2000 complexes were rescored using ZRANK. The overall 1000 best scoring complexes were then re-ranked a second time using Firedock, a program that takes into account limited protein flexibility when scoring protein complexes. For all calculations default parameters as recommended in the software manuals were used unless mentioned explicitly. The best 100 complexes were finally clustered, using the program kmlocal,[131] an implementation of the k-means algorithm.

For analysis of the surface residues of both the NCoR2-DAD and HDAC3 we used the program cons-PPISP,[132] online version of which is available at http://pipe.scs.fsu.edu/meta-ppisp.html. The program uses the output of three different web-servers for protein-protein interaction site prediction, [133-135] and based on this data calculates a consensus result from a linear regression model. The output provides a number for each residue that is proportional to the estimated probability of this residue for being part of, or close to, a protein-protein interaction site. The program Chimera[136] was used for visualization of molecules and surfaces.

4.3 Results and discussion

4.3.1 HDAC3/NCoR2-DAD modified by diazide probes reported by western blot

The results presented in Figure 24A showed that all three diazide probes successfully photocrosslinked to both HDAC3 and NCoR2-DAD. For HDAC3, this result was expected since the probe was bound to the HDAC3 active site at the time of photoactivation, which has been proved by the competitive binding of probe **3** and monoazide **2** (Figure 24B), probe HD-74 and probe 2 (Figure 24C), HD-74 and SAHA (Figure 25).

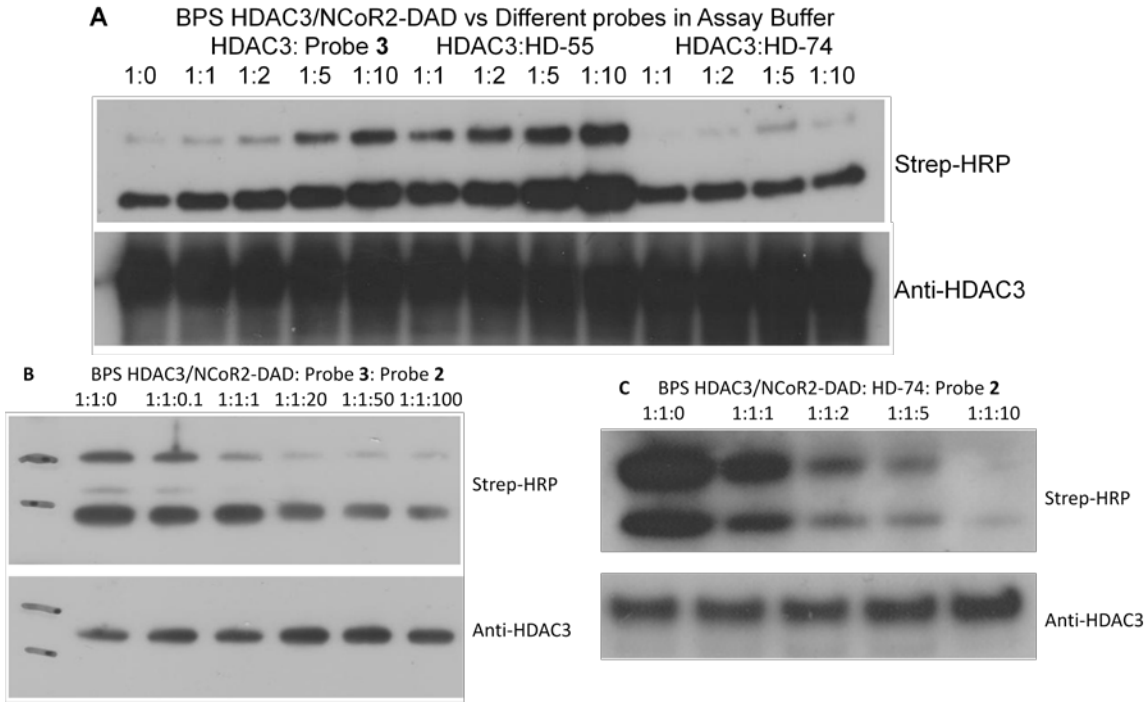

Figure 24: Photolabeling and competition experiment of HDAC3/NCoR2-DAD. *A:* Western blot analysis of dose-dependent photocrosslinking of probe **3,** HD-55 and HD-74 to HDAC3 and NCoR2-DAD visualized by strep-HRP, which binds to the biotin tag[107] covalently attached to the second azide group of the diazide probes via click chemistry. Equal protein loading was confirmed by anti-HDAC3 antibodies. *B:* Competitive binding of probe **3** with monoazide **2** shows a dose-dependent decrease in biotinylation of HDAC3 and NCoR2-DAD as **3:2** ratio increases. *C:* Same as B with diazide probe HD-74.

The specific modifications on HDAC3/NCoR2-DAD complex by photoaffinity probes were revealed by competitive binding of monoazide **2** or SAHA. When the binding pocket of HDAC3 was occupied by probe **2** or SAHA, it was unable to be accessed by BT. As a consequence; the protein-probe complex could not be identified by Strep-HRP and thereby resulting in a decrease of photolabeling signals.

The competition experiment presented in Figure 24 proved that photolabeling of HD-74 and **3** to HDAC3/NCoR2-DAD can be competed out by the adduction of monoazide probe **2**. The dose-dependent signal decrease manner of biotinylated HDAC3 was

visualized when the concentration of competing reagent was raised. Such dose-dependent pattern suggested that the monoazide probe binds to the same place as diazide probe does; however, it is not necessarily the active site of HDAC3. Therefore, another competitive experiment was conducted to confirm that the probes bind to the HDAC active site (Figure 25).

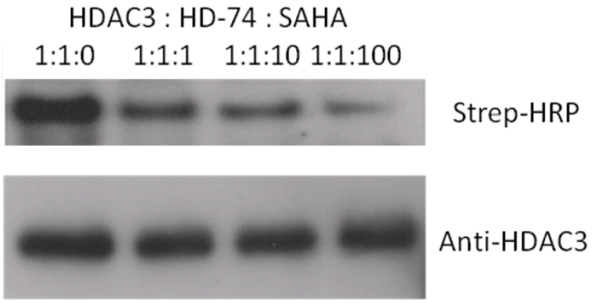

Figure 25: Competitive binding of HD-74 to HDAC3/NCoR2-DAD by SAHA

The HDAC3/NCoR2-DAD was incubated with HD-74 in a 1:1 ratio while the concentrations of the competitor--SAHA increased from 0 to 100 equivalents. The biotinylated HDAC3 signals declined in the blot as the increment of concentrations of SAHA, implying that SAHA and HD-74 were competing for the HDAC3 active site. Since SAHA is known to directly bind to HDAC3 active site, the photoaffinity probes specifically target to the same site as well.

On the other hand, binding to the NCoR2-DAD can only occur when the NCoR2-DAD is positioned within the reach of the UV-activated nitrene moiety of photoaffinity diazide probe free or bound to HDAC3. To decipher between these two possibilities and to exclude the possibility of non-specific binding to NCoR2-DAD, different concentrations

of HD-74 was incubated with NCoR2-DAD alone (Figure 26). The equal protein loading was assessed by coomassie staining.

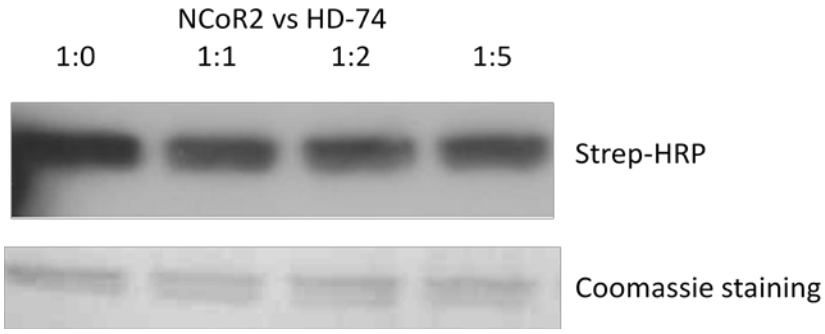

Figure 26: NCoR2 incubated with HD-74 reported by western blot.

The amount of HD-74 was increased as relative to the NCoR2 in the ratio of 0:1 to 5:1. As shown in Figure 23, no change in signal intensity of biotinylated NCoR2 was observed, thus implying that no interactions exist between NCoR2 and the photoaffinity probe. The signals detected may be attributed to the nonspecific binding of biotin tag to NCoR2. The results therefore suggest that probe HD-74 does not react in a dose-dependent manner with NCoR2 in absence of HDAC3.

To exclude the possibility of our probes non-specifically binding to the HDAC3/NCoR2-DAD, an inactive probe (Figure 16, probe **4**) was used on photolabeling with HDAC3/NCoR2-DAD (Figure 27, right panel). This probe adopts the same structure as HD-74, but was inactivated by removing the hydroxamate portion (IC_{50}> 66 μM).

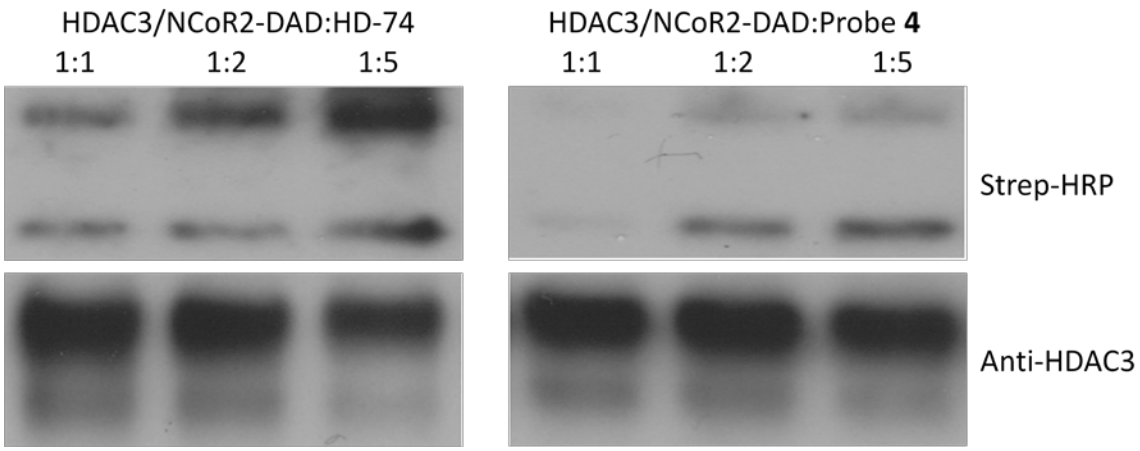

Figure 27: Comparison of photolabeling of active/inactive diazide probes

Similarly, the amount of probe **4** was increased from 0 to 5 equivalents of NCoR2. We observed no change in biotinylated HDAC3 signal intensity and a slight increase of biotinylated NCoR2 upon incubating with probe **4**. It indicated that probe **4** can slightly react with NCoR2-DAD but not with HDAC3 even at the higher molar ratio investigated. The interactions between zinc binding group (ZBG) on the probe and HDAC active site are required for the photolabeling. Therefore, we proved that the binding to NCoR2 is dependent on the photo-crosslinking to HDAC3. The signal intensity of biotinylated HDAC3 and NCoR2 decreased in a proportional manner in the competition experiment, thereby revealing that the NCoR2-DAD should be in close proximity to the HDAC3 binding site in order to be photocrosslinked by activated photoaffinity probes.

The biotinylated NCoR2 signal observed when probed with probe **4** may be attributed to the nonspecific binding of biotin tag to NCoR2. The NCoR2 and HDAC3/NCoR2-DAD were directly incubated with BT to evaluate the non-specific background noise (Figure 28).

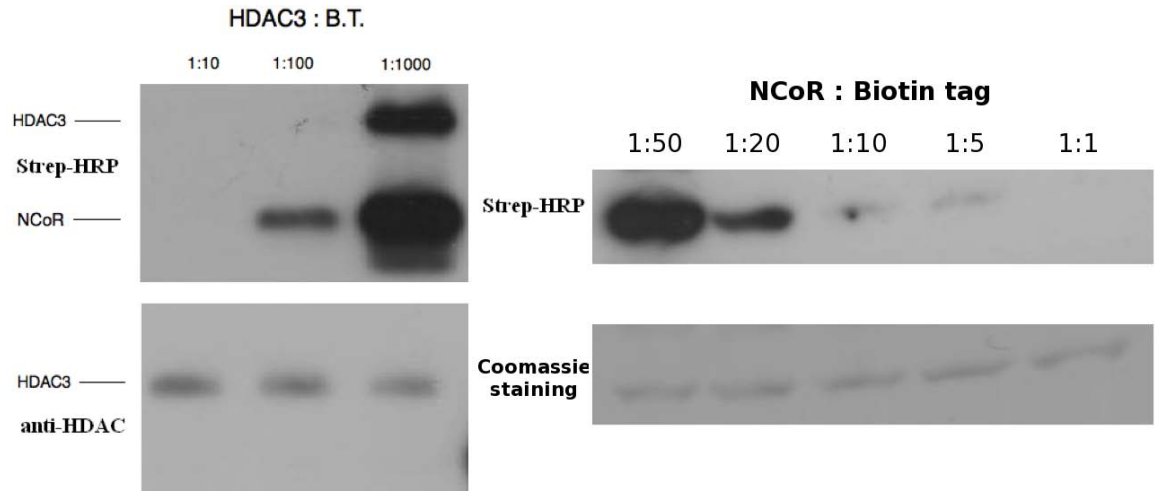

Figure 28: Nonspecific binding of B.T to NCoR2-DAD

As illustrated on the left panel of Figure 28, there was no background noise detected for HDAC3 until the protein-tag ratio reaches 1:100. On the right panel, when incubated with NCoR2, the background noises appeared at the ratio of 1:20. Therefore, the signal displayed in Figure 26 can be attributed to the nonspecific binding of BT to NCoR2.

4.3.2 MALDI-ToF analysis of HDAC3/NCoR-DAD photolabeling

Selective modification of HDAC3 and NCoR2-DAD by the photoaffinity labeling inhibitor was further confirmed using MALDI time-of-flight mass spectrometry (Figure 29). The HDAC3/NCoR2-DAD complex was incubated with HD-74 at different molar ratios of protein to probe, and the samples were UV irradiated as described in the supplemental material. In parallel incubations, HDAC8 was used as a control for non-specific modification by the probe. Modification of HDAC3/NCoR2-DAD by the photoaffinity probe was observed using positive ion MALDI mass spectrometry as a dose-dependent increase in protein mass.[137] There was little change in the mass of the

HDAC8 control due to the low affinity (IC_{50} = 650 nM) of the photoaffinity probe HD-74 for this protein (Figure 29). The ionization of intact ion was relatively low due to the high salt concentration in protein storage buffer and not enough matrix was used.

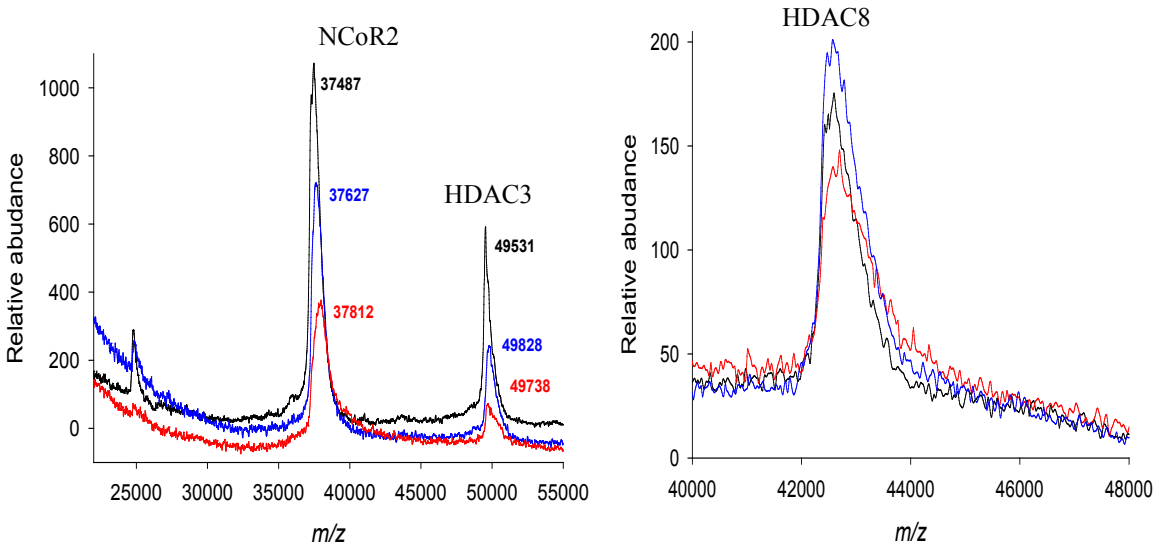

Figure 29: MALDI time-of-flight mass spectra of HDAC3/NCoR-DAD and HDAC8. The HDACs were incubated with the HD74 and UV irradiation at different molar ratios. HDAC: HD-74= 1:0 ; 1:5 ; 1:10 .

4.3.3 Tryptic peptide mapping and identification of modified HDAC3/NCoR2-DAD

After confirming that significant modification of HDAC3/NCoR-DAD-DAD occurred upon UV irradiation of the protein-inhibitor complex, we performed a tryptic digestion followed by peptide sequencing using microcapillary HPLC coupled with high resolution tandem mass spectrometry on an FTICR mass spectrometer to find the sites of photoaffinity modification of HDAC3 and NCoR2-DAD by the inhibitor. MassMatrix proteomics data analysis software was used to identify modified peptides with less than 10 ppm mass tolerance. Two NCoR2-DAD tryptic peptides (amino acids 407 to 424 and 444 to 461) and one HDAC3 tryptic peptide (amino acids 283 to 300) were found to be

modified by the photoaffinity probe at a protein/probe molar ratio of 1:1 (Table IX). Specifically, F409, F457, and amino acid residues between 420 and 424 (Figure 31) and between 455 and 458 were identified as modification sites of the NCoR2-DAD tryptic peptides. These covalently modified regions of NCoR2-DAD are located near the R426 and F444 surface interaction regions of DAD with HDAC3 that had been reported by Codina et al.[130] An amino acid residue between 293 and 297 of HDAC3, which lies in the probe binding region, was a modification site (data not shown). Not just one but two azide groups on the aromatic ring of photolabeling inhibitor HD-74 were found to be activated upon UV irradiation in 50% aqueous methanol solution resulting in formation of both water and methanol adducts. Therefore, two different activation events of azide groups by UV irradiation were considered to identify covalently modified HDAC3 and NCoR2-DAD peptides.

TABLE IX: SUMMARY OF IDENTIFIED HDAC3/NCOR2-DAD AND HDAC8 PEPTIDES MODIFIED BY HD74 (1:1 MOLAR RATIO).

Proteins	Peptide	Sequence (start-end)	$[M+H]^+$	m/z	Charge state	Mods by
HDAC3	SFNIPPLVLGGGGYTVR	283-300	2780.4	927.5	3	2B
NCoR2	IKFINMNGLMADPM*KVYK	406-423	3155.5	789.9	4	A+B +oxi M
	FM*QHPKNFGLLASFLERK	443-460	3196.6	640.1	5	2B +oxi M
HDAC8	No alkylated peptide found					

oxi M indicates oxidation of Met. Structures of A and B are shown in Figure 30.

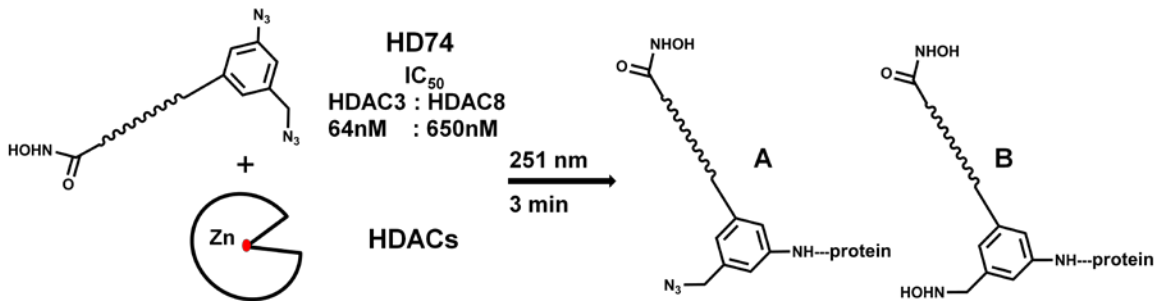

Figure 30: General structures of photoaffinity probe HD-74 after UV-irradiation.

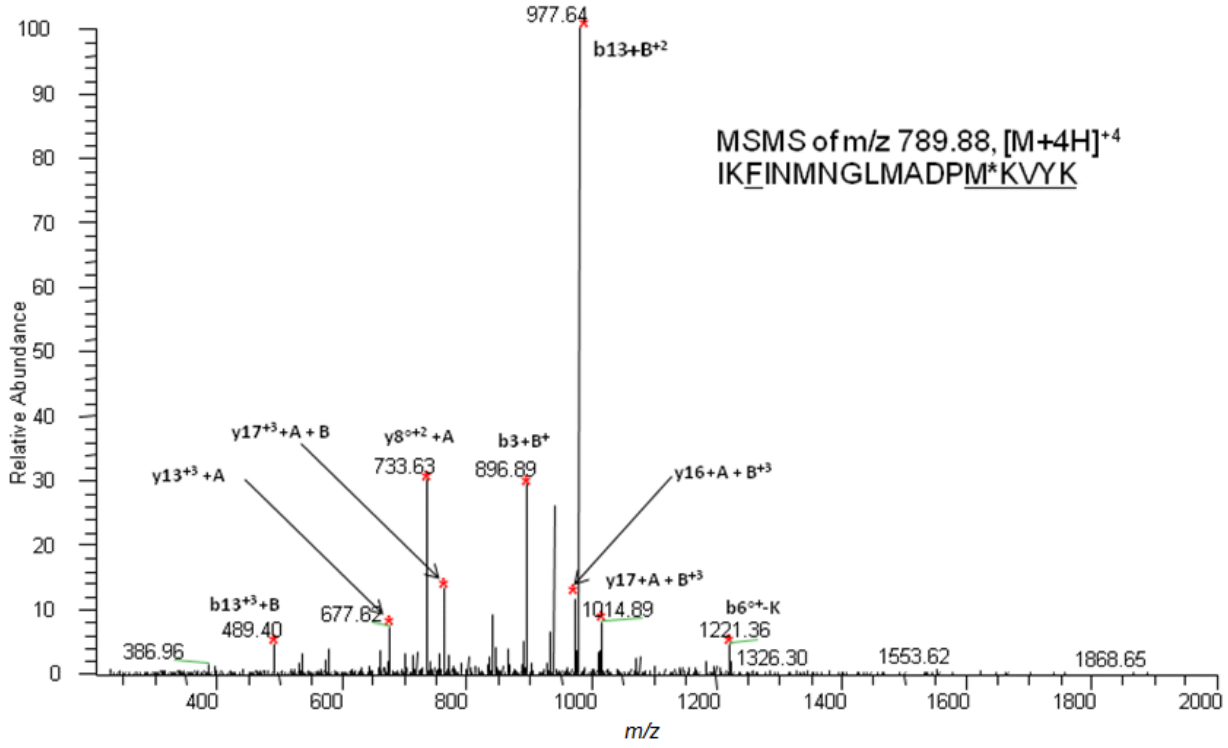

Figure 31: Product ion tandem mass spectrum of NCoR2 tryptic peptide. IKFINMNGLMADPMKVYK, showing alkylation at Phe and a residue among MKVYK. ^{o} and * denote neutral loss of H_2O and NH_3, respectively

4.3.4 Exploring with short diazide probe **5**

Encouraged by these results, we synthesized probe **5** (Figure 16) with a much shorter surface binding group (SBG). The experiments shown in Figure 24**A** were repeated for probe **5** (Figure 32). We found that despite the difference, probe **5** can still crosslink to both HDAC3 and NCoR2-DAD, suggesting that NCoR2-DAD is positioned no farther than roughly 7-8 Å from the entrance to the catalytic site.

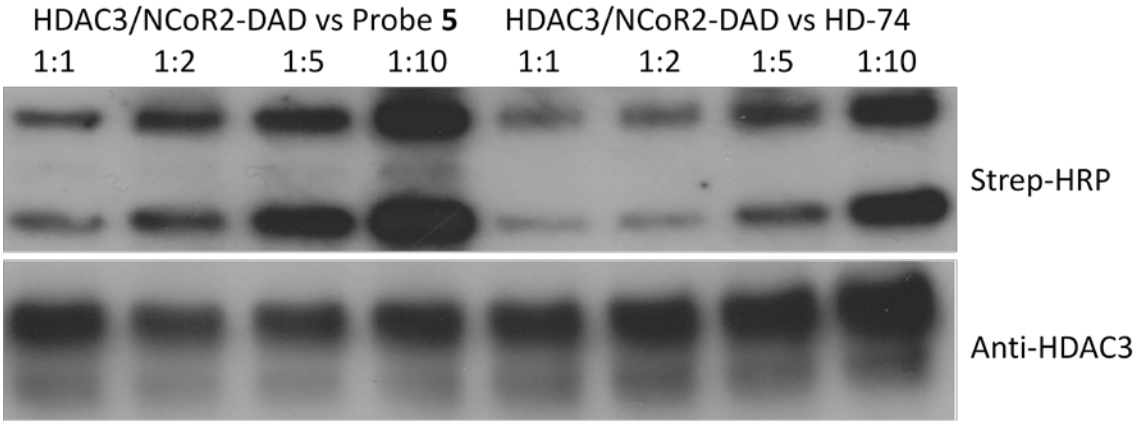

Figure 32: Exploration of HDAC3/NCoR2-DAD with short diazide probe **5**

4.3.5 Docking and computational modeling

In agreement with the experimental results and the surface analysis presented above, most high ranking solutions correspond to poses with the NCoR2-DAD located close to the HDAC3 probe-binding site (Figure 33). The centers of all clusters are shown in Figure 33A demonstrating that the majority (77%) of high ranking poses, and the biggest

clusters correspond to a location of NCoR2-DAD in groove 1 next to the HDAC3 binding site entrance.

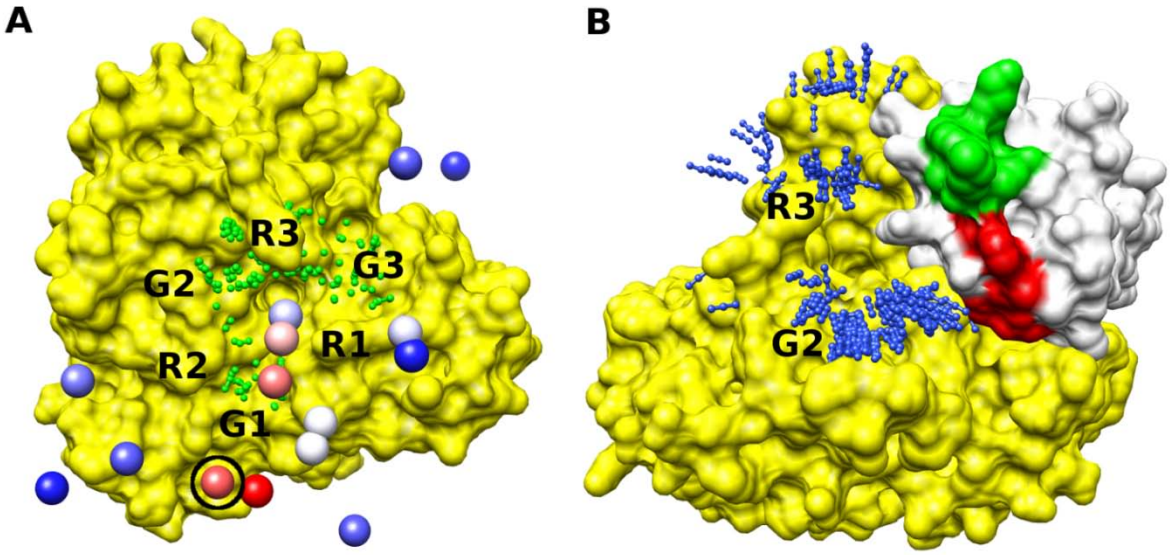

Figure 33: Location of NCoR2-DAD on the HDAC3 surface.
A: The results of docking calculations are shown as the centers of mass of 15 groups of NCoR2-DAD poses obtained from clustering of the 100 highest scoring NCoR2-DAD poses on the surface of an HDAC3 model. The size, N, of each cluster is indicated by the color, white (N=1) to red (N=17). Small green spheres indicate the possible locations of the reactive azide group obtained through docking of probe **5** to uncomplexed HDAC3 models. The grooves (G1-G3) and ridges (R1-R3) formed by the protein surface are designated similar to those for HDAC8.[107] *B*: An NCoR2-DAD pose that represents one of the largest clusters (black circle in Figure 33A) and complies with constraints from the Western blot and mass-spectrometry analysis. The two segments of NCoR2-DAD that were tagged by HD-74 (Table IX) are colored red and green respectively. Also, the triads of blue spheres shown are the reactive azide groups of HD-74 obtained by docking this compound to the uncomplexed HDAC3.

Diazide probe **5** was docked to multiple aligned HDAC3 structures using GOLD[138] and the coordinates of the reactive azide groups in the resulting poses were recorded. Exclusion of those NCoR2-DAD docking poses that either correspond to NCoR2-DAD

side chains extending into the binding site or show at least one of the two tagged regions (Table IX) being further away than 10 Å from any azide group left only six very similar poses, all members of one of the largest clusters identified. The center of mass of this cluster is highlighted in Figure 33A, and a representative pose is shown in Figure 33B.

4.4 Conclusion

The notable difference between experimental approaches commonly used to elucidate the details of the protein-protein interfaces (e.g. electrostatic analysis, point directed mutagenesis, or H/D-exchange) and the approach used in this study is that the latter can not only determine the interface between the proteins but also the relative orientation of the proteins and their accessibility by the inhibitors. We expect a combination of docking with experimental constraints as done here to provide an excellent means for generating hypothesis that can assist structure-based drug design when the target represents a protein-protein complex. Our work demonstrated the value of photoreactive probes for studying the structure of HDAC-containing complexes, and this approach can be readily extended to study other macromolecular complexes.

The results presented in this study showed that our combined approach can not only delineate the regions involved in the interface between two interacting proteins but also lead to structural models where the relative orientation of the proteins and their accessibility by small molecule inhibitors are defined. We anticipate that a combination of small molecule photoreactive probes/inhibitors acting as “nanorules” with docking and liquid chromatography-mass spectrometry analysis. We also envision that this approach can be enhanced to design even more sophisticated probes, e.g. “nanoprotractors”, to

stimulate further exploration of new chemical scaffolds and reactions and how they can be used in the study of protein-protein complexes in cell or animal models.

CHAPTER 5 EXPLORATION OF RELATIONSHIP BETWEEN IC_{50} AND PHOTOLABELING EFFICIENCY

5.1 Introduction

Photoaffinity labeling is often used to determine the site of probe incorporation within a protein. Phenyl azide-based photoprobes are widely used in photoaffinity-labeling studies. Therefore, understanding of the reactivity of aryl azide with amino acid analogs is important. Despite the widespread use of aryl azides as photoaffinity labels, there have been a few reports by us and others, utilizing a diazide containing probe in photoaffinity labeling. probeprobeIn our recent publication we developed the isoxazole- and pyrazole- based inhibitors with photoactive diazide groups.[139] After conducting a series of photolabeling experiments we realized that sometimes even potent photoreactive HDAC inhibitorsprobe gave poor yields of the photolabeled adducts.

There are many factors influencing the outcome of photoaffinity labeling. Although the potency of inhibitor is usually the main criteria to evaluate photoaffinity probes, several research groups mentioned that the photolabeling signal could not be solely ascribed to potency in protein binding.[140-142] Salisbury compared the specific HDAC labeling and inhibitory activities of 15 activity-based photoreactive probes with diverse structures and realized that the differences observed in proteome labeling among the various probes were not directly correlated with their respective affinities for HDACs.[140] They suggested that other factors, such as the location and orientation of the cross-linking moiety are critical for converting a tight-binding reversible inhibitor into optimal performing photoaffinity probe. Likewise, the binding affinity did not foretell

photolabeling efficiency of the 6 Lck photoprobes, instead, Kawamura[141] attributed photolabeling efficiency to conformational flexibility through structure-activity relationship (SAR) study. Similarly, Geurink[142] pointed that the inhibitory efficiency is not directly correlated to photoaffinity labeling and tentatively ascribe labeling efficiency to the close proximity of photoreactive group to amino acid nearby.

So far, no systematic study was conducted on the factors that affect the photolabeling efficiency of the HDAC photoreactive probes. Apart from probe binding and conformational flexibility, factors such as reactivity/specificity of the photoreactive group, non-specific photolabeling, efficiency of the click reaction, the ability of probes to correctly orient and covalently cross-linked to protein, the aggregation of probes/tags, accessibility of the reactive groups for click chemistry ligation, and availability of the biotin tag for recognition when using biotin tag as visualization reagent need to be considered. While the reactivity/stability of the photoreactive moiety during photolysis will be explored by other students/postdocs in Dr. Petukhov's group, a series of experiments were conducted in this thesis to explore probe potency, crosslinking efficiency, irradiation requirements and accessibility/ availability of the probes for visualization.

5.2 Methods and Materials

5.2.1 Synthesis of probes and tags

All the organic synthesis work was done by Dr. Raghupathi Neelarapu and Dr. Subash Velaparthi. The synthetic route for regular aromatic azide probe **2** and **3** was illustrated in our previous publication.[107] The strategy for the synthesis of pyrazole-

HD-55 and isoxazole-based HD-74 photoaffinity probe was identical to that we published previously.[139] Biotin tag linker group length was varied to evaluate the impact of accessibility for recognition of Strep-HRP on western blot. The long biotin analogue (LBT) was prepared as outlined in (Figure 34). A coupling reaction between biotin (6) and amine (7) using CDI in DMF gave (8). Deprotection of Boc-group of 8 using TFA followed by another coupling reaction with pentynoic acid using NMM, isobutyl chloroformate in DMF afforded LBT.

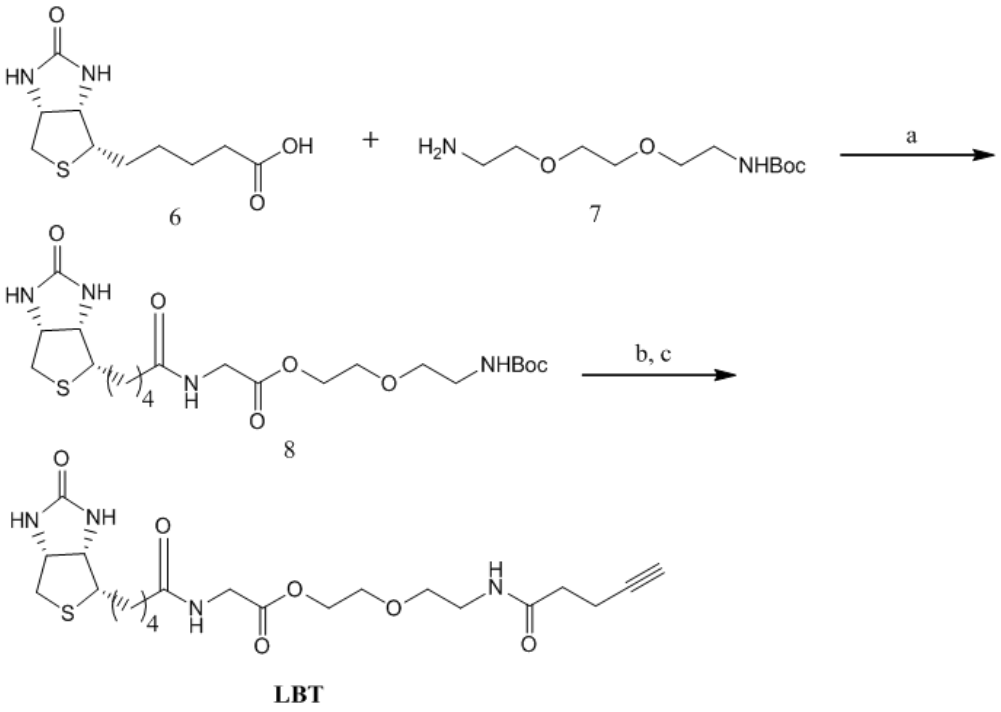

Figure 34: Synthesis of Long biotin tag (LBT)
Reagents and conditions: a) biotin, CDI, DMF, 0 °C-rt, 1 h, then 7, overnight; b) TFA, CH_2Cl_2, 0 °C-rt; c) pentynoic acid, NMM, isobutyl chloroformate, DMF, rt.

5.2.2 HDAC inhibitory assay

Three diazide photoaffinity probes were tested for inhibition of HDAC3 and HDAC8 isoforms, the general class I/II HDAC inhibitor suberoylanilide hydroxamic acid (SAHA) and trichostatin A (TSA) were tested as control. The procedure was identical to what was published before[107] except 0.1% triton X-100 was used as detergent to examine aggregation of probes. The inhibition of HDAC8 was measured using HM HDAC8 and acetylated HDAC substrate *Fluor de Lys* (BML-KI178, Enzolife), for HDAC3, commercial available HDAC3 (BPS bioscience, CA) and acetylated HDAC substrate (Boc-Lys-Acety, Chem-Impex) were used.

5.2.3 Enzyme kinetics study

The probes at various concentrations were tested to determine the type of inhibition on HDAC3 and gain insight into the mode of inhibitor binding. The inhibition profile of the probes was acquired when incubated with various predetermined concentration of substrate in assay buffer for 30 min. The reaction was quenched for 30 min and read on Optima micro-plate reader. The Lineweaver-Burk plot was generated and model of HDAC inhibition by different probes was confirmed by non-linear regression analysis of data using Graphpad Prism 5.0 (Graphpad software Inc. CA).

5.2.4 Photolabeling of diazide probes to HDAC3 and HDAC8

Recombinant human HDAC3/NCoR-DAD or HM HDAC8 (0.5 μg in 5 μL of assay buffer or assay buffer with 0.1% triton X-100) was incubated with various concentrations of probe **3**, HD-55 and HD-74 with or without competent SAHA for three hours in the

dark, after which the formation of a covalent bond between the azide group present in the probe and reactive side chains of the HDAC was initiated by UV irradiation (λ= 254 nm) for 3×1 min with 1 min rest. Then "click chemistry" was used to attach BT to the diazide probes attached covalently to the protein. The biotin tag was added to all the tubes at a final concentration of 50 μM, and the chemical reaction was initiated by addition of TCEP (0.5 mM final concentration), TBTA (0.1 mM) and $CuSO_4$ (1 mM). After 60 min incubation at room temperature, protein samples were analyzed by SDS-PAGE and western blot using an anti-biotin primary antibody, streptavidin conjugated to horseradish peroxidase (Pierce, Rockford IL) and ECL (Pierce, Rockford IL). In order to evaluate the effect of certain click-chemistry catalyst on photolabeling efficiency, different combinations of catalyst were applied after UV-irradiation and analyzed on western blot.

5.2.5 Direct measurement of modification by MALDI-ToF

HDAC protein was treated with different diazide probes at the ratio of 1:1 to 1:20 and UV-irradiated to induce covalent cross-linking. The protein-probe complex was diluted with 50% methanol in water to make 2 μM as final concentration, mixed with saturated sinapic acid. 1 μL of the mixture was spotted onto a MALDI plate and air-dried before analysis. Positive ion MALDI TOF mass spectra were acquired using an Applied Biosystems (Foster City, CA) Voyager-DE pro MALDI-TOF mass spectrometer in linear mode. A total of 500 or more laser shots were acquired and signal averaged per mass spectrum.

5.2.6 Effect of biotin length on photolabeling

The isoxazole-containing probe HD-74 was preincubated with HDAC3/NCoR-DAD or HDAC8 for 3 hours, UV irradiated and mixed with click chemistry catalyst and two different biotin tags: regular biotin tag or longer version of biotin tag. Allow 1 hour for click chemistry cycloaddition and the reaction mixture was then separated on SDS-PAGE and probed by Strep-HRP.

5.3 Results and discussion

5.3.1 Inhibitory potency and detergent effect

Many studies have demonstrated that most of hits found in high throughput screening are due to the promiscuous inhibition by colloid-like aggregates of the small molecule.[143-147] The particles are usually formed in the aqueous buffer, leading to the nonspecific inhibition of enzymes.[148] It was reported that at 30 μM, up to 19% of "drug like" molecules can form aggregates.[149] Even at concentrations as low as 5 μM, about 1-2% of "drug like" molecules still tend to aggregate. This is not trivial, since the hit rate of HTS itself is usually less than 1%.[149] At the same time, the aggregation of photoaffinity probes is likely to yield stronger photolabeling signals when probed with strep-HRP on western blot. In order to preclude the possibility that the inhibitory potency of our probes for HDAC proteins was aggregation-based nonspecific inhibition, we adopted non-ionic detergent to explore the potential aggregation of our probes. 0.1% Triton X-100 detergent was applied in HDAC acitivity assay during the IC_{50} screenings. The probe **3**, HD-55, HD-74 and SAHA were tested in HDAC assay buffer in the presence of 0.1% triton X-100 detergent following the same protocol against HDAC3 and

HDAC8 (Section 3.2.1). The inhibitory activity of three diazide probes and SAHA tested in detergent was compared with which in assay buffer and data was listed in Table X.

TABLE X: COMPARISON OF INHIBITORY ACTIVITY (IC_{50}, MM) OF SAHA, PROBE **3**, HD-55, AND HD-74 AGAINST HDAC3/8 IN HDAC ASSAY BUFFER AND DETERGENT

HDAC3/A.B.	IC50 (μM)	SD (μM)	Ki (μM)	**HDAC3/D.T.**	IC50 (μM)	SD (μM)	Ki (μM)
SAHA	0.05	0.00	0.04	SAHA	0.05	0.00	0.04
Probe **3**	4.13	0.04	1.41	Probe **3**	0.37	0.01	0.13
HD-55	0.39	0.03	0.28	HD-55	0.20	0.01	0.15
HD-74	0.08	0.01	0.03	HD-74	0.07	0.01	0.02
HDAC8/A.B.				**HDAC8/D.T.**			
SAHA	0.24	0.02	0.24	SAHA	0.30	0.00	0.30
Probe **3**	2.87	0.06	2.86	Probe **3**	0.80	0.02	0.80
HD-55	0.06	0.00	0.06	HD-55	0.05	0.00	0.05
HD-74	1.04	0.04	1.04	HD-74	1.20	0.14	1.20

A.B.: HDAC assay buffer
D.T.: Detergent in HDAC assay buffer

In the assay buffer, among three probes, probe **3** inhibited HDAC8 and HDAC3 with the lowest potency. HD-55 exhibited the highest potency inhibiting HDAC8 whereas HD-74 was the most active inhibitor for HDAC3. On the other hand, SAHA showed comparable inhibitory activity on both HDAC3 and HDAC8.

Compared to the data acquired in the HDAC assay buffer, there was no significant IC_{50} value change observed (within 2 fold difference) among SAHA, HD-55 and HD-74 for HDAC3 and HDAC8. However, IC_{50} of probe **3** determined with HDAC3 in assay buffer has decreased by about 10 fold after introduction of detergent. Similarly, for HDAC8, the

IC_{50} value of probe **3** in the detergent was about three to four fold lower than which was tested in assay buffer.

Unlike promiscuous inhibitors, our probes did not lose their inhibitory potency for HDACs upon application of detergent. In fact, the HDAC inhibitory potency of probe **3** became more pronounced while assayed in detergent. This is to be expected because like the other two probes, probe **3** is confirmed to be an HDAC competitive inhibitor (data shown in section 5.3.4) as well. The aggregation of the specific inhibitor lowered the nominal concentration of free inhibitor in solution. While enzyme activity was similar after introduction of detergent (data not shown), the detergent separates the aggregates, increases the amounts of free inhibitors in the solution, and lowers the IC_{50} values as a consequence. Therefore, by comparing the IC_{50} values of three diazide probes and SAHA in the assay buffer with or without detergent, we can gain some insight into the aggregation of inhibitors under the similar conditions used in the photolabeling assay. Probe **3** is more prone to aggregate than SAHA and other two diazide probes and it is more likely to yield higher than usual photolabeling signal on western blot.

5.3.2 Photolabeling efficiency on HDAC3 and HDAC8

The photolabeling in aqueous buffer usually suffered non-specific binding and resulted in a high background signal.[150] The photolabeling of HDAC8 by probe **2** and **3** was illustrated in Figure 18, panel A and the photolabeling of HDAC3 by probe **3**, HD-55 and HD-74 was shown in Figure 24, panel A. There was strong biotinylated HDAC8 signal shown even when HM HDAC8 was incubated with biotin tag alone, whereas there was almost no signal observed for HDAC3 at similar condition, indicating the possible

aggregation of biotin tag with HDAC8 but not with HDAC3. Therefore, the detergent was applied to explore the effect of aggregation of biotin tag brought to photolabeling of HDAC8 (Figure 35).

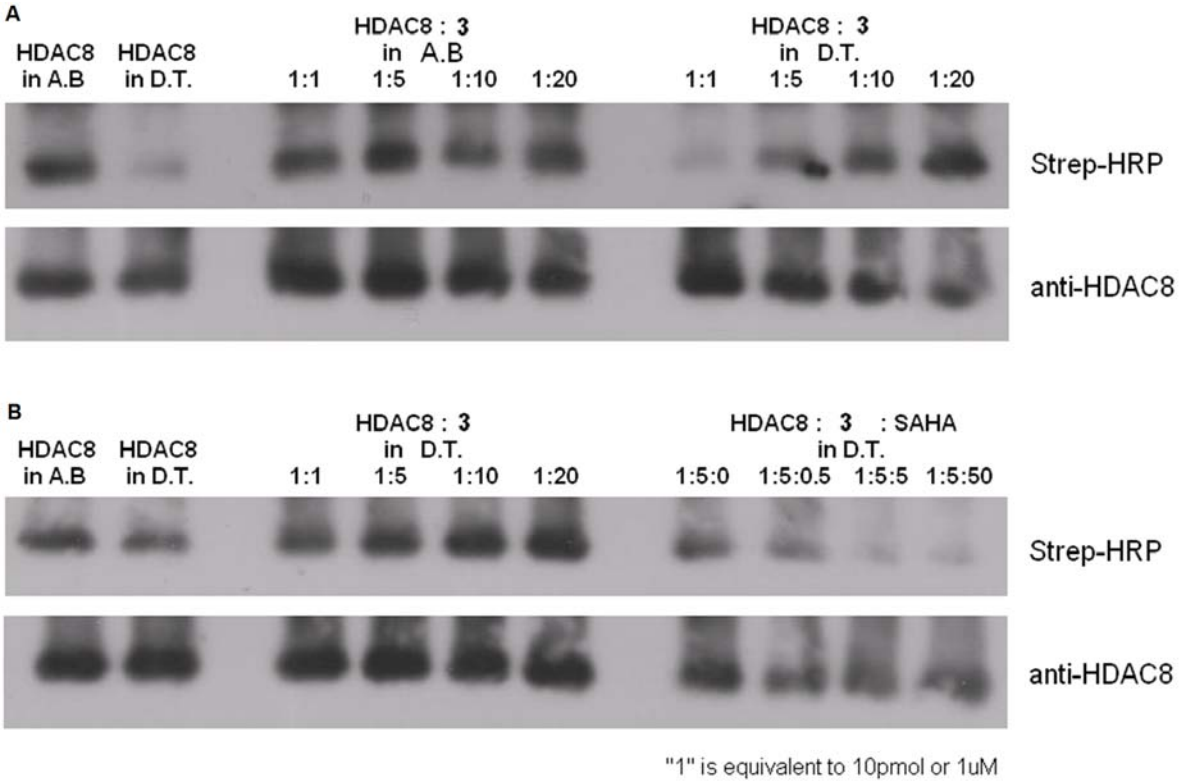

Figure 35: Detergent effect on photolabeling of HM HDAC8

The leftmost bands in Figure 35 illustrated that even in absence of photoaffinity probes, the incubation of HDAC8 with biotin tag alone yielded strong bands, indicating that the aggregation of biotin tag in assay buffer could be recognized by anti-biotin antibody. Similarly, when photolabeling performed in assay buffer, as shown in Figure 35 panel A, the modification of HDAC8 by photoaffinity probes was shielded by the background noise and there was no significant signal increase when amount of probe **3** increased from

1 to 20 equivalent of HDAC8 protein. On the other hand, dose-dependent increase pattern re-emerged when photolabeling performed in detergent. This pattern was reproduced in Figure 35 panel B. Furthermore, after the introduction of detergent, while keeping probe **3** constant, blots intensity decreased in a dose-dependent manner by raising the competition reagent SAHA concentration. The addition of non-ionic detergent separated the biotin tags and reduced background noise. This observation led to the conclusion that our diazide photoaffinity probe **3** could specifically modify HDAC8 and binds to the same sites as SAHA, and we should have detergent included in the assay buffe in order to get more accurate photolabeling signal of HDAC8.

To evaluate the photolabeling efficiency between three diazide probes, the photolabeling of HDAC3 and HDAC8 was performed in assay buffer and detergent, respectively. The data was shown in Figure 36.

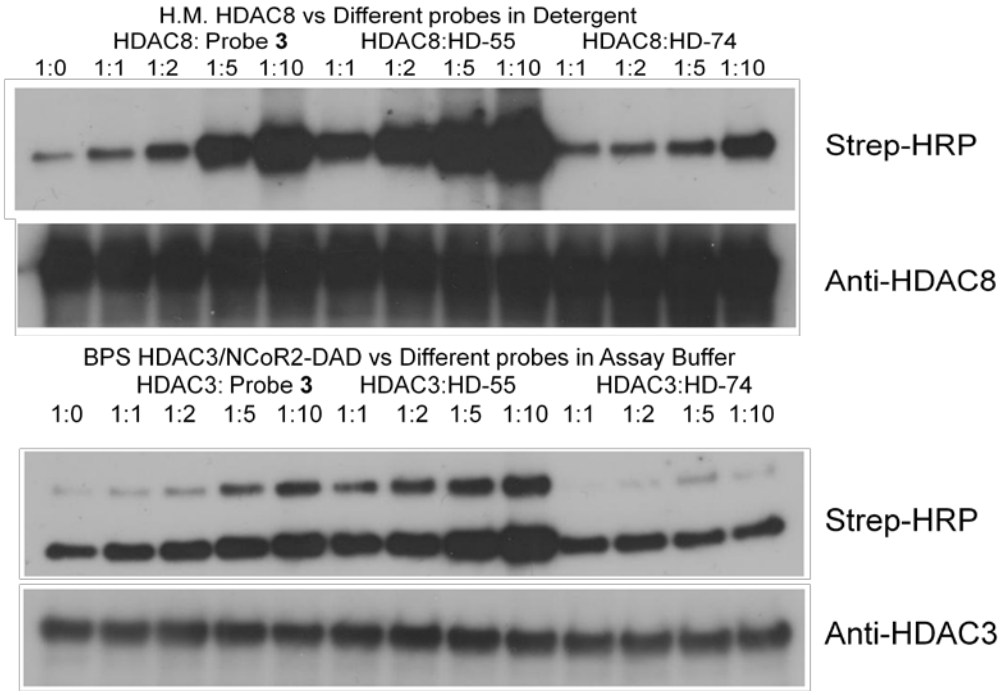

Figure 36: Photolabeling of three diazide probes to HDAC3/8 and visualized by biotin tagging

The pyrazole-containing diazide HD-55 displayed highest band intensity for both HDAC3 and HDAC8 while isoxazle-containing HD-74 always the weakest. There is clearly discrepancy between the order of probe inhibitory potency and band intensity: for HDAC3, HD-74 is much more potent than HD-55 and probe **3** while the blot intensity is the weakest. Similarly, for HDAC8 in detergent, the similar potency of HD-74 and probe **3** disagreed with the much thinner blot size of HD-74.

5.3.3 Aggregation of biotin tag and background noise

The non-specific labeling of HDAC by biotin tag alone would contribute to photolabeling outcome as illustrated in 5.3.2. The effect of biotin tag concentration on background noise was thus explored (Figure 37). 10, 100 and 1000 equivalents of biotin tag was incubated directly with HDAC3 or HDAC8 protein followed by SDS-PAGE and

western blotting. Since no probe introduced in this study, the signal shown on blots was solely resulted from non-specific labeling of biotin tag. As shown on Figure 37, HDAC8 had stronger background than HDAC3 at the same biotin concentration as expected. At 1:50 of the protein:biotin ratio applied in this work, the detergent should be used for HDAC8 to reduce the background noise results from biotin aggregation.

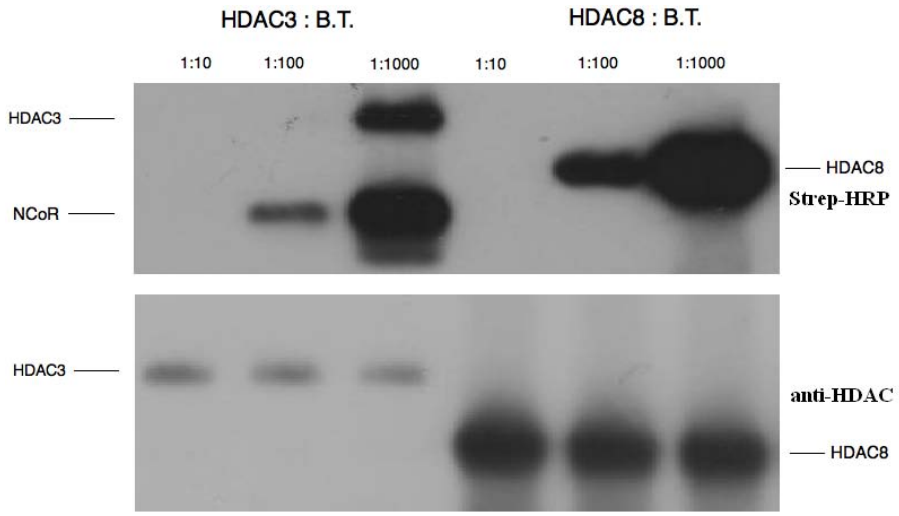

Figure 37: Non-specific background noise with respect of tagging concentration.

The background noise of photolabeling could be ascribed to non-specific interaction with click-chemistry catalyst, therefore, the effect of catalyst and UV-irradiation were explored while maintain the biotin tag concentration constant. In the panel A of Figure 38, no signal was detected under the condition in the absence of the catalyst regardless UV irradiation. On the other hand, strong signal was observed in the reaction mixture after incubating with click-chemistry catalyst, even without UV-irradiation. It is clear that the

UV-irradiation has little to do with non-specific photolabeling signal while the catalysts are responsible for background noise. To further understand the role of different catalysts in generating photolabeling signal, varies of combinations of catalysts were applied as shown in Figure 38 panel B. Similar to panel A, the UV-irradiation or not did not make significant difference in background noise. There was no background signal shown except TCEP and $CuSO_4$ were both applied. TBTA stabilizes the Cu^{+1} ion generated from $CuSO_4$ and TCEP, since Cu^{+1} catalyzes the click-addition of biotin tag to diazide probe, as predicted, the higher background noise is observed after introduction of TBTA.

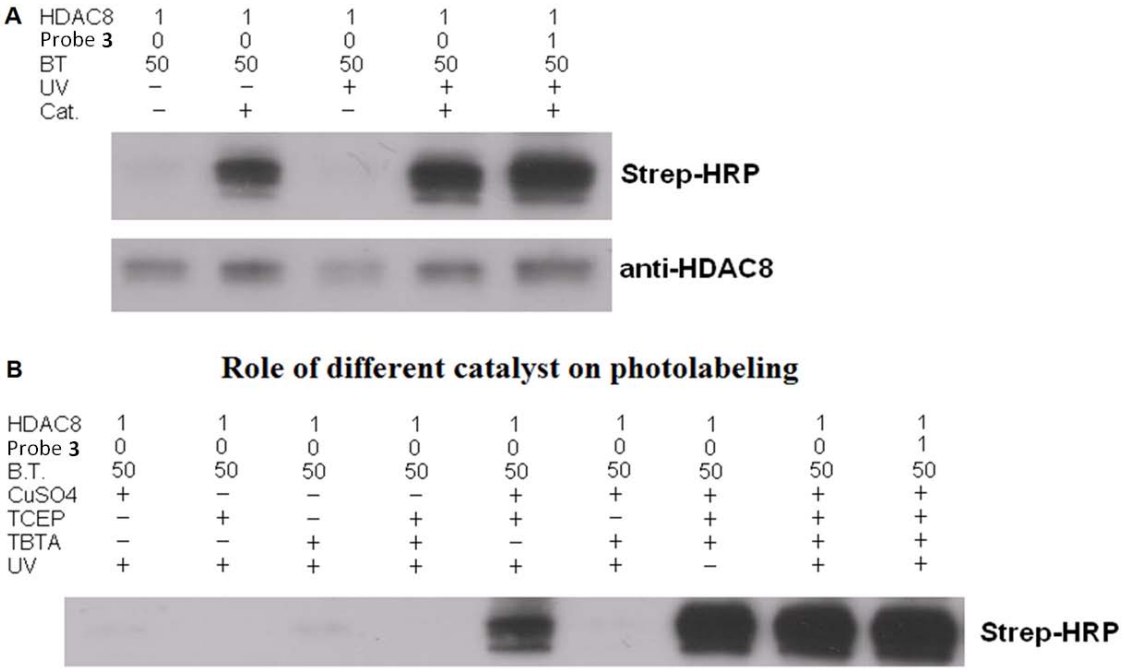

Figure 38: Exploration of different click-chemistry catalysts in photolabeling background noise

5.3.4 Enzyme kinetics study

The type of inhibition of HDAC enzyme by photoaffinity probes determines where and how the probes interact with HDAC, therefore, the enzyme kinetics is of critical importance to understand the probe binding and photolabeling. Hydroxamic acid based HDAC inhibitor trichostatin A was reported to be a noncompetitive inhibitor for HDACs[151, 152], implying that it acts at a site other than HDAC catalytic site. However, the crystal structure of HDAC8 complexed with TSA and SAHA, showed that these inhibitors fit into the catalytic site of protein, suggesting that they are competitive inhibitors as well.[120] Sekhavat et al demonstrated that TSA and butyrate are competitive inhibitors for HDACs through HDAC assays and enzyme kinetic studies.[153] In this study, we investigated the interactions between the diazide probes and HDAC3 protein, and provided the evidence that SAHA and three diazide probes all act as competitive inhibitors for HDAC3. A kinetic analysis of SAHA and three probes inhibition of HDAC activity were performed (Figure 39). The test results were shown in a Lineweaver-Burk plot (*1/V versus 1/S*).

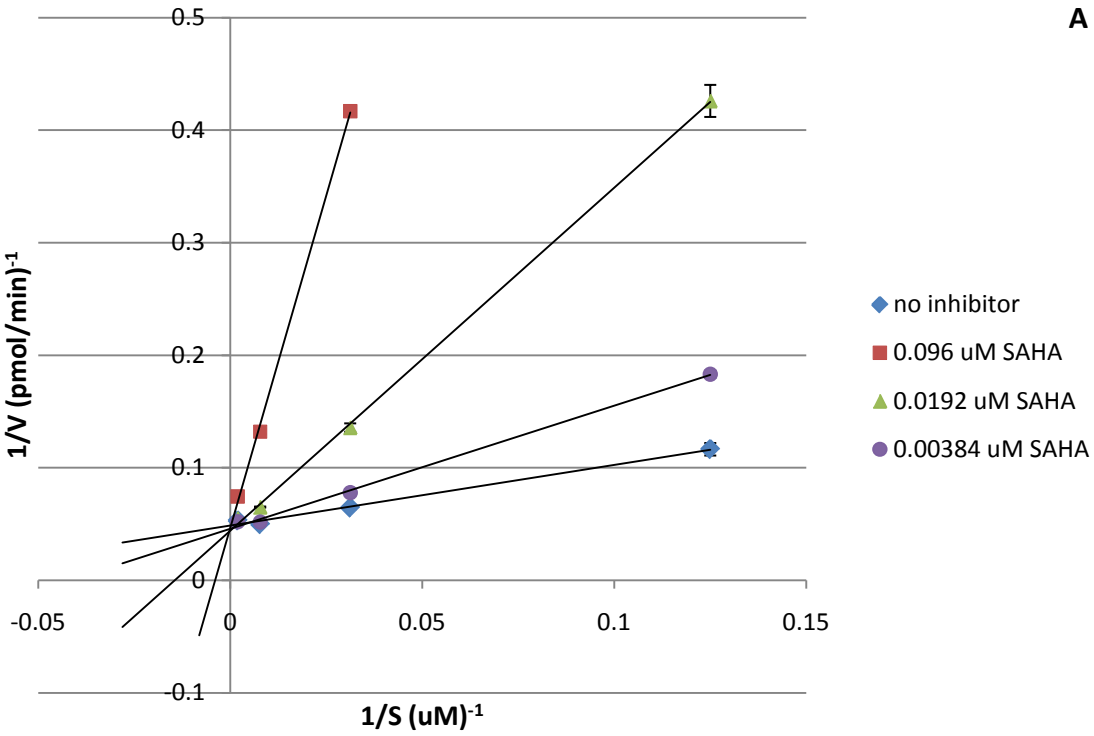
A
0.5
0.4
0.3
0.2
0.1
0
-0.1
-0.05
0
0.05
0.1
0.15
1/V (pmol/min)-1
1/S (uM)-1
no inhibitor
0.096 uM SAHA
0.0192 uM SAHA
0.00384 uM SAHA

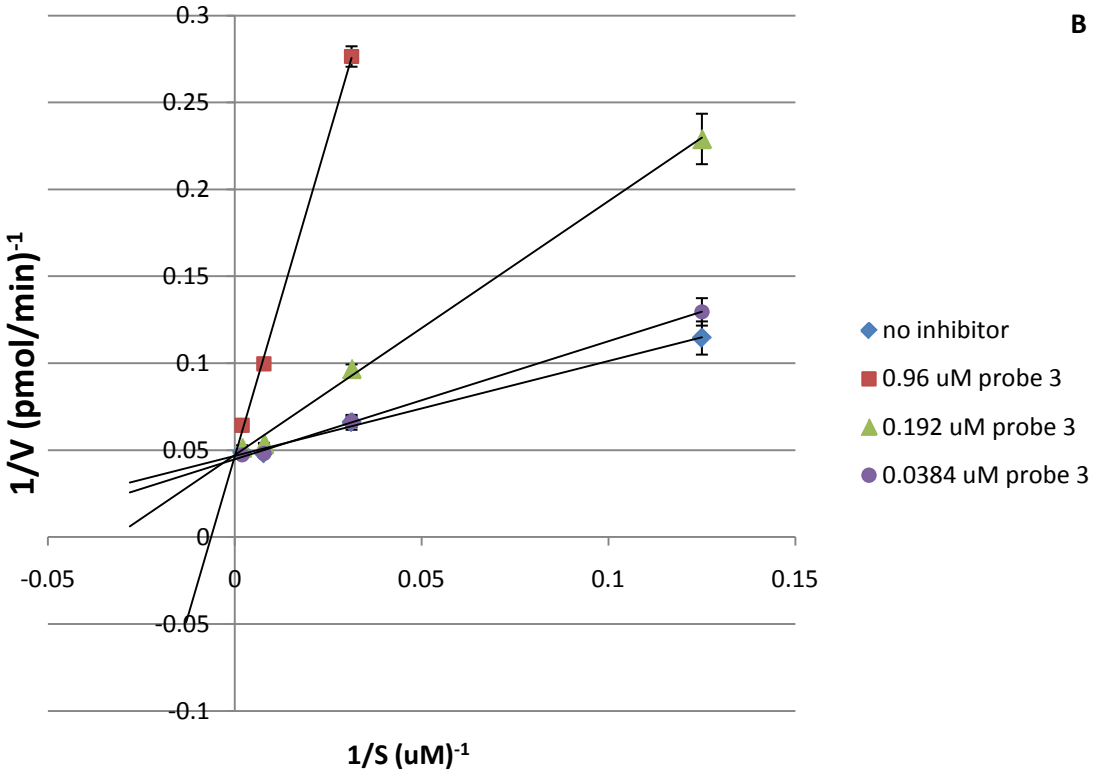
B
0.3
0.25
0.2
0.15
0.1
0.05
0
-0.05
-0.1
-0.05
0
0.05
0.1
0.15
1/V (pmol/min)-1
1/S (uM)-1
no inhibitor
0.96 uM probe 3
0.192 uM probe 3
0.0384 uM probe 3

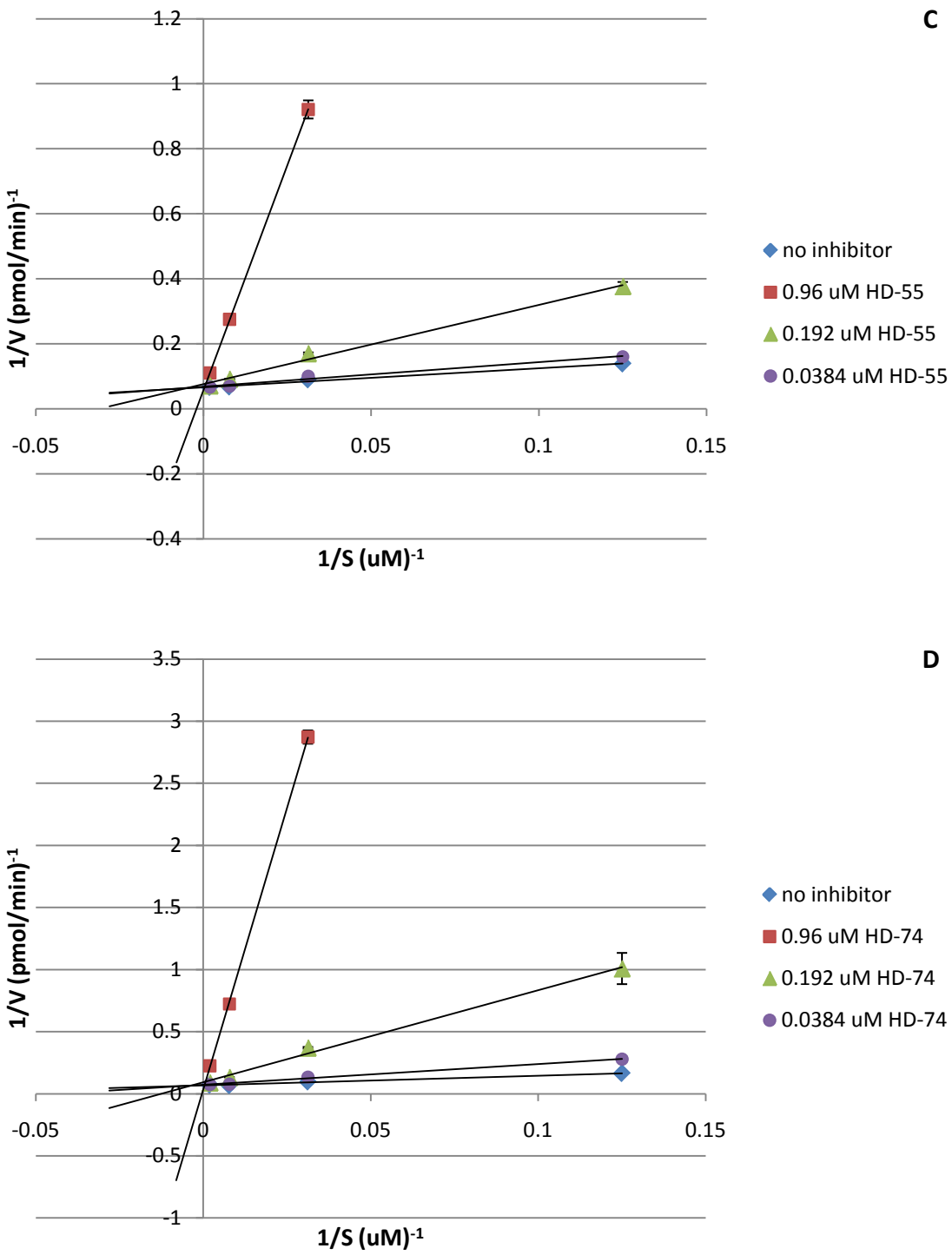

Figure 39: Kinetic analysis of HDAC3 inhibition by SAHA, probe **3**, HD-55 and HD-74. (A): HDAC3 activity in the presence of 0 (◆), 3.84 nM (●), 19.2(▲) and 96 nM (■) of SAHA is presented as a Lineweaver-Burk plot. (B, C, D) HDAC3 activity in the presence of 0 (◆), 38.4 nM (●), 192(▲) and 960 nM (■) of probe **3**, HD-55 and HD-74 is presented as a Lineweaver-Burk plot. Standard error of the mean is presented.

As shown in Figure 39, the *y* intercepts appeared similar with the concentrations of probes being increased, implying the presence of probes did not affect V_{max}. All three diazide probes as well as SAHA are competitive HDAC inhibitor utilizing hydroxamic acid to chelate the zinc ion in the active site of HDAC, and this interaction becomes a prerequisite of photolabeling.

5.3.5 MALDI-ToF direct measurement of protein modification

Matrix-assisted laser desorption ionization time-of-flight technique (MALDI-ToF) is a soft ionization technique used in mass spectrometry for analysis of biomolecules (biopolymers such as proteins, peptides and sugars), which tend to be vulnerable to fragmentation when ionized by conventional ionization methods. A laser beam is used for triggering ionization and a matrix is used to protect the protein from being destroyed by direct laser beam and to facilitate vaporization and ionization. In such way, MALDI-ToF measures the total mass of intact peptide or protein.[154] Similarly, MALDI-ToF could be utilized to examine mass shift of modified protein due to the covalent modifications by photoaffinity probes. The more probes labeled, the higher mass shift would be yielded. Noticeably, since the molecular weight of probes is different, at the same ratio of labeling, the mass shift will be different. However, considering the limited resolution of MALDI-ToF mass spectrometry in the range between 15 and 70 kD as well as the heterogeneity of sample prepared, quantitative analysis of probes photolabeled to protein would be difficult.[155] Therefore, MALDI-ToF-MS here in this study was adopted to qualitatively compare molar fraction of HDAC3/8 modified by three diazide probes, the standard deviation between measurements of the same probe should be considered to

determine whether there is significant difference between probes. The mass shift of modified HDAC compared with native HDAC protein was shown on Table XI.

TABLE XI: MASS SHIFT OF HOMEMADE HDAC8 MODIFIED BY DIAZIDE PROBES

Mass shift	**1:1**		**1:5**		**1:20**	
	avg.	sd.	avg.	sd.	avg.	sd.
Probe **2**	4	41.3	113.5	37.1	256.8	37.1
Probe **3**	3	15.4	13.2	7.5	60.1	77.6
HD-55	6.4	11.8	42.7	23.9	406.5	17.2
HD-74	6.4	11.8	10.9	15.7	15.5	10.4
HDAC8 alone	42799.8	9.8				

The mass shift increased in a dose-dependent manner as probe concentration. Mass shift of HD-55 is the highest among three diazide probes while HD-74 the lowest. This agrees with our observation of IT-ToF probe stability data. HD-55 is the most active probe upon UV-irradiation, therefore, the highest amount of HD-55 could be labeled to HDAC protein nearby leading to highest mass shift.

5.3.6 Effect of B.T length on photolabeling

In order to complete click-chemistry attachment, the aryl azido group on the probe has to be accessible by biotin tag. To explore the accessibility of acryl azido group, the longer version of biotin tag was synthesized and applied in photolabeling of HDAC3 and HDAC8. Different concentration of HD-74 was cross-linked with short and long biotin tags for comparison (Figure 40).

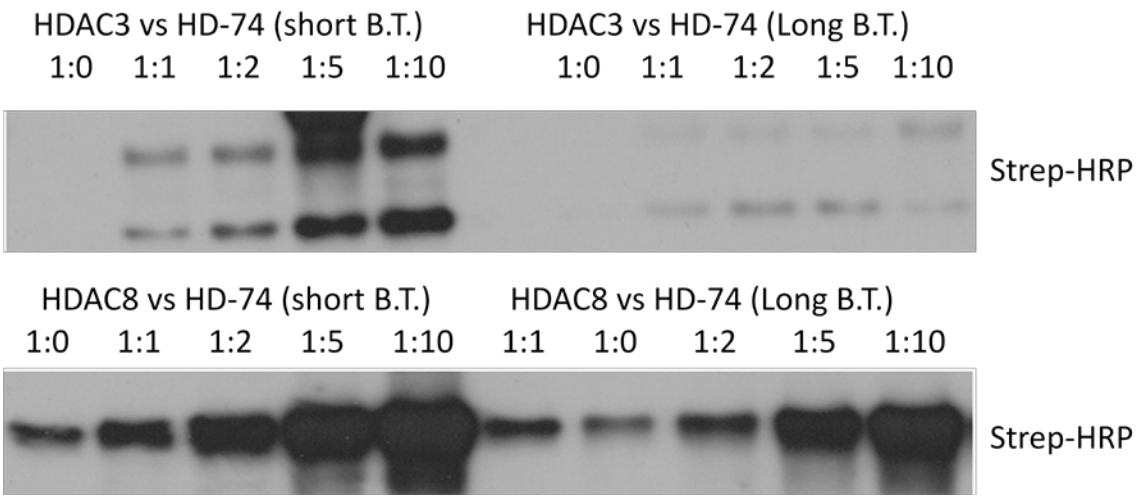

Figure 40: Effect of biotin tag on photolabeling

Similar to the study performed for HDAC8, the regular (short) biotin tag exhibited stronger signal for HDAC3 than the longer version. This may be attributed to the higher energy barrier of longer tag to rotate due to the steric hindrance effects, which prohibits the intermediate state from formation. In conclusion, a shorter biotin tag is advantageous in enhancing photolabeling efficiency.

5.4 Conclusion

We recently developed several potent photoreactive probes for HDAC8 and other isoforms.[107, 139] Since photolabeling efficiency of probes is critical for photolabeling and there is no systematic research exploring it, we decided to identify the major factors affecting the photolabeling efficiency. To answer this question, three diazide probes with different scaffold – regular aromatic ring, isoxazole- and pyrozole- were compared. Through enzyme kinetics study, inhibitor activity assay, biotin length exploration, in-vitro photolabeling and competition experiment, IT-ToF and MALDI-ToF mass spectrometry direct measurement of modification and photoreactive moiety stability, we

systematically investigated photolabeling efficiency of photoaffinity probes and possible influential factors.

When the activity assay was performed in assay buffer, SAHA and all diazide probes exhibited promising potency for HDAC3 and HDAC8. Probe **3** has the lowest potency for HDAC3 and HDAC8, HD-55 ranks the best for HDAC8 while HD-74 is the best inhibitor for HDAC3. Upon introduction of detergent, the decrease of IC_{50} value of probe **3** for both HDAC3 and HDAC8 implied that the addition of detergent separates the aggregates and increases the free probe **3** concentration in solution. Probe **3** is prone to aggregate under the condition of photolabeling, therefore, probe **3** is tend to yield higher photolabeling signal than usual.

In kinetic study performed against HDAC3, the V_{max} determined in Lineweaver-Burk plot with or without probes was very similar to each other. The modification on the linker and surface binding group of SAHA did not change the type of inhibition and all three diazide probes were confirmed to be competitive inhibitor for HDAC3. The probes compete with substrate for binding to active site of HDAC3.

In photolabeling experiment, the application of detergent separated biotin aggregation and significantly reduced background noise. With the help of detergent, the dose-dependent photolabeling signal change was observed while varying photoaffinity probe concentration or SAHA concentration. Therefore, the influence of biotin aggregation needs to be taken into consideration when comparing photolabeling efficiency.

Direct measurement of HDAC8 modification by photoaffinity probes using MALDI-ToF was performed on three independent experiments at three concentrations in assay buffer. Standard deviation was considered to identify significant difference between three probes. As a result, HD-55 has the strongest ability to cross-link HDAC8 while HD-74 is proven to be the photoaffinity probe with the lowest cross-linking efficiency. The more probe cross-linking, the higher photolabeling signal yielded.

The weaker signal intensity of long biotin tag implied that higher energy barrier of longer tag due to the bulky size prohibits the intermediate state from formation. Therefore, the steric effect of biotin tag needs to be taken into consideration for optimization of photolabeling efficiency.

In conclusion, besides binding affinity of probes to target enzymes, we explored other factors that may influence photolabeling efficiency and shed some light in photoaffinity probe and reporter group design for future.

CHAPTER 6 SUMMARY AND FUTURE DIRECTION

In this study we have explored the binding poses of HDAC3 and HDAC8 using activity-based photoaffinity probes. The combination of activity-based photolabeling, mass spectrometry analysis and computational modeling supplies a unique power in analysis of the binding of ligands to their macromolecular targets by expanding the data typically obtained in the protein X-ray crystallography or providing an alternative tool when cocrystallization of the protein with the ligand of interest has failed. Most importantly, the binding poses determined in this study are determined in solution and, thus, the captured "snapshots" reflect the dynamic nature of the ligand and its macromolecular target conformations.

Our findings demonstrated that multiple binding poses of HDAC ligands are likely to contribute to the binding of HDAC8. The data also helped to determine the binding modes of photoaffinity probes to HDAC3/NCoR2-DAD and suggested that NCoR2-DAD is positioned no further than roughly 7-8 Å from the entrance of the channel leading to HDAC3 binding site. It was shown that our combined approach can not only delineate the regions involved in the interface between two interacting proteins but also lead to structural models where the relative orientation of the proteins and their accessibility by small molecule inhibitors are defined.

Our ongoing and future studies will be directed towards refinement of the BEProFL approach. Minimization of the fragmentation of the probe is highly desirable to facilitate the analysis of MS/MS data. The mechanism of nonspecific tagging of the HDAC8 protein upon incubation with biotin tag remains unclear, warranting further investigation.

To further explore the factors which influence the photolabeling efficiency, the stability of photoreactive moiety during UV irradiation will be evaluated using mass spectrometry. The flexibility of probes in the HDAC active site may have significant impact on the insertion reaction with nearby protein residues, which will be reflected in the outcomes of the photolabeling experiment. Therefore, we will perform molecular simulation to investigate the orientation/flexibility of the probes.

Our future plans also include conducting BEProFL experiments with all class I HDAC proteins to enhance our understanding of the binding poses of the probes and gather more information for further refinement of the docking approaches for HDACs and solvent exposed binding sites in general, extension of the BEProFL approach to experiments in cells, identification of the potential targets of photoaffinity probes in cytoplasm and nuclei, evaluation of histone acetylation upon treatment with probes, completion of the HDAC isoform profiling, and extensive investigation of SAR of the promising pyrazole- and isoxazole-based histone deacetylase probes.

CITED LITERATURE

1. Wolffe, A.P., *Histone deacetylase: a regulator of transcription.* Science, 1996. **272**(5260): p. 371-2.

2. Taunton, J., C.A. Hassig, and S.L. Schreiber, *A mammalian histone deacetylase related to the yeast transcriptional regulator Rpd3p.* Science, 1996. **272**(5260): p. 408-11.

3. Bhasin, M., E.L. Reinherz, and P.A. Reche, *Recognition and classification of histones using support vector machine.* J Comput Biol, 2006. **13**(1): p. 102-12.

4. Luger, K., et al., *Crystal structure of the nucleosome core particle at 2.8 A resolution.* Nature, 1997. **389**(6648): p. 251-60.

5. Valkonen, K.H. and R.S. Piha, *Isoelectric focusing and isoelectric points of bovine liver histones.* Anal Biochem, 1980. **104**(2): p. 499-505.

6. Jenuwein, T. and C.D. Allis, *Translating the histone code.* Science, 2001. **293**(5532): p. 1074-80.

7. Xu, W.S., R.B. Parmigiani, and P.A. Marks, *Histone deacetylase inhibitors: molecular mechanisms of action.* Oncogene, 2007. **26**(37): p. 5541-52.

8. Gregory, P.D., K. Wagner, and W. Horz, *Histone acetylation and chromatin remodeling.* Exp Cell Res, 2001. **265**(2): p. 195-202.

9. Di Gennaro, E., et al., *Acetylation of proteins as novel target for antitumor therapy: review article.* Amino Acids, 2004. **26**(4): p. 435-41.

10. Das, C. and T.K. Kundu, *Transcriptional regulation by the acetylation of nonhistone proteins in humans -- a new target for therapeutics.* IUBMB Life, 2005. **57**(3): p. 137-49.

11. Bolden, J.E., M.J. Peart, and R.W. Johnstone, *Anticancer activities of histone deacetylase inhibitors.* Nat Rev Drug Discov, 2006. **5**(9): p. 769-84.

12. de Ruijter, A.J., et al., *Histone deacetylases (HDACs): characterization of the classical HDAC family.* Biochem J, 2003. **370**(Pt 3): p. 737-49.

13. McKinsey, T.A., et al., *Signal-dependent nuclear export of a histone deacetylase regulates muscle differentiation.* Nature, 2000. **408**(6808): p. 106-11.

14. Glozak, M.A. and E. Seto, *Histone deacetylases and cancer.* Oncogene, 2007. **26**(37): p. 5420-32.

15. Lin, R.J., et al., *Transcriptional regulation in acute promyelocytic leukemia.* Oncogene, 2001. **20**(49): p. 7204-15.

16. Choi, J.H., et al., *Expression profile of histone deacetylase 1 in gastric cancer tissues.* Jpn J Cancer Res, 2001. **92**(12): p. 1300-4.

17. Halkidou, K., et al., *Upregulation and nuclear recruitment of HDAC1 in hormone refractory prostate cancer.* Prostate, 2004. **59**(2): p. 177-89.

18. Wilson, A.J., et al., *Histone deacetylase 3 (HDAC3) and other class I HDACs regulate colon cell maturation and p21 expression and are deregulated in human colon cancer.* J Biol Chem, 2006. **281**(19): p. 13548-58.

19. Zhang, Z., et al., *Quantitation of HDAC1 mRNA expression in invasive carcinoma of the breast*.* Breast Cancer Res Treat, 2005. **94**(1): p. 11-6.

20. Huang, B.H., et al., *Inhibition of histone deacetylase 2 increases apoptosis and p21Cip1/WAF1 expression, independent of histone deacetylase 1.* Cell Death Differ, 2005. **12**(4): p. 395-404.

21. Song, J., et al., *Increased expression of histone deacetylase 2 is found in human gastric cancer.* APMIS, 2005. **113**(4): p. 264-8.

22. Bertrand, P., *Inside HDAC with HDAC inhibitors.* Eur J Med Chem. **45**(6): p. 2095-116.

23. Gui, C.Y., et al., *Histone deacetylase (HDAC) inhibitor activation of p21WAF1 involves changes in promoter-associated proteins, including HDAC1.* Proc Natl Acad Sci U S A, 2004. **101**(5): p. 1241-6.

24. Dokmanovic, M., C. Clarke, and P.A. Marks, *Histone deacetylase inhibitors: overview and perspectives.* Mol Cancer Res, 2007. **5**(10): p. 981-9.

25. Minucci, S. and P.G. Pelicci, *Histone deacetylase inhibitors and the promise of epigenetic (and more) treatments for cancer.* Nat Rev Cancer, 2006. **6**(1): p. 38-51.

26. Yoo, C.B. and P.A. Jones, *Epigenetic therapy of cancer: past, present and future.* Nat Rev Drug Discov, 2006. **5**(1): p. 37-50.

27. McLaughlin, F. and N.B. La Thangue, *Histone deacetylase inhibitors open new doors in cancer therapy.* Biochem Pharmacol, 2004. **68**(6): p. 1139-44.

28. Marks, P.A. and M. Dokmanovic, *Histone deacetylase inhibitors: discovery and development as anticancer agents.* Expert Opin Investig Drugs, 2005. **14**(12): p. 1497-511.

29. Sweet, M.J., et al., *HDAC inhibitors: modulating leukocyte differentiation, survival, proliferation and inflammation.* Immunol Cell Biol. **90**(1): p. 14-22.

30. Stimson, L., et al., *HDAC inhibitor-based therapies and haematological malignancy.* Ann Oncol, 2009. **20**(8): p. 1293-302.

31. Marks, P.A., V.M. Richon, and R.A. Rifkind, *Histone deacetylase inhibitors: inducers of differentiation or apoptosis of transformed cells.* J Natl Cancer Inst, 2000. **92**(15): p. 1210-6.

32. Park, J.H., et al., *Class I histone deacetylase-selective novel synthetic inhibitors potently inhibit human tumor proliferation.* Clin Cancer Res, 2004. **10**(15): p. 5271-81.

33. Weichert, W., et al., *Association of patterns of class I histone deacetylase expression with patient prognosis in gastric cancer: a retrospective analysis.* Lancet Oncol, 2008. **9**(2): p. 139-48.

34. Miyake, K., et al., *Expression of hypoxia-inducible factor-1alpha, histone deacetylase 1, and metastasis-associated protein 1 in pancreatic carcinoma: correlation with poor prognosis with possible regulation.* Pancreas, 2008. **36**(3): p. e1-9.

35. Weichert, W., et al., *Histone deacetylases 1, 2 and 3 are highly expressed in prostate cancer and HDAC2 expression is associated with shorter PSA relapse time after radical prostatectomy.* Br J Cancer, 2008. **98**(3): p. 604-10.

36. Weichert, W., et al., *Class I histone deacetylase expression has independent prognostic impact in human colorectal cancer: specific role of class I histone deacetylases in vitro and in vivo.* Clin Cancer Res, 2008. **14**(6): p. 1669-77.

37. Oehme, I., et al., *Targeting of HDAC8 and investigational inhibitors in neuroblastoma.* Expert Opin Investig Drugs, 2009. **18**(11): p. 1605-17.

38. Alland, L., et al., *Role for N-CoR and histone deacetylase in Sin3-mediated transcriptional repression.* Nature, 1997. **387**(6628): p. 49-55.

39. Heinzel, T., et al., *A complex containing N-CoR, mSin3 and histone deacetylase mediates transcriptional repression.* Nature, 1997. **387**(6628): p. 43-8.

40. Cress, W.D. and E. Seto, *Histone deacetylases, transcriptional control, and cancer.* J Cell Physiol, 2000. **184**(1): p. 1-16.

41. Hartman, H.B., et al., *The histone-binding code of nuclear receptor co-repressors matches the substrate specificity of histone deacetylase 3.* EMBO Rep, 2005. **6**(5): p. 445-51.

42. Grant, P.A. and S.L. Berger, *Histone acetyltransferase complexes.* Semin Cell Dev Biol, 1999. **10**(2): p. 169-77.

43. Glozak, M.A., et al., *Acetylation and deacetylation of non-histone proteins.* Gene, 2005. **363**: p. 15-23.

44. Rosato, R.R. and S. Grant, *Histone deacetylase inhibitors: insights into mechanisms of lethality.* Expert Opin Ther Targets, 2005. **9**(4): p. 809-24.

45. Zhao, L.J., et al., *Acetylation by p300 regulates nuclear localization and function of the transcriptional corepressor CtBP2.* J Biol Chem, 2006. **281**(7): p. 4183-9.

46. Ficner, R., *Novel structural insights into class I and II histone deacetylases.* Curr Top Med Chem, 2009. **9**(3): p. 235-40.

47. Marmorstein, R. and R.C. Trievel, *Histone modifying enzymes: structures, mechanisms, and specificities.* Biochim Biophys Acta, 2009. **1789**(1): p. 58-68.

48. Hildmann, C., et al., *Substrate and inhibitor specificity of class 1 and class 2 histone deacetylases.* J Biotechnol, 2006. **124**(1): p. 258-70.

49. Finnin, M.S., et al., *Structures of a histone deacetylase homologue bound to the TSA and SAHA inhibitors.* Nature, 1999. **401**(6749): p. 188-93.

50. Mai, A., et al., *Histone deacetylation in epigenetics: an attractive target for anticancer therapy.* Med Res Rev, 2005. **25**(3): p. 261-309.

51. Cravatt, B.F., A.T. Wright, and J.W. Kozarich, *Activity-based protein profiling: from enzyme chemistry to proteomic chemistry.* Annu Rev Biochem, 2008. **77**: p. 383-414.

52. Evans, M.J. and B.F. Cravatt, *Mechanism-based profiling of enzyme families.* Chem Rev, 2006. **106**(8): p. 3279-301.

53. Amara, N., et al., *Covalent inhibition of bacterial quorum sensing.* J Am Chem Soc, 2009. **131**(30): p. 10610-9.

54. Geurink, P., et al., *Photoaffinity Labeling in Activity-Based Protein Profiling.* p. 85-113.

55. Monica, B., et al., *Human caliciviruses in symptomatic and asymptomatic infections in children in Vellore, South India.* J Med Virol, 2007. **79**(5): p. 544-51.

56. Kidd, D., Y. Liu, and B.F. Cravatt, *Profiling serine hydrolase activities in complex proteomes.* Biochemistry, 2001. **40**(13): p. 4005-15.

57. Lennon-Dumenil, A.M., et al., *Analysis of protease activity in live antigen-presenting cells shows regulation of the phagosomal proteolytic contents during dendritic cell activation.* J Exp Med, 2002. **196**(4): p. 529-40.
58. Liu, Y., M.P. Patricelli, and B.F. Cravatt, *Activity-based protein profiling: the serine hydrolases.* Proc Natl Acad Sci U S A, 1999. **96**(26): p. 14694-9.
59. Kalesh, K.A., et al., *The use of click chemistry in the emerging field of catalomics.* Org Biomol Chem, 2010. **8**(8): p. 1749-62.
60. Brunner, J., *New photolabeling and crosslinking methods.* Annu Rev Biochem, 1993. **62**: p. 483-514.
61. Singh, A., E.R. Thornton, and F.H. Westheimer, *The photolysis of diazoacetylchymotrypsin.* J Biol Chem, 1962. **237**: p. 3006-8.
62. Chowdhry, V. and F.H. Westheimer, *Photoaffinity labeling of biological systems.* Annu Rev Biochem, 1979. **48**: p. 293-325.
63. Tanaka, Y., M.R. Bond, and J.J. Kohler, *Photocrosslinkers illuminate interactions in living cells.* Mol Biosyst, 2008. **4**(6): p. 473-80.
64. Vodovozova, E.L., *Photoaffinity labeling and its application in structural biology.* Biochemistry (Mosc), 2007. **72**(1): p. 1-20.
65. Nielsen, P.E., ed. *Photochemical Probes in Biochemistry*. NATO ASI Series. Vol. 272. 1989, Kluwer Academic Publishers: Dordrecht / Boston / London.
66. Buchmueller, K.L., et al., *RNA-tethered phenyl azide photocrosslinking via a short-lived indiscriminant electrophile.* J Am Chem Soc, 2003. **125**(36): p. 10850-61.
67. Schnapp, K.A., et al., *Exploratory photochemistry of fluorinated aryl azides. Implications for the design of photoaffinity labeling reagents.* Bioconjug Chem, 1993. **4**(2): p. 172-7.
68. Staros, J.V., et al., *Reduction of aryl azides by thiols: implications for the use of photoaffinity reagents.* Biochem Biophys Res Commun, 1978. **80**(3): p. 568-72.
69. Weber, P.J. and A.G. Beck-Sickinger, *Comparison of the photochemical behavior of four different photoactivatable probes.* J Pept Res, 1997. **49**(5): p. 375-83.
70. Saxon, E. and C.R. Bertozzi, *Cell surface engineering by a modified Staudinger reaction.* Science, 2000. **287**(5460): p. 2007-10.
71. Rostovtsev, V.V., et al., *A stepwise huisgen cycloaddition process: copper(I)-catalyzed regioselective "ligation" of azides and terminal alkynes.* Angew Chem Int Ed Engl, 2002. **41**(14): p. 2596-9.
72. Speers, A.E., G.C. Adam, and B.F. Cravatt, *Activity-based protein profiling in vivo using a copper(i)-catalyzed azide-alkyne [3 + 2] cycloaddition.* Journal of the American Chemical Society, 2003. **125**(16): p. 4686-7.

73. Baskin, J.M., et al., *Copper-free click chemistry for dynamic in vivo imaging.* Proc Natl Acad Sci U S A, 2007. **104**(43): p. 16793-7.

74. Ning, X., et al., *Visualizing metabolically labeled glycoconjugates of living cells by copper-free and fast huisgen cycloadditions.* Angew Chem Int Ed Engl, 2008. **47**(12): p. 2253-5.

75. Poloukhtine, A.A., et al., *Selective labeling of living cells by a photo-triggered click reaction.* J Am Chem Soc, 2009. **131**(43): p. 15769-76.

76. Adam, G.C., et al., *Mapping enzyme active sites in complex proteomes.* Journal of the American Chemical Society, 2004. **126**(5): p. 1363-8.

77. Sieber, S.A., et al., *Microarray platform for profiling enzyme activities in complex proteomes.* Journal of the American Chemical Society, 2004. **126**(48): p. 15640-1.

78. Speers, A.E. and B.F. Cravatt, *A tandem orthogonal proteolysis strategy for high-content chemical proteomics.* Journal of the American Chemical Society, 2005. **127**(28): p. 10018-9.

79. Hanson, S.R., et al., *Tailored glycoproteomics and glycan site mapping using saccharide-selective bioorthogonal probes.* Journal of the American Chemical Society, 2007. **129**(23): p. 7266-7.

80. Li, W., J.L. Blankman, and B.F. Cravatt, *A functional proteomic strategy to discover inhibitors for uncharacterized hydrolases.* Journal of the American Chemical Society, 2007. **129**(31): p. 9594-5.

81. Salisbury, C.M. and B.F. Cravatt, *Activity-based probes for proteomic profiling of histone deacetylase complexes.* Proceedings of the National Academy of Sciences of the United States of America, 2007. **104**(4): p. 1171-6.

82. Kolb, H.C. and K.B. Sharpless, *The growing impact of click chemistry on drug discovery.* Drug Discov Today, 2003. **8**(24): p. 1128-37.

83. Huisgen, R., *1,3-Dipolar cycloaddition - introduction, survey, mechanism. 1,3-Dipolar Cycloaddition Chemistry*, 1984. **1**: p. 1-176.

84. Yan, W. and S.S. Chen, *Mass spectrometry-based quantitative proteomic profiling.* Brief Funct Genomic Proteomic, 2005. **4**(1): p. 27-38.

85. Wu, S., et al., *An integrated top-down and bottom-up strategy for broadly characterizing protein isoforms and modifications.* J Proteome Res, 2009. **8**(3): p. 1347-57.

86. Han, X., A. Aslanian, and J.R. Yates, 3rd, *Mass spectrometry for proteomics.* Curr Opin Chem Biol, 2008. **12**(5): p. 483-90.

87. Siuti, N. and N.L. Kelleher, *Decoding protein modifications using top-down mass spectrometry.* Nat Methods, 2007. **4**(10): p. 817-21.

88. Parks, B.A., et al., *Top-down proteomics on a chromatographic time scale using linear ion trap fourier transform hybrid mass spectrometers.* Anal Chem, 2007. **79**(21): p. 7984-91.

89. Zabrouskov, V. and J.P. Whitelegge, *Increased coverage in the transmembrane domain with activated-ion electron capture dissociation for top-down Fourier-transform mass spectrometry of integral membrane proteins.* J Proteome Res, 2007. **6**(6): p. 2205-10.

90. Ge, Y., et al., *Top down characterization of secreted proteins from Mycobacterium tuberculosis by electron capture dissociation mass spectrometry.* J Am Soc Mass Spectrom, 2003. **14**(3): p. 253-61.

91. Ge, Y., et al., *Top down characterization of larger proteins (45 kDa) by electron capture dissociation mass spectrometry.* J Am Chem Soc, 2002. **124**(4): p. 672-8.

92. Sze, S.K., et al., *Plasma electron capture dissociation for the characterization of large proteins by top down mass spectrometry.* Anal Chem, 2003. **75**(7): p. 1599-603.

93. Abzalimov, R.R., et al., *Protein conformations can be probed in top-down HDX MS experiments utilizing electron transfer dissociation of protein ions without hydrogen scrambling.* J Am Soc Mass Spectrom, 2009. **20**(8): p. 1514-7.

94. Zabrouskov, V., et al., *Unraveling molecular complexity of phosphorylated human cardiac troponin I by top down electron capture dissociation/electron transfer dissociation mass spectrometry.* Mol Cell Proteomics, 2008. **7**(10): p. 1838-49.

95. Bunger, M.K., et al., *Automated proteomics of E. coli via top-down electron-transfer dissociation mass spectrometry.* Anal Chem, 2008. **80**(5): p. 1459-67.

96. Jung, M., A. Kozikowski, and A. Dritschilo, *Rational design and development of radiation-sensitizing histone deacetylase inhibitors.* Chem Biodivers, 2005. **2**(11): p. 1452-61.

97. Acharya, M.R., et al., *Rational development of histone deacetylase inhibitors as anticancer agents: a review.* Mol Pharmacol, 2005. **68**(4): p. 917-32.

98. Korner, M. and U. Tibes, *Histone deacetylase inhibitors: a novel class of anti-cancer agents on its way to the market.* Prog Med Chem, 2008. **46**: p. 205-80.

99. Hahnen, E., et al., *Histone deacetylase inhibitors: possible implications for neurodegenerative disorders.* Expert Opin Investig Drugs, 2008. **17**(2): p. 169-84.

100. Brandl, A., T. Heinzel, and O.H. Kramer, *Histone deacetylases: salesmen and customers in the post-translational modification market.* Biol Cell, 2009. **101**(4): p. 193-205.

101. Gurard-Levin, Z.A. and M. Mrksich, *The activity of HDAC8 depends on local and distal sequences of its peptide substrates.* Biochemistry, 2008. **47**(23): p. 6242-50.

102. Hu, E., et al., *Cloning and characterization of a novel human class I histone deacetylase that functions as a transcription repressor.* J Biol Chem, 2000. **275**(20): p. 15254-64.

103. Moreth, K., et al., *An active site tyrosine residue is essential for amidohydrolase but not for esterase activity of a class 2 histone deacetylase-like bacterial enzyme.* Biochem J, 2007. **401**(3): p. 659-65.

104. Huber, K., et al., *Inhibitors of histone deacetylases: correlation between isoform specificity and reactivation of HIV type 1 (HIV-1) from latently infected cells.* J Biol Chem. **286**(25): p. 22211-8.

105. Girish, V. and A. Vijayalakshmi, *Affordable image analysis using NIH Image/ImageJ.* Indian J Cancer, 2004. **41**(1): p. 47.

106. Eliceiri, K.W. and C. Rueden, *Tools for visualizing multidimensional images from living specimens.* Photochem Photobiol, 2005. **81**(5): p. 1116-22.

107. He, B., et al., *Binding ensemble profiling with photoaffinity labeling (BEProFL) approach: mapping the binding poses of HDAC8 inhibitors.* J Med Chem, 2009. **52**(22): p. 7003-13.

108. Wang, D.F., et al., *Toward selective histone deacetylase inhibitor design: homology modeling, docking studies, and molecular dynamics simulations of human class I histone deacetylases.* J Med Chem, 2005. **48**(22): p. 6936-47.

109. Rajagopalan, K., D.S. Watt, and B.E. Haley, *Orientation of GTP and ADP within their respective binding sites in glutamate dehydrogenase.* Eur J Biochem, 1999. **265**(2): p. 564-71.

110. Olcott, M.C., M.L. Bradley, and B.E. Haley, *Photoaffinity labeling of creatine kinase with 2-azido- and 8-azidoadenosine triphosphate: identification of two peptides from the ATP-binding domain.* Biochemistry, 1994. **33**(39): p. 11935-41.

111. Hosoya, T., et al., *Novel bifunctional probe for radioisotope-free photoaffinity labeling: compact structure comprised of photospecific ligand ligation and detectable tag anchoring units.* Organic & Biomolecular Chemistry, 2004. **2**(5): p. 637-41.

112. Sun, P., et al., *Synthesis of a bis-azido analogue of acromelic acid for radioisotope-free photoaffinity labeling and biochemical studies.* Bioorganic & Medicinal Chemistry Letters, 2006. **16**(9): p. 2433-2436.

113. Hosoya, T., et al., *Design of dantrolene-derived probes for radioisotope-free photoa.nity labeling of proteins involved in the physiological Ca2+ release from sarcoplasmic reticulum of skeletal muscle.* . Bioorg. Med. Chem. Lett., 2005. **15**: p. 1289-1294.

114. Saxon, E., J.I. Armstrong, and C.R. Bertozzi, *A "traceless" Staudinger ligation for the chemoselective synthesis of amide bonds.* Organic Letters, 2000. **2**(14): p. 2141-3.

115. Saxon, E., et al., *Investigating cellular metabolism of synthetic azidosugars with the Staudinger ligation.* Journal of the American Chemical Society, 2002. **124**(50): p. 14893-902.

116. Kiick, K.L., et al., *Incorporation of azides into recombinant proteins for chemoselective modification by the Staudinger ligation.* Proc Natl Acad Sci U S A, 2002. **99**(1): p. 19-24.

117. Vocadlo, D.J. and C.R. Bertozzi, *A strategy for functional proteomic analysis of glycosidase activity from cell lysates.* Angew Chem Int Ed Engl, 2004. **43**(40): p. 5338-42.

118. Vocadlo, D.J., et al., *A chemical approach for identifying O-GlcNAc-modified proteins in cells.* Proceedings of the National Academy of Sciences of the United States of America, 2003. **100**(16): p. 9116-21.

119. Al-Mawsawi, L.Q., et al., *Discovery of a small-molecule HIV-1 integrase inhibitor-binding site.* Proceedings of the National Academy of Sciences of the United States of America, 2006. **103**(26): p. 10080-5.

120. Somoza, J.R., et al., *Structural snapshots of human HDAC8 provide insights into the class I histone deacetylases.* Structure, 2004. **12**(7): p. 1325-34.

121. Li, J., et al., *Both corepressor proteins SMRT and N-CoR exist in large protein complexes containing HDAC3.* Embo J, 2000. **19**(16): p. 4342-50.

122. Guenther, M.G., O. Barak, and M.A. Lazar, *The SMRT and N-CoR corepressors are activating cofactors for histone deacetylase 3.* Mol Cell Biol, 2001. **21**(18): p. 6091-101.

123. Guenther, M.G., et al., *A core SMRT corepressor complex containing HDAC3 and TBL1, a WD40-repeat protein linked to deafness.* Genes Dev, 2000. **14**(9): p. 1048-57.

124. Sali, A. and T.L. Blundell, *Comparative protein modelling by satisfaction of spatial restraints.* J Mol Biol, 1993. **234**(3): p. 779-815.

125. Dowling, D.P., et al., *Structural studies of human histone deacetylase 8 and its site-specific variants complexed with substrate and inhibitors.* Biochemistry, 2008. **47**(51): p. 13554-63.

126. Vannini, A., et al., *Crystal structure of a eukaryotic zinc-dependent histone deacetylase, human HDAC8, complexed with a hydroxamic acid inhibitor.* Proc Natl Acad Sci U S A, 2004. **101**(42): p. 15064-9.

127. Vannini, A., et al., *Substrate binding to histone deacetylases as shown by the crystal structure of the HDAC8-substrate complex.* EMBO Rep, 2007. **8**(9): p. 879-84.

128. Wiehe, K., et al., *ZDOCK and RDOCK performance in CAPRI rounds 3, 4, and 5.* Proteins, 2005. **60**(2): p. 207-13.

129. Janin, J., *Sailing the route from Gaeta, Italy, to CAPRI.* Proteins-Structure Function and Bioinformatics, 2005. **60**(2): p. 149-149.

130. Codina, A., et al., *Structural insights into the interaction and activation of histone deacetylase 3 by nuclear receptor corepressors.* Proceedings of the National Academy of Sciences of the United States of America, 2005. **102**(17): p. 6009-6014.

131. Kanungo, T., et al., *An efficient k-means clustering algorithm: Analysis and implementation.* Ieee Transactions on Pattern Analysis and Machine Intelligence, 2002. **24**(7): p. 881-892.

132. Qin, S. and H.X. Zhou, *meta-PPISP: a meta web server for protein-protein interaction site prediction.* Bioinformatics, 2007. **23**(24): p. 3386-7.

133. Chen, H. and H.X. Zhou, *Prediction of interface residues in protein-protein complexes by a consensus neural network method: test against NMR data.* Proteins, 2005. **61**(1): p. 21-35.

134. Liang, S., et al., *Protein binding site prediction using an empirical scoring function.* Nucleic Acids Res, 2006. **34**(13): p. 3698-707.

135. Neuvirth, H., R. Raz, and G. Schreiber, *ProMate: a structure based prediction program to identify the location of protein-protein binding sites.* J Mol Biol, 2004. **338**(1): p. 181-99.

136. Pettersen, E.F., et al., *UCSF chimera - A visualization system for exploratory research and analysis.* Journal of Computational Chemistry, 2004. **25**(13): p. 1605-1612.

137. Liu, G., et al., *Screening method for the discovery of potential cancer chemoprevention agents based on mass spectrometric detection of alkylated Keap1.* Anal Chem, 2005. **77**(19): p. 6407-14.

138. Verdonk, M.L., et al., *Improved protein-ligand docking using GOLD.* Proteins, 2003. **52**(4): p. 609-23.

139. Neelarapu, R., et al., *Design, synthesis, docking, and biological evaluation of novel diazide-containing isoxazole- and pyrazole-based histone deacetylase probes.* J Med Chem, 2011. **54**(13): p. 4350-64.

140. Salisbury, C.M. and B.F. Cravatt, *Optimization of activity-based probes for proteomic profiling of histone deacetylase complexes.* J Am Chem Soc, 2008. **130**(7): p. 2184-94.

141. Kawamura, A., et al., *Binding is not enough: flexibility is needed for photocrosslinking of Lck kinase by benzophenone photoligands.* Bioorg Med Chem, 2008. **16**(19): p. 8824-9.

142. Paul P. Geurink, T.K., Laurette Prèly, Krisztina Paal, Michiel A. Leeuwenburgh, Gijs A. van der Marel, Henk F. Kauffman, Herman S. Overkleeft and Rainer Bischoff, *Design of Peptide Hydroxamate-Based Photoreactive Activity-Based Probes of Zinc-Dependent Metalloproteases* European journal of organic chemistry, 2010. **2010**(11): p. 2100-2112.

143. Rishton, G.M., *Nonleadlikeness and leadlikeness in biochemical screening.* Drug Discov Today, 2003. **8**(2): p. 86-96.

144. Hann, M.M. and T.I. Oprea, *Pursuing the leadlikeness concept in pharmaceutical research.* Curr Opin Chem Biol, 2004. **8**(3): p. 255-63.

145. Roche, O., et al., *Development of a virtual screening method for identification of "frequent hitters" in compound libraries.* J Med Chem, 2002. **45**(1): p. 137-42.

146. DeWitte, R.S., *Avoiding physicochemical artefacts in early ADME-Tox experiments.* Drug Discov Today, 2006. **11**(17-18): p. 855-9.

147. Coan, K.E. and B.K. Shoichet, *Stoichiometry and physical chemistry of promiscuous aggregate-based inhibitors.* J Am Chem Soc, 2008. **130**(29): p. 9606-12.

148. McGovern, S.L., et al., *A common mechanism underlying promiscuous inhibitors from virtual and high-throughput screening.* J Med Chem, 2002. **45**(8): p. 1712-22.

149. Feng, B.Y., et al., *A high-throughput screen for aggregation-based inhibition in a large compound library.* J Med Chem, 2007. **50**(10): p. 2385-90.

150. Kooper, G.N., et al., *Photoaffinity labeling of opiate receptors using intrinsically photoactive 3H-opiates.* Mol Pharmacol, 1988. **33**(3): p. 316-26.

151. Yoshida, M., et al., *Potent and specific inhibition of mammalian histone deacetylase both in vivo and in vitro by trichostatin A.* J Biol Chem, 1990. **265**(28): p. 17174-9.

152. Cousens, L.S., D. Gallwitz, and B.M. Alberts, *Different accessibilities in chromatin to histone acetylase.* J Biol Chem, 1979. **254**(5): p. 1716-23.

153. Sekhavat, A., J.M. Sun, and J.R. Davie, *Competitive inhibition of histone deacetylase activity by trichostatin A and butyrate.* Biochem Cell Biol, 2007. **85**(6): p. 751-8.

154. Laiko, V.V., M.A. Baldwin, and A.L. Burlingame, *Atmospheric pressure matrix-assisted laser desorption/ionization mass spectrometry.* Anal Chem, 2000. **72**(4): p. 652-7.

155. Kislinger, T., A. Humeny, and M. Pischetsrieder, *Analysis of protein glycation products by matrix-assisted laser desorption ionization time-of-flight mass spectrometry.* Curr Med Chem, 2004. **11**(16): p. 2185-93.

VITA

NAME:
HE BAI

EDUCATION

University of Illinois at Chicago, 2007.5 – present
Chicago, IL
Ph. D program in Medicinal chemistry / Dept. of Med. Chem. and Pharmacognosy.

University of Illinois at Chicago, 2005.8 – 2007.5
Chicago, IL
Master of Science in Chemistry/ Dept. of Chemistry

Zhejiang University, **1999.9 – 2003.6**
Hangzhou, CHINA
Bachelor of Science in Chemistry / Dept. of Chemistry

WORK EXPERIENCE

Johnson & Johnson, Centocor, Jan 2011 – Jul 2011
Radnor, PA
Graduate Co-op program

- Design and perform protein stability and biophysical characterization studies.
- Determine the effect of silicone oil coating on pre-filled syringe.
- Evaluate protein compatibility with pre-filled syringe components and interfaces.
- Develop a platform to support early stage formulation development.
- Analyze data and present results in internal research group meetings

Bristol-Myers Squibb, May 2010 – Aug 2010
Hopewell, NJ
Summer internship

- Study the colloidal interactions (B2) effects of pharmaceutically relevant kosmotropic buffers on PEG by multi-angle light scattering (MALS).
- Explore the conformational effects of kosmotropic buffers on PEG by measuring solution viscosities.
- Investigate the solution interactions of PEG under pharmaceutically relevant conditions.
- Perform biophysical characterization of PEG, native protein and PEGylated proteins.

Sichuan Times Pharm. Group, Jul 2003 – Jun 2005
Chengdu, China
Quality Control Specialist

- Maintain inventory and analytical instruments LC-MS, HPLC, UV-VIS and FTIR
- Analyze and characterize raw materials, intermediates and final products
- Assess short and long-term stability of formulations isolate

RESEARCH EXPERIENCE

University of Illinois at Chicago, May 2007 – present
Chicago, IL
Research assistant

- Design, validate and perform in-vitro and cellular inhibitor assay
- Over-express and purify HDAC8 protein in Hek-293 mammalian cells
- Validate ligand binding of protein by ELISA, immunoblotting and MALDI-ToF
- Identify post translational modification of protein by FT-MS
- Visualize cellular imaging tagged probes in live Hela cells by Confocal microscopy
- Analyze cell extract of modified protein by LC-MS

University of Illinois at Chicago, Aug 2005 – May 2007
Chicago, IL
Research assistant

- Over-express and purify erythroid alpha-spectrin protein in E. Coli
- Characterize Alpha-spectrin protein and conduct stability tests
- Evaluate mutation effects on association alpha-spectrin with beta-spectrin

RESEARCH SKILLS

- Proficiency with mass spectrometry and scientific analysis software such as Xcalibur, SEQUEST, Mascot, ImageJ, Voyager, Graphpad Prism, ChemOffice, PyMOL

- Protein over-expression in mammalian and bacterial cell culture; Confocal Microscopy cellular imaging, Protein purification through Fast Protein Liquid Chromatography (FPLC) system [Ion-exchange Column (IEC), Immobilized metal ion affinity chromatography, Size Exclusion Column (SEC)]; Analysis of enzyme activity by High Performance Liquid Chromatography (HPLC).

- Hands on experience with protein formulation, characterization and stability evaluation techniques: Isothermal Titration Calorimetry (ITC), Circular Dichroism (CD), Multi-angle Light Scattering (MALS), Dynamic Light Scattering (DLS), m-VROC viscometer, Fluorescence Spectroscopy, Fourier transform infrared spectroscopy (FTIR), ZebraSci ZS40 silicone oil characterization system, LTQ-FT Mass Spectrometry and Ultraviolet Spectroscopy

- Molecular biology techniques: Sodium Dodecyl Sulphate-Polyacrylamide Gel Electrophoresis (SDS-PAGE), Enzyme-linked immunosorbent assay (ELISA), western blot, immunoprecipitation, DNA purification and transfection, gel extraction, preparation of competent cells, in vitro fluorometric and cell based assays, protein crystallization (grow single crystals for data collecting).
- Word processing with Word, Excel, PowerPoint, Symyx electronic lab notebook

PUBLICATION AND PRESENTATIONS

- Hazem Abdelkarim, Michael Brunsteiner, Bai H., Yong Soo Choi, Raghupathi Neelerapu, Subash Veleparthi, Richard van Breemen, Sylvie Y. Blond, Pavel A. Petukhov. (2012) Photoreactive HDAC3 inhibitors act as "nanorulers" probing the details of HDAC3/NCoR2-DAD complex. J. Am. Chem. Soc. (in preparation)
- Neelarapu R., Vaidya A.S., Bai H., Mendonca E., Brunsteiner M., , van Breemen RB, Blond S.Y., Petukhov P.A. (2012) Novel HDAC8 Ligands without a Bidentate Zinc Chelating Group: Exploring an upside-down binding pose. J. Med. Chem (in preparation)
- Neelarapu R., Holzle D.L., Velaparthi S., Bai H., Brunsteiner M., Blond S.Y., Petukhov P.A. (2011) Design, synthesis, docking, and biological evaluation of novel diazide-containing isoxazole- and pyrazole-based histone deacetylase probes. J. Med. Chem. 54, 4350-4364
- Bai H., Velaparthi S., Pieffet G., Pennington C., Mahesh A., Holzle D.L., Brunsteiner M., van Breemen RB, Blond S.Y., Petukhov P.A. (2009) Binding Ensemble Profiling with Photoaffinity Labeling (BEProFL) Approach: Mapping the Binding Poses of HDAC8 Inhibitors. J. Med. Chem. 52, 7003-7013.
- Chakrabarty S., Jasmine, Bhadaliya C., Sinha B. N., Mahesh A., Bai H., Blond S.Y., Jayaprakash V. (2010) Inhibitors of Human Histone Deacetylase: Synthesis and Enzyme Assay of Hydroxamate with Piperazine Linker. Arch. Pharm. Chem. Life Sci. 343, 167-172.
- Bai H., (2009) Exploring binding of HDAC isoforms with inhibitors by photoaffinity probes, American Chemical Society Conference March 2009, Salt Lake City, Utah.

HONORS AND MEMBERSHIP

- Received Joseph frank Celer scholarship, which is presented for outstanding research performance in cancer research by Department of Medicinal Chemistry and Pharmacognosy, The University of Illinois at Chicago.

  2008
- Membership in Rho Chi Pharmacy Honors Society

  2007-2009
- Awarded the third Prize of Excellent Undergraduate Scholarship by Zhejiang University

  2002
- Awarded Specialized scholarship of Recreational Activities by Zhejiang University

  2001